Physics Lib.

NOV 8 -

DO NOT TAKE FROM LIBRARY

copy 2

THE PHYSICAL REVIEW

VOLUME 48 *Second Series* NUMBER 9

NOVEMBER 1, 1935

Published for the

AMERICAN PHYSICAL SOCIETY

by the

AMERICAN INSTITUTE OF PHYSICS

Incorporated

LANCASTER, PA., AND NEW YORK, N. Y.

THE AMERICAN PHYSICAL SOCIETY

OFFICERS OF THE SOCIETY

R. W. WOOD, *President*
The Johns Hopkins University
Baltimore, Maryland

F. K. RICHTMYER, *Vice President*
Cornell University
Ithaca, New York

W. L. SEVERINGHAUS, *Secretary*
Columbia University
New York, New York

G. B. PEGRAM, *Treasurer*
Columbia University
New York, New York

JOHN T. TATE, *Editor*
University of Minnesota
Minneapolis, Minnesota

L. B. LOEB, *Local Secretary for the Pacific Coast*
University of California
Berkeley, California

THE PHYSICAL REVIEW

BOARD OF EDITORS

JOHN T. TATE, *Editor*

J. W. BUCHTA, *Assistant Editor*

Associate Editors

K. K. DARROW
J. C. HUBBARD
A. E. RUARK
A. ELLETT
L. A. TURNER
G. E. UHLENBECK
W. V. HOUSTON
R. S. MULLIKEN
I. I. RABI

THE PHYSICAL REVIEW, which was established in 1893, is a journal of experimental and theoretical physics. It is published for the American Physical Society by the American Institute of Physics Incorporated. There are two volumes annually with twelve issues in each volume.

Manuscripts for publication should be submitted to John T. Tate, University of Minnesota, Minneapolis, Minnesota.

Proof and all correspondence concerning papers in the process of publication, should be addressed to the Editorial Secretary, American Institute of Physics, 11 East 38th Street, New York, New York.

Subscription price: United States and Possessions and Canada, $15.00; Foreign, $16.50. Subscriptions and orders for back numbers should be addressed to Prince and Lemon Streets, Lancaster, Pennsylvania, or to the American Institute of Physics, 11 East 38th Street, New York, New York.

Advertising is not accepted for the *Physical Review* but attention is called to the *Review of Scientific Instruments with Physics News and Views*, a companion publication of the Institute, and a medium through which the field of physics can be reached most effectively. Rates and other information will be furnished on request to the Editorial Secretary.

Changes of address and complaints of failure to receive the *Physical Review*, in the case of members of the American Physical Society, should be addressed to the Treasurer; in the case of other subscribers, to the Editorial Secretary. New copies can be sent free in response to complaints of non-delivery only if notice of non-delivery is received within three months of date of issue.

The Physical Review is published semi-monthly at Prince and Lemon Streets, Lancaster, Pennsylvania.

Entered at the Post Office at Lancaster, Pennsylvania, as second class matter.

Acceptance for mailing at special rate of postage provided for in section 1103, Act of October 3, 1917, authorised September 6, 1926.

THE
PHYSICAL REVIEW
A Journal of Experimental and Theoretical Physics
VOL. 48, NO. 9 NOVEMBER 1, 1935 SECOND SERIES

Beryllium Deuteride Spectra

PHILIP G. KOONTZ,* *Sloane Physics Laboratory, Yale University*
(Received July 15, 1935)

The spectra of the BeD green bands and of the ultraviolet BeD^+ bands have been photographed at high dispersion. A Be arc in a deuterium atmosphere was the source. Rotational analyses of the BeD bands, and rotational and vibrational analyses of the BeD^+ bands are presented. The electronic isotope shift in the ultraviolet system is 0.8 cm^{-1}. The values $B_e^* = 5.6807$ for the lower state of BeD and $B_e^* = 5.9546$ for the lower state of BeD^+ are found. Comparison of these values with the corresponding values of the hydrides gives ratios 0.55110 and 0.55073, respectively, whereas $\rho^2 = 0.55060$. Calculation of the J. L. Dunham corrections to B_e for the anharmonic oscillator are shown to affect the B_e ratio inappreciably. The variation of the ratio of the B_e^*'s from ρ^2 and the small electronic isotope shift are briefly discussed.

INTRODUCTION

AN accurate comparison of the spectra of the deuterides with those of the corresponding hydrides is important in the study of the dynamical behavior of diatomic molecules. Such studies as have been made for DCl,[1] AlD,[2] CaD,[3] NaD,[4] LiD,[5] and AgD,[6] CdD[7] show, in many cases, an interesting variation of the ratios of the molecular constants from the predictions of the simple isotope theory. This theory predicts an equality between the ratio of the reduced masses, ρ^2, and the ratio of the rotational constant B_e for the nonrotating vibrationless isotopic molecules, but experiment shows the latter to be appreciably larger than ρ^2 in some cases. In no case has the ratio B_e^i/B_e been found to be smaller than ρ^2. Since different views[2, 8] of the explanation of these departures have developed, it is desirable to compare accurately the spectra of other hydrides and deuterides. The $^1\Sigma \rightarrow {}^1\Sigma$ BeH^+ bands[9, 10, 11] in the region 2200–3100A and the $^2\Pi \rightarrow {}^2\Sigma$ BeH bands[9, 12, 13, 14] near 4990A, which have been carefully analyzed, offer good material for this study. The results of analyses of the corresponding spectra of the deuterides BeD^+ and BeD are here presented.

* Part of a dissertation presented to the Faculty of the Graduate School of Yale University in candidacy for the degree of Doctor of Philosophy.

[1] Hardy, Barker, and Dennison, Phys. Rev. **42**, 279 (1932).

[2] W. Holst and E. Hulthén, Nature **133**, 496 (1934); **133**, 796 (1934); Zeits. f. Physik **90**, 712 (1934).

[3] W. W. Watson, Phys. Rev. **46**, 319 (1934); **47**, 27 (1935).

[4] E. Olsson, Nature **134**, 697 (1934); Zeits. f. Physik **93**, 206 (1935).

[5] F. H. Crawford and T. Jorgensen, Jr., Phys. Rev. **47**, 358 (1935); **47**, 932 (1935).

[6] P. G. Koontz, Phys. Rev. **48**, 138 (1935).

[7] E. Svensson, Stockholm, 1935.

[8] R. de L. Kronig, Physica **1**, 617 (1934).

[9] W. W. Watson, Phys. Rev. **32**, 600 (1928); **34**, 372 (1929).

[10] E. Bengtsson, Nature **123**, 529 (1929); Nova Acta Reg. Soc. Sci. Uppsala (IV) **8**, 65 (1932).

[11] R. Mecke, Zeits. f. Physik **72**, 155 (1931).

[12] M. Petersen, Phys. Rev. **31**, 1130 (1928).

[13] W. Watson and A. Parker, Phys. Rev. **36**, 1019 (1930); **37**, 167 (1931).

[14] E. Olsson, Zeits. f. Physik **73**, 732 (1932).

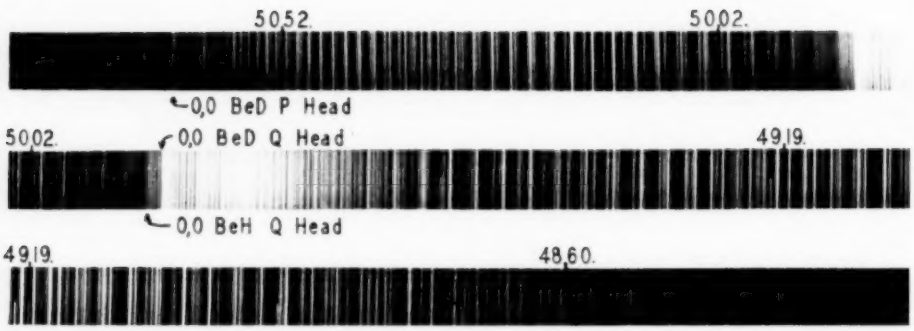

FIG. 1. Spectrogram of the BeD green bands at 4990A.

EXPERIMENTAL PROCEDURE

The light source, used in the production of the BeD^+ and BeD bands, was a d.c. arc between two Be electrodes in an atmosphere of deuterium gas at about 3 cm of Hg pressure. The deuterium was obtained from the reaction of 99 percent deuterium oxide with metallic Ca in a vacuum. The BeD bands near 4990A were photographed in the third order of a 21-ft. concave grating in a stigmatic mounting, with a dispersion of 1.29A mm. Exposure times of 5 to 10 minutes with currents of 4 to 6 amperes were sufficient to produce intense spectrograms. The BeD^+ bands in the region 2200–3100A were photographed with a Hilger E-1 spectrograph in a Littrow mounting having a dispersion of 2.7A/mm at 2500A. Exposure times for the prism instrument were of the order of 1 to 4 minutes. Although the hydride spectra were present as an impurity on all spectrograms, the hydrogen coming from the hot electrodes and electrode mountings, they were much weaker than those of the corresponding deuteride spectra. The presence of the hydride system did not present any difficulties in the quantum assignments since the spacing of the lines for the hydride is nearly twice that for the deuteride.

BeD GREEN BANDS

It is well known that the green bands of BeH[9, 12, 13, 14] at 4990A belong to a $^2\Pi \rightarrow {}^2\Sigma$ transition and that the system consists almost entirely of a few bands in the $\Delta v = 0$ sequence, the origin of the 1,1 band being very close to that of the 0,0 band. The $^2\Pi$ state can be described as Hund's case *b*, since the ratio $A/B = 0.191$ for this state. Only a few of the rotational lines near the origin show a detectable spin doubling due to the $^2\Pi$ level, while the spin doubling for the lower $^2\Sigma$ state is negligible. This means that the bands have the appearance of $^1\Pi \rightarrow {}^1\Sigma$ bands with only three branches, and that the equations for a $^1\Pi \rightarrow {}^1\Sigma$ transition may be used instead of the more complicated ones for $^2\Pi \rightarrow {}^2\Sigma$ bands which have appreciable spin multiplet separations.

Fig. 1 is a spectrogram of the BeD green bands. The strong head is that of the *Q* branch of the 0,0 band, while the weak head on the long wave-length side is that of the *Q* branch of the corresponding BeH 0,0 band. Because of the much smaller spacing of the lines in the deuteride spectra, the *P* and *R* branches belonging to the hydride can easily be distinguished from

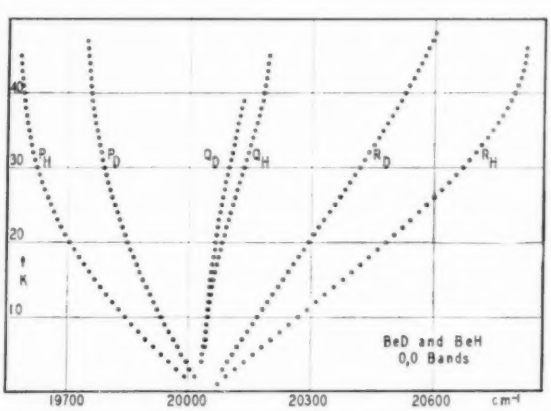

FIG. 2. Fortrat diagram of BeD green bands.

those of the deuteride. Fig. 2 is a Fortrat diagram comparing the 0,0 bands for BeD and BeH. This shows the Q branches rising very rapidly with the P and R branches extending out to either side. The upward curve of the R branches has been attributed to rotational distortion.

Rotational Constants

The assignment of frequencies to the P, Q, and R branches of the 0,0 and 1,1 bands is given in Table I. The usual combination differences may be obtained from Table I in the customary manner by means of the relations

$$\begin{aligned} R(K-1)-P(K+1)&=\Delta_2F''(K),\\ R(K)-Q(K+1)&=\Delta_1F''(K+\tfrac{1}{2})+Z_{K+1},\\ Q(K)-P(K+1)&=\Delta_1F''(K+\tfrac{1}{2})-Z_K \end{aligned} \quad (1)$$

for the lower state, and the equations

$$\begin{aligned} R(K)-P(K)&=\Delta_2F_d'(K),\\ R(K)-Q(K)&=\Delta_1F_e'(K+\tfrac{1}{2})+Z_{K+1}\\ &=\Delta_1F_d'(K+\tfrac{1}{2})+Z_K,\\ Q(K+1)-P(K+1)&=\Delta_1F_e'(K+\tfrac{1}{2})-Z_K\\ &=\Delta_1F_d'(K+\tfrac{1}{2})-Z_{K+1} \end{aligned} \quad (2)$$

for the upper state, where Z_K represents the Λ doubling of the $^2\Pi$ state. The expressions for ΔF are easily shown to have the well-known form

$$\Delta_2F(K)=(4K+2)\{B_v+2D_v(K^2+K+1)+F_v(3K^4+6K^3+13K^2+10K+4)\}$$

and

$$\Delta_1F(K+\tfrac{1}{2})=(2K+2)\{B_v+2D_v(K^2+2K+1)+F_v(3K^4+12K^3+19K^2+14K+4)\}.$$

Table I. *Rotational assignments for BeD bands.*

K	0,0 Band P	Q	R	1,1 Band P	Q	R
1						
2	20015.82			20032.02		
3	004.72		20083.65	021.87		
4	19993.92		095.86	011.18		
5	983.31		107.71	000.74		20122.01
6	972.66	20040.51	119.97	19990.44	20056.00	134.16
7	962.46	041.54	132.08	980.25	057.43	146.08
8	952.45	042.60	144.57	970.36	058.29	157.85
9	942.67	043.84	156.89	960.62	059.46	169.85
10	933.05	045.17	169.25	951.16	060.67	181.72
11	923.73	046.64	181.72	941.82	061.94	193.65
12	914.47	048.29	194.32	932.63	063.21	205.76
13	905.50	050.07	206.85	923.73	064.86	217.81
14	896.83	051.92	219.38	915.11	066.45	229.86
15	888.33	053.92	232.06	906.57	068.39	241.92
16	880.07	056.00	244.65	898.31	070.17	253.99
17	872.01	058.29	257.04	890.20	071.95	266.55
18	864.25	060.67	269.99	882.33	074.04	278.08
19	856.72	063.21	282.63	874.67	076.04	289.99
20	849.41	065.76	295.19	867.30	078.81	302.06
21	842.49	068.39	307.78	860.18	080.53	313.95
22	835.69	071.26	320.38	853.17	082.99	325.92
23	829.18	074.04	332.89	846.50	085.57	337.64
24	822.99	077.28	345.26	840.10	087.99	349.26
25	816.86	080.53	357.70	833.85	090.37	360.93
26	811.29	083.65	370.02	827.84		372.44
27	805.71	086.91	382.29	822.11		383.84
28	800.58	090.37	394.39	816.43		395.17
29	795.68	093.67	406.53	810.77		406.53
30	790.92	097.38	418.45	805.71		417.31
31	786.45	101.02	430.38	800.58		428.21
32	782.33	104.63	441.93			438.89
33	778.48	108.67	453.57			449.48
34	774.72	112.31	465.04			459.79
35	771.22	116.12	476.29			470.02
36	768.13	119.97	487.40			480.02
37	765.17	124.04	498.22			489.76
38	762.44	127.98	509.07			499.32
39	759.94	132.08	519.65			508.51
40	757.67		529.95			517.59

The rotational constants B, D, and F for the lower state are evaluated in the usual semi-graphical manner:

(1) The experimental values for $\Delta_2F(K)/(4K+2)$ are plotted against K, using a large scale.

(2) The expression for $\Delta_2F(K)/(4K+2)$ is applied successively to any three points on the curve. The resulting equations are solved simultaneously for the desired constants.

The points are chosen in the region $K=8$ to $K=25$ to eliminate error due to fluctuations of the experimental points for low K values, and the influence of a fourth constant which is effective only for high values of K. An average of ten such determinations for each value gives $B_0''=5.6198\pm0.0004$ and $B_1''=5.4980\pm0.0002$. Using the relation $B_e=B_v+\alpha(v+\frac{1}{2})$ and the above values of B_0 and B_1, one finds $\alpha=0.1218$ and $B_e''=5.6807$. The resulting constants are given in Table II.

Table II. *Rotational constants for BeD bands.*

Lower $^2\Sigma$ state	Upper $^2\pi$ state
$B_0^*=5.6198$	$B_{0e}^*=5.6926$
$B_1^*=5.4980$	$B_{0d}^*=5.6937$
	$B_{1d}^*=5.5623$
$D_0=-3.074\times10^{-4}$	$D_0=-3.169\times10^{-4}$
$D_1=-3.204\times10^{-4}$	$D_1=-3.255\times10^{-4}$
$F_0=1.29\times10^{-6}$	$F_0=1.40\times10^{-6}$
$F_1=2.79\times10^{-6}$	$F_1=2.58\times10^{-6}$
$\alpha=0.1218$	$\alpha_d=0.1314$
$B_e^*=5.6198+\frac{1}{2}\alpha=5.6807$	$B_e^*=5.6926+\frac{1}{2}\alpha=5.7583$

The upper state rotational constants may be obtained in a similar manner if the Λ doubling Z_K is evaluated and substituted into Eqs. (2).

TABLE III. *Rotational assignments for BeD^+ bands.*

J	R	P	J	R	P	J	R	P	J	R	P
	0,1 BAND			0,2 BAND			0,3 BAND			3,0 BAND	
0	37550.20		0			0			0		
1		37529.09	1			1		34455.73	1		42313.52
2		37513.65	2		35954.15	2		34441.72	2		42296.95
3	37552.93	37494.62	3		35936.50	3		34424.09	3		42276.09
4	37543.61	37471.76	4		35914.50	4		34403.67	4		42252.02
5	37532.29	37446.69	5		35889.95	5	34465.20	34380.62	5		42222.33
6	37519.22	37416.72	6	35963.85	35862.04	6	34455.73	34354.40	6	42287.04	42189.84
7	37501.00	37383.21	7	35947.73	35830.76	7	34441.72	34324.08	7	42265.76	42152.75
8	37479.23	37346.76	8	35928.98	35796.27	8	34424.09	34291.86	8	42237.77	42111.80
9	37454.41	37306.10	9	35907.04	35760.61	9	34403.67	34256.89	9	42206.18	42066.23
10	37426.05	37262.04	10	35880.64	35717.46	10	34380.62	34217.95	10	42172.38	42016.80
11	37393.88	37214.85	11	35851.66	35672.47	11	34354.40	34174.93	11	42134.19	41963.07
12	37358.10	37164.15	12	35818.39	35624.75	12	34324.08	34131.09	12	42089.86	41905.15
13	37319.03	37109.90	13	35783.82	35574.30	13	34291.86	34083.46	13	42043.07	41843.49
14	37276.90	37052.36	14	35744.51	35520.63	14	34256.89	34033.46	14	41990.52	41777.78
15	37230.03	36991.60	15	35702.56	35463.61	15	34217.95	33980.94	15	41936.81	41708.30
16	37180.98	36927.98	16	35656.87	35403.59	16	34174.93	33925.22	16	41876.33	41634.88
17	37127.77	36860.30	17	35608.58	35340.71	17	34132.23	33865.81	17	41812.82	41557.71
18	37072.99	36790.09	18	35556.66	35274.92	18	34088.14	33804.50	18	41745.64	41476.42
19	37012.08	36715.85	19	35501.99	35206.24	19	34039.53	33741.27	19	41673.73	41391.61
20	36949.71	36639.67	20	35442.68	35134.18	20	33985.42	33674.72	20	41598.60	41303.39
21	36882.83	36559.46	21	35383.25	35060.05	21	33929.59	33605.99	21	41519.37	41211.39
22	36813.76	36476.53	22	35319.48	34982.95	22	33872.06	33535.04	22	41436.77	41115.19
23	36741.21	36392.43	23	35253.60	34903.22	23	33811.24	33460.63	23	41350.60	41015.91
24	36665.39	36301.61	24	35183.82	34820.77	24	33748.21	33385.56	24	41260.10	40912.36
25	36587.19	36210.27	25	35112.06	34735.98	25	33681.99	33305.87	25	41166.35	40807.12
26	36505.16	36115.95	26	35036.82	34647.23	26	33614.20	33225.66	26	41069.21	40697.16
27	36421.59	36019.46	27	34959.64	34557.97	27	33545.77	33139.07	27	40969.39	40584.78
28	36334.24	35919.48	28	34880.06	34464.91	28	33471.64		28	40863.73	40468.86
29	36243.79	35818.39	29	34797.55	34370.99	29	33395.00		29	40755.50	40349.17
30	36150.94	35712.38	30	34712.07					30	40645.18	40227.73
31	36056.63	35608.57	31	34623.86					31	40528.61	40100.95
32	35963.85		32	34533.71					32	40411.32	39969.69
33	35862.04		33	34441.48					33	40290.22	
34	35760.61		34	34347.38							
35	35656.87										

	2,0 BAND			3,2 BAND			1,1 BAND	
0			0			0		
1			1			1		38608.58
2		41254.95	2	39172.22	39134.47	2		38593.67
3		41234.91	3	39168.29	39115.99	3	38629.83	38575.52
4	41279.83	41211.39	4		39094.34	4	38620.26	38552.64
5	41267.07	41183.05	5	39150.02	39067.79	5	38608.58	38524.13
6	41249.67	41150.30	6	39135.25	39038.15	6	38593.67	
7	41228.26	41115.19	7	39116.48	39004.32	7	38575.52	38458.69
8	41203.04	41073.94	8	39094.34	38967.62	8	38552.64	38422.02
9	41173.34	41029.35	9	39067.79	38927.10	9	38527.26	38380.33
10	41139.61	40981.14	10	39038.15	38882.50	10	38497.34	38335.98
11	41102.31	40928.34	11	39004.32	38834.40	11		38287.36
12	41060.79	40872.31	12	38967.62	38783.12	12	38426.41	38235.08
13	41015.91	40812.15	13	38927.10	38728.59	13	38385.97	38180.25
14	40965.20	40747.83	14	38882.50	38669.58	14	38342.94	38121.19
15	40912.36	40679.18	15	38834.40	38608.58	15	38293.66	38058.42
16	40853.79	40608.30	16	38783.12	38542.86	16	38241.90	37992.60
17	40792.60	40532.71	17	38728.59	38474.08	17	38187.15	37923.77
18	40727.38	40453.52	18	38669.58	38402.68	18	38129.33	37851.32
19	40658.36	40370.77	19	38608.58	38327.84	19	38067.16	37774.80
20	40584.78	40283.61	20	38542.86	38246.86	20	38000.76	
21	40508.65	40195.35	21	38474.08	38167.60	21	37933.09	
22	40426.47	40100.95	22	38402.68	38083.08	22	37860.62	
23	40344.41	40004.07	23	38327.84	37995.82	23	37786.33	
24	40257.18	39903.86	24	38246.86	37904.50			
25	40165.71	39800.03	25	38167.60	37810.48			

According to Mulliken and Christy,[15] the B_v's in the expression for the rotational energy term for the $^2\Pi$ state represent a more complicated expression than that which the usual B_v signifies and they should be designated as B_v^*. The B_v's should carry the subscript d or c to indicate the side of the Λ doublet to which they belong. The constants for the $^2\Pi$ state are given in Table II. Of course the B_v constants resulting from this analysis of the lower $^2\Sigma$ state are also B^* values,[15] and we therefore place a superscript (*) on all these constants in Table II.

[15] R. S. Mulliken and A. Christy, Phys. Rev. **38**, 87 (1931).

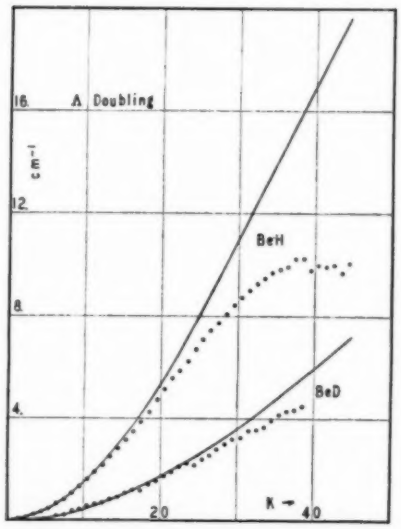

FIG. 3. Λ doubling of $^2\Pi$ state of BeD.

The importance of this in connection with isotope effect theory we shall mention in the last section.

Λ Doubling

The doubling of each rotational level, known as Λ doubling, is attributed to a difference of energy resulting from Λ being parallel or anti-parallel to the electric field along the internuclear axis when a magnetic field due to rotation is present. This doubling is zero for Σ states but is appreciable for Π states. For a case *b*Π state Mulliken and Christy[15] express this doubling as

$$\Delta\nu_{dc}(K)=qK(K+1).$$

If allowance is made for rotational stretching, the coefficient q should change with K. Thus

$$q=q_0/[1+u^2K(K+1)]^2.$$

where $u^2=-D_e/B_e$, and q_0 is the value of q for low values of K. Fig. 3 shows the Λ doubling curves for both BeD and BeH. In this figure the points represent experimental values while the solid lines are drawn according to the above expressions. The experimental values for $\Delta\nu_{dc}$ for BeH are the average values from data of Watson[9] and Olsson.[14] Values of $q_0=0.014$ for BeH from Mulliken and Christy and $q_0=0.0043$ for BeD are used. The deviation at high K values of the experimental points from the theoretical curve is well known for BeH and is probably due to failure of the simple relation from which the expression for q was derived. Since the theoretical expression for q_0 contains B_e^2, the transformation ratio for the two isotopic molecules should be equal to ρ^4. The ratio of the above values of q_0 does equal ρ^4 to within the accuracy with which the values can be determined.

Ultraviolet BeD^+ Bands

In contrast to the BeH system, which consists chiefly of a strong $\Delta v=0$ sequence with the band origins of the sequence very closely spaced—indicating a very narrow Condon parabola and a small change in ω_e for the two states—the $^1\Sigma-{}^1\Sigma$ BeH^+ system has no long sequences and its strongest bands form a wide Condon parabola. The ω_e values are 1476.1 and 2220.0 cm^{-1}, respectively, for the excited and the ground states. The individual bands, which consist of only two branches, do not form prominent heads since the R branches turn at very low quantum numbers. The appearance of the BeD^+ bands is very similar to that of the BeH^+ system except for a smaller pattern both for the distribution of the band origins and for the spacing of the lines within a band.

Rotational Analyses

The rotational constants B and D were evaluated in the manner described in the case of the BeD bands. Since no prominent heads are formed, some difficulty was experienced in locating the branches. Table III gives the quantum assignments for seven bands. Table IV gives the results of the rotational analyses. A comparison of the B_e values for the isotopic molecules will be made in a later section.

TABLE IV. *Rotational constants for BeD^+ bands.*

	Lower $^1\Sigma$ state		Upper $^1\Sigma$ state	
	B	D	B	D
0	5.8930	−0.0002912	3.9423	−0.0001913
1	5.7714	2986	3.8860	1877
2	5.6464	3036	3.8267	1829
3	5.5038	2783	3.7633	1892
	$\alpha=0.1233$		$\alpha=0.0578$	
	$B_e^*=5.9546$		$B_e^*=3.9712$	

TABLE V. *$v'-v''$ diagram of band origins, * denotes BeD$^+$ others are BeH$^+$.*

$v'v''\rightarrow$ ↓	0	1	2	3	4
		37540.30*	35980.80*	34465.89*	
0	39051.4	31911.5	34852.5	32875.3	
		38619.33*			
1	40496.4			34320.4	32426.9
	41282.76*				
2	41908.3				
	42323.95*		39161.67*		
3	43284.5				
4	44621.7				

VIBRATIONAL ANALYSIS

In order to find the vibrational constants ω_e, $x_e\omega_e$, and $y_e\omega_e$ for both states, it is necessary to determine the origin of each band with all possible accuarcy. Of several methods tried, the most satisfactory one consisted in the application, for example, of the equation of the P branch to an individual line in this branch, using the previously determined values for the B's and D's. This equation was then solved for ν_0. The final value given is the average of ten or more such determinations from the P branch and of a similar set obtained from the R branch. Table V gives a $v'-v''$ table of band origins for BeH$^+$ as given by Bengtsson[10] and for BeD$^+$ as found by the above method, the latter being designated by an asterisk. Bengtsson showed that the constant $y_e\omega_e$ should be included in the vibrational expression for both the lower and upper states of BeH$^+$. If we include these constants for BeD$^+$, it means that we have to evaluate seven constants ν_e, ω_e', $x_e'\omega_e'$, $y_e'\omega_e'$, ω_e'', $x_e''\omega_e''$, and $y_e''\omega_e''$, from seven equations, and that we have no other bands with which to check the result. But Bengtsson's values for the $y_e\omega_e$ constants are not large:

$$y_e'\omega_e' = 0.40 \quad \text{and} \quad y_e''\omega_e'' = 0.15.$$

According to simple isotope theory the transformation ratio of this constant for the two molecules should be ρ^3, which is approximately equal to 0.4087 as calculated from the ratio of the reduced masses. Assuming this transformation ratio to hold exactly, $y_e'\omega_e' = 0.16$ and $y_e''\omega_e'' = 0.06$ for BeD$^+$. On evaluating the remaining constants in the usual way, the vibrational equation is found to be

$$\nu_e = 39416.2 + 1096.4(v'+\tfrac{1}{2}) - 8.5(v'+\tfrac{1}{2})^2 - 0.16(v'+\tfrac{1}{2})^3 - [1647.6(v''+\tfrac{1}{2}) - 21.9(v''+\tfrac{1}{2})^2 - 0.06(v''+\tfrac{1}{2})^3].$$

The corresponding equation for BeH$^+$ as given by Bengtsson[10] is

$$\nu_e = 39417.0 + 1476.1(v'+\tfrac{1}{2}) - 14.8(v'+\tfrac{1}{2})^2 - 0.4(v'+\tfrac{1}{2})^3 - [2220.0(v''+\tfrac{1}{2}) - 39.8(v''+\tfrac{1}{2})^2 - 0.15(v''+\tfrac{1}{2})^3].$$

TABLE VI. *Comparison of vibrational constants.*

	BeH	TRANSFORMATION RATIO	BeD$^+$ CALCULATED	BeD$^+$ EXPERIMENTAL
ν_e	39417.0			39416.2
ω_e'	1476.1	ρ	1095.43	1096.41
$x_e'\omega_e'$	14.8	ρ^2	8.15	8.49
ω_e''	2220.0	ρ	1647.49	1647.64
$x_e''\omega_e''$	39.8	ρ^2	21.92	21.85

Table VI gives a comparison of the vibrational constants for BeH$^+$ with the experimental values for BeD$^+$ and with the calculated values for BeD$^+$ as determined by means of simple isotope theory. The difference in the values of the ν_e for the two isotopic molecules BeH$^+$ and BeD$^+$ indicates a shift of the system origin of about 0.8 cm^{-1}. An explanation of the so-called electronic isotope shifts has been given recently by Dieke[16] as arising from certain terms of the complete Hamiltonian which are usually neglected. On account of the comparatively large B_e values for the BeD$^+$ and BeH$^+$ molecules, that part of these perturbation terms which involves the reaction of the nuclei to the precession of the electronic angular momentum about the internuclear axis would contribute an electronic isotope shift of about 6 cm^{-1} if a $p\Sigma$ state is involved. Since the electronic configuration for the upper state involved is $(2s\sigma)(2p\sigma)$, the lower state being $(2s\sigma)^2$, the smallness of the observed shift is puzzling. It is possibly to be attributed to a like contribution of the opposite sign from the $\partial^2\phi/\partial r^2$ term.

[16] G. H. Dieke, Phys. Rev. **47**, 661 (1935).

Comparison of B_e Constants with Mass Ratios

Simple isotope theory predicts that the ratio of the B_e constants for the isotopic molecules should be exactly equal to ρ^2, the ratio of the reduced masses. With Olsson's[14] value $B_e = 10.308$ for the ground state of BeH and the above value $B_e = 5.6807$ for BeD, the ratio is 0.55110. Although there is some uncertainty in the proper method of calculating ρ^2,[6] the use of atomic weights H = 1.0081, D = 2.0148, Be = 9.0155 gives $\rho^2 = 0.55060$. (The use of the old atomic masses of hydrogen and deuterium increases this value slightly.) Thus the ratio of the B_e constants exceeds ρ^2 by 0.09 percent, the discrepancy being larger than the experimental error.

A possible explanation of this discrepancy which should be considered is the correction to B_e given by J. L. Dunham[17] in his extended treatment of the rotating vibrator. With his notation, the corrected value is $Y_{01} = B_e[1 - 0.00015]$ for BeH. This correction cannot be calculated exactly for BeD without the analysis of at least one additional band, but an approximate solution gives $Y_{01} = B_e[1 - 0.00008]$. The ratio of the corrected B_e values is 0.55110. Apparently the discrepancy can be only partially explained in this way.

It should be recalled that these B values are really B^* values, differing from the true B_v values by uncoupling terms arising from the interaction with certain other states of the molecule. Mulliken and Christy[15] have shown that the two electronic states involved in these BeH bands interact almost solely with each other. Assuming this interaction to be exactly that of "pure precession," the true B_e values may be calculated[3] with the relation $B^* - B_v = -2B_v^2 l \times (l+1)/\nu(\Pi, \Sigma)$. With the known Λ doubling values, however, this correction makes $B_e = 10.3237$ for the normal state of BeH, while for BeD the correction is smaller, so that $B_e = 5.6855$. The ratio of these two B_e's is 0.55072, a value fairly close to that for the ratio of the reduced masses. Since inclusion of these uncoupling terms in order to get true B_e values for the B states of CaH and CaD has been shown by Watson[3] to give similarly near equality of the ratio of the B's and ρ^2, it may be that this effect is responsible for the largest part of the discrepancy between these ratios for all corresponding diatomic hydride and deuteride molecules.

With Bengtsson's[10] value $B_e^* = 10.813$ for the ground state of BeH^+ and the above value $B_e^* = 5.9546$ for BeD^+, the ratio is 0.55073. This is but very slightly larger, about 0.02 percent, than the value of ρ^2. It is to be noted that the discrepancy is much less for the ionized molecule than for the neutral molecule. An adequate explanation of the discrepancy should account for this fact. Kronig's recent treatment of the diatomic molecule including certain terms in the Hamiltonian of the diatomic molecule which are usually omitted, predicts a variation between the ratio of the B_e's and ρ^2 if the united atom has an L value different from 0, the amount of the variation being dependent upon L. Since the L value of the united atom for BeD^+ is 0, while that for BeD is 1, the experimental results are in accordance with his theory. The upper state constants are not compared because of the probable larger influence of nearby levels as discussed by Kronig.

The author wishes to express his appreciation to Professor W. W. Watson, who suggested the problem, for his interest and for many helpful discussions.

[17] J. L. Dunham, Phys. Rev. **41**, 721 (1932).

The Far Ultraviolet Absorption Spectrum of Oxygen

W. C. PRICE AND GEORGE COLLINS, *Rowland Physical Laboratory, The Johns Hopkins University*

(Received August 8, 1935)

The far ultraviolet absorption spectrum of oxygen has been photographed under high dispersion in the region 1300–650A. The bands are explained as going to the various excited states of O_2^+ as limits and are attributed to the removal of $v\pi$, $\omega\pi$ and $x\sigma$ electrons, respectively, from the normal state of O_2. The results strongly support Mulliken's assignment of the visible O_2^+ bands to the transition $^4\Sigma_g^- \rightarrow {}^4\Pi_u$. The distances of the $^4\Pi_u$ and $^4\Sigma_g^-$ states of O_2^+ from the ground state of O_2 are given as 16.1 and 18.2 volts, respectively, with possible errors of about a tenth of a volt. The appearance and nonappearance of strong electronic series going to known ionization potentials are also discussed.

THE ultraviolet absorption spectrum of oxygen begins with the Schumann-Runge bands.[1] Under normal conditions these start around 1970A and extend toward shorter wave-lengths until they are concealed by a strong continuous absorption. The intensity of this absorption diminishes to zero at about 1350A. Below this there is a system of absorption bands extending from 1250A which are evident only when relatively high pressures of O_2 are used. On the short wave-length side of this system are the Hopfield bands[2] which extend down to 680A. Unfortunately no emission bands of O_2 are known in the ultraviolet. The authors and others have tried several methods to obtain the Hopfield bands in emission, but without success. It is therefore very desirable to work out the absorption spectrum of O_2 as completely as possible. The original photographs of Hopfield were probably not taken under sufficiently high dispersion to allow a good analysis to be made. The work was therefore repeated under much higher dispersion, the Lyman continuum being used as a source of continuous radiation.

The instrument used was a two-meter grazing incidence vacuum spectrograph having a dispersion of about 2A/mm in the region 1200–600A. The discharge tube and the methods of obtaining the spectra have been described in a previous article.[3] The Hopfield bands in oxygen appear at such extremely low pressures that it was found convenient when taking the low pressure pictures to use a mixture of oxygen and helium in order that a sufficient pressure for the satisfactory operation of the discharge tube could be obtained. The helium was originally purified by passing it over charcoal cooled with liquid air. Mixtures varying from one to ten parts of oxygen in a hundred parts of helium were used to obtain plates at different pressures. The mixture was admitted into the spectrograph through the discharge tube by means of a fine capillary. It was pumped out continuously through the main pumps. The conditions were such that the partial pressures of oxygen varied from about 0.01 mm to 0.001 mm and the length of the absorbing path was about 1.5 meters. To obtain the absorption bands above 1000A, oxygen was admitted without dilution at a pressure of about 0.1 mm.

The photographs obtained as described above are shown in Fig. 1. A comparison of this absorption spectrum with those of N_2 and H_2O in the same region showed that no bands due to these possible impurities were present in appreciable amounts. It was found, however, that excited oxygen was always present in small quantities in the spectrograph, as strips of polished copper introduced into the instrument became tarnished in the course of an exposure. However, control experiments showed that none of the absorption bands which are reported here could be attributed to absorption in such excited molecules.

The emission spectrum of H_2[4] is a convenient comparison spectrum for the wave-length determination of the bands above 1000A. For the bands below 1000A emission lines in the continuum which were identified as due to highly

[1] S. W. Leifson, Astrophys. J. **63**, 73 (1926).
[2] J. J. Hopfield, Astrophys. J. **72**, 133 (1930).
[3] G. B. Collins and W. C. Price, Rev. Sci. Inst. **5**, 423 (1934).
[4] H. H. Hyman, Phys. Rev. **36**, 187 (1930).

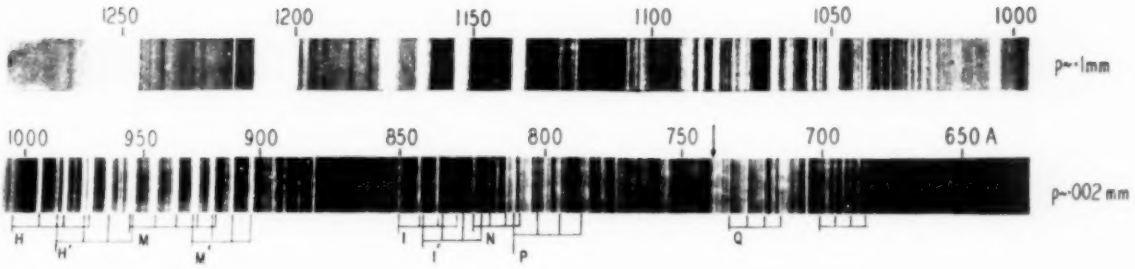

FIG. 1. The far ultraviolet absorption spectrum of oxygen.

ionized states of O and N were used as standards, their wave-lengths being taken from Edlén.[5] The accuracy of the measurements on the sharp bands is probably such that their frequencies can be given to within ± 5 cm^{-1}. The errors in the measurement of broad and diffuse bands and those which fall close to emission lines in the continuum are considerably greater than this. The inaccuracy of these determinations may be at first thought rather large, but it must be remembered that the factor $\Delta\nu/\Delta\lambda$ at 800A is about twenty-five times as great as it is around 4000A. A large number of plates taken under different conditions were measured and a reasonable average of the wave-lengths so obtained was taken.

BANDS ABOVE 1000A

It has been shown[6] that the far ultraviolet absorption spectra of a number of molecules consist of various electronic series, with or without vibrational patterns, which go to a limit agreeing fairly well with the ionization potention of the molecule as determined by electron impact. Some molecules show strong Rydberg series going to the minimum ionization potential, while others show strong series going to one or more higher ionization potentials, the series going to the minimum ionization potential being apparently very weak. Examples of the latter type are the far ultraviolet absorption spectra of O_2, NO, N_2 and CO. It can be said at least that the electronic series and ionization continua corresponding to the first ionization potentials of these molecules do not appear at the low pressures which are usually adequate to bring them out in other molecules (cp. C_2H_2, H_2S, CH_3I). The bands going to the other ionization potentials of these molecules, i.e., Hopfield's Rydberg series[7] in nitrogen and the shorter wave-length bands of oxygen to be discussed here exhibit more usual behavior. Without attempting any explanation of this, we wish to record here the empirical facts.

The bands in oxygen above 1000A come out at relatively high pressures (0.1 mm). They are of the character of electronic series going to a limit between 12 and 12.5 volts. The value 12.5 ± 0.1 volts is the first ionization potential of O_2 as obtained by electron impact.[8] A more exact value depending on the extrapolation over a very small range of the vibrational levels of the $^2\Pi_u$ excited state of O_2^+ to its heat of dissociation turns out to be 12.2 ± 0.1 volts.[9] Actually no bands of the long wave-length set we obtained were observed below 1018A (12.1 volts). The first bands in the region 1250–1200A are somewhat predissociated, probably due to the proximity of the potential curve of the $\sigma^2\pi^3\pi^3$, $^3\Sigma_u$ state or other predicted states. They are very strong and apparently not accompanied by any vibrations, which is in agreement with the fact that 'r' and 'ω' are not very greatly different for the ground states of O_2 and O_2^+. The shorter wave-length bands are very much weaker and

[5] B. Edlén, Zeits. f. Physik **85**, 85 (1933).
[6] R. S. Mulliken, Phys. Rev. **46**, 144 (1934); H. J. Henning, Ann. d. Physik **13**, 599 (1932); W. C. Price, Phys. Rev. **47**, 419, 444, 510, 788 (1935); J. Chem. Phys. **3**, 256, 365 (1935).
[7] J. J. Hopfield, Phys. Rev. **36**, 789A (1930).
[8] J. T. Tate and P. T. Smith, Phys. Rev. **39**, 270 (1932).
[9] R. S. Mulliken and D. S. Stevens, Phys. Rev. **44**, 720 (1933).

though they appear to converge to a limit $\sim 1015A \equiv 12.15$ volts, they could not be arranged in any Rydberg series. Even if it had been possible to do this, the intensities of the electronic series would have been very unusual, as the long wave-length bands are very much stronger than the shorter wave-length bands (i.e., the intensities fall off much more rapidly than for the electronic series going to an ionization continuum which have been observed in other molecules). No ionization continuum could be found for these bands though a slight weakening of the background was observed to extend from 1105A toward shorter wave-lengths (probably due to weak transitions to repulsion curves).

As the internuclear distance of the ground state of O_2^+ is less than that of O_2 one would expect bands going to the former state as a limit to be shaded toward the violet. This is only true of some of the bands we observe. Some are shaded toward the red and some are so narrow that it is difficult to say in what direction they are shaded.

A very similar situation occurs in NO. The bands which might be regarded as the first members of a set going to the minimum ionization potential were obtained by Leifson.[1] They are strong and form two good vibrational progressions for which 'ω' is not much different from that in the ground state. We have photographed the NO bands at shorter wave-lengths and found that the bands go to a limit which is close to the value 9.4 volts determined by electron impact. However, the upper members lose the simplicity of the lower ones. They suffer great diminutions in intensity and cannot be arranged in Rydberg series. Even at the highest pressure used (~ 0.3 mm) they do not give an ionization continuum.

Another example of what has been discussed above is nitrogen. The first ionization potential of nitrogen is accurately known to be about 15.55 volts[10] and thus one might expect a Rydberg series with an ionization continuum starting at 794A to appear in absorption (little vibrational structure would be expected as 'r' and 'ω' are not greatly different for the ground states of N_2 and N_2^+). This has not been found by Hopfield.[11] In more recent work by one of us (P) at higher pressures, a continuum has been found in this region but the bands going to it cannot be identified with the type of bands one would expect to approach the ground state of N_2^+. Their interpretation is as yet uncertain.

In CO as in NO the first few states are found fairly strongly with frequencies differing little from the ground state. Hopfield and Birge[12] have obtained the bands as far as 920A but do not get any higher series members. The absorption past the first ionization potential (14.1 volts $\equiv 875$A) has been done by Henning.[6] Discrete bands were found as far down as 783A and no continuum corresponding to the first ionization potential was observed. However, Henning reports evidence of a second ionization potential which is close to Mackay's[13] value of 15.6 volts for the second I.P. of CO.

While it is disappointing not to be able to get direct spectroscopic evidence of the first ionization potentials of the above molecules, it is considered important to point out the instances in which such evidence cannot be easily obtained.

Bands From 1000–650A

The Hopfield bands extend from a little above 1000A to as far down as 650A. The pressures at which they appear are so low that all the longer wave-length bands are practically entirely absent. They thus correspond to bands which have enormously high transition probabilities. They were found to consist of fairly short vibrational progressions having about four or five members. The various vibrational progressions are indicated in Fig. 1 and listed in Table I. There is a break in the absorption between 900 and 850A. The bands start again on the short wave-length side of this with diminished intensity. Around 800A the bands overlap so much that little can be done with them. This is exactly what one would expect if the bands were due to the vibrational progressions of various terms of an electronic series going to an ionization potential.

On the basis of evidence to be presented below the bands are interpreted as transitions

[10] R. S. Mulliken, Phys. Rev. **46**, 144 (1934).

[11] J. J. Hopfield, Phys. Rev. **36**, 789A (1930).

[12] J. J. Hopfield and R. T. Birge, Phys. Rev. **29**, 922A (1927).

[13] C. A. Mackay, Phys. Rev. **24**, 327 (1924).

TABLE I. *Table of frequencies of various progressions in the Hopfield bands in O_2.*

I	ν	$\Delta\nu$	I	ν	$\Delta\nu$	I	ν	$\Delta\nu$	I	ν	$\Delta\nu$
	H			*H'*			*N*			*N'*	
3	99630		4	101440		8	121064			——	
		1070			1090			899			
8	100700		8	2530		8	121963			——	
		1020			1050			867			
10	1720		10	3580		7	122830			——	
		1000			1010			830			
8	2820		7(b)	4590		4	123670			——	
	M			*M'*			*P*			*Q*	
8b	104470		8	107150		10	123330		8	136559	
		1030			1020			1340			1166
10	5500		9	8170		8(o)	4670		6	7725	
		1010			960			1290			1121
9	6510		8	9130		6	5960		4	8846	
		950			860			1250			1088
7	7460		6	9990		4	7210		2	9924	
		900									
3(o)	8360										
	I			*I'*			*V*			*W*	
3	117200		2	118500		4	142670		5	143300	
		1012			1030			1180			1150
5	8212		4	9530		4	3850		6	4450	
		983			990			1120			1100
6	9195		5	120540		3	4970		4	5550	
		950			970			1070			
4	120145		3	1510		2	6040				
					950						
			1	2460							

from the ground state of O_2 to upper electronic states which approach as limits the excited states of O_2^+. Two of these states can be identified as the upper and lower states of the visible bands of O_2^+. Their term values with respect to the ground state of O_2 are found here to be $\sim$18.2 volts and $\sim$16.1 volts with a probable error of 0.1 volt. It has not yet been possible to analyze the structure of the visible O_2^+ bands but Mulliken[14] has tentatively assigned them to the transition $^4\Sigma_g^- \rightarrow {}^4\Pi_u$ identifying the $^4\Pi_u$ state with the second ionization potential (16.1 volts) determined by electron impact. Our results are in complete agreement with this assignment.

The interpretation of the far ultraviolet absorption spectra of some molecules as going to excited states of the ion has already been applied by Mulliken[14] to Hopfield's Rydberg series in nitrogen which go to the well-known A', $^2\Sigma_u^+$ state of N_2^+ as a limit. The difference between these bands and the ones we shall describe is that while in N_2 each electronic state gives only one band ('r' and 'ω' are changed very little by the excitation), in oxygen each electronic state has a vibrational progression associated with it ('r' and 'ω' are changed very considerably by the excitation). Rathenau[15] has interpreted the far ultraviolet absorption spectra of CO_2 as going to excited states of CO_2^+, but no correlation with the emission bands of CO_2^+ has yet been made.

The data on the Hopfield bands in oxygen are given in Table I. The lettering scheme is such that bands in the groups $HIJ\cdots$, $MNO\cdots$, $PQR\cdots$ belong to Rydberg series approaching the limit characteristic of each particular group. On account of their similarity in vibrational frequencies, intensity distribution, appearance, etc., the progressions "H" and "I" are assigned to the same Rydberg series. If their first members are introduced into a Rydberg formula, the limit so obtained is $\sim$130,300 cm^{-1}. In the same way "H"' and "I"' are assigned to another Rydberg series which has a limit $\sim$131,400 cm^{-1}. This

[14] R. S. Mulliken, Rev. Mod. Phys. **4**, 56 (1932).

[15] G. Rathenau, Zeits. f. Physik **87**, 32 (1933).

agreement between the limits is considered fair in view of the uncertainty of the identification of the first members of the progressions and the possible departure of the electronic states from a Rydberg series. Their average, 130,800 cm^{-1}, corresponds to an ionization potential of 16.14 volts which is in good agreement with the value 16.1 volts obtained by Tate and Smith[8] by electron impact for the second ionization potential of oxygen.

The vibration frequencies of these bands approach that of the lower state of the visible bands of O_2^+. This is especially so in the "*I*" progression where incidentally the measurements are best. For this state ω_e turns out to be ~ 1042 cm^{-1} and $x_e\omega_e \sim 15$ cm^{-1} as compared with the values 1037.2 and 11.1 for O_2^+. Further the intensity distribution of the bands is approximately what one would expect for such a transition. The internuclear distance of normal O_2 is 1.204A. That of the lower state of the visible bands of O_2^+ is not accurately known but is probably ~ 1.4A. Thus one would expect the first band to be weak, the second and third somewhat stronger and subsequent members weaker. This is found to be the case. Under the dispersion used here the bands appear as doublets. The maxima of the two components are separated by about 75 cm^{-1}. The minima in between these is a very narrow region of transparency not more than a few wave numbers broad. All the members of the *A* and *B* systems were found to have this structure.

From the above it is indicated that the lower state of the visible O_2^+ bands has a term value ~ 16.1 volts with respect to the ground state of O_2. We shall later show that the bands approaching the upper state due to absorption from normal $^3\Sigma_g^-$, O_2 are single headed and go to a limit ~ 18.2 volts. The $\Delta V = 18.2 - 16.1 = 2.1$ volts agrees with the observed $\nu_e = 2.05$ volts of the visible bands of O_2^+. It thus appears that our results strongly support Mulliken's assignment of the transition $^4\Sigma_g^- \rightarrow {}^4\Pi_u$ to these bands.

With regard to the probable nature of the upper levels of the *H*, *I*, *J* series a few things may be said. The states which go to the state of O_2^+ should include $(^4\Pi_{\frac{1}{2}})nx$, $(^4\Pi_{\frac{1}{2}})nx$, $(^4\Pi_{3/2})nx$ and $(^4\Pi_{5/2})nx$ with probably $\Omega - s$ type coupling. If nx is $nx\sigma$ then the states would correspond to $^5\Pi$ and $^3\Pi$. The question of selection rules is rather complicated but transitions to some components of both states (all of $^3\Pi$) should occur.

Two other strong progressions *M* and *M'* were found in the bands between 1000 and 900A. These appear at somewhat shorter wave-lengths than the *HH'* progressions and have smaller values of 'ω.' They are of the same character as the *H*, *I*, *J*$\cdots$ bands having two components separated by a fine line. Only one of the "*N*" progressions could be found at shorter wave-lengths; *N'* is apparently lost in the confusion produced by the overlapping of a number of electronic states in the region 820–770A. By introducing *M* and *N* into a Rydberg formula one obtains 16.5 volts for the ionization potential of these bands. On account of the fact that the value of $\omega_e \sim 915$ cm^{-1} for *N* is close to that of the $^2\Pi_u$ state of O_2^+ ($\omega_e = 898.9$) it seems possible that the bands go to this state as a limit. From the ultraviolet bands of O_2^+ the $^2\Pi_u$ state is known to be 4.73 volts above the ground state of O_2^+. With the value of Mulliken and Stevens for the ionization potential of O_2, the distance of the $^2\Pi_u$ state of O_2^+ relative to the ground state of O_2 is $12.2 + 4.73 = 16.9$ volts. While the value 16.5 volts which we have obtained has a possible error of a few tenths of a volt, it is doubtful whether it could be raised as high as 16.9 volts. The other excited states of O_2^+ which are predicted in this region[16] can probably be ruled out as limits of our series since they are produced by the removal of a $w\pi$ electron from the metastable states $^1\Delta_g$ and $^1\Sigma_g^+$ of O_2. However it is conceivable that the excitation could be accompanied by an interval rearrangement of the $v\pi_g^2$ group. One could then get the ionic states $^2\Phi_u$, $^2\Pi_u$ (corresponding to the removal of one $w\pi_u$ from $\sigma_g^2\pi_u^4\pi_g^2$, $^1\Delta_g$) or the $^2\Pi_u$ corresponding to the removal of one electron from the $\sigma_g^2\pi_u^4\pi_g^2$, $^1\Sigma_g^+$ state. While the probability of such a process is small it cannot be entirely neglected.

In connection with the ionization potential of the *MNO* system we might look for an ionization continuum. Such a continuum is apparently found. It starts fairly sharply around 740A $\equiv$ 16.7 volts which seems close enough to our value of the ionization potential of this system to be

[16] R. S. Mulliken, Rev. Mod. Phys. **4**, 56 (1932).

identified with it. However, the possibility that the continuum is a dissociation continuum cannot be eliminated. If the latter is the case then the continuum may be explained as transitions to repulsion curves giving the same products of dissociation as the H or M systems.

A third set of bands Q appears in the continuum mentioned previously. These are quite sharp and good measurements could be made on them. They are single headed and are shaded toward the red. The values of $\omega_e \sim 1205$ cm^{-1} and $x_e\omega_e \sim 20$ cm^{-1} indicate that the electronic state is approaching the upper state of the visible O_2^+ bands for which $\omega_e = 1198.1$ cm^{-1} and $x_e\omega_e = 17.8$ cm^{-1}. As has been previously mentioned, Mulliken has tentatively designated this state as $^4\Sigma_g^-$. This is supported by the fact that the bands are single headed. The intensity distribution of the bands is different from that of the H and M bands. The first member of the progression is strongest and subsequent members become gradually weaker. This indicates that the internuclear distance of the excited state is not greatly different from the ground state of O_2.

A progression marked P which is very similar to the Q progression can be picked out at longer wave-lengths. The first band is strong single headed and shaded towards the red. It is very similar to the first band in the Q progression. Good measurements could not be made on the subsequent members of the progression as they are partially obscured by the overlapping in the region around 800A. Introducing P and Q into a Rydberg formula we obtain 18.25 volts as the ionization potential of the PQR system. This is probably a little too high, as ω_e and D are somewhat greater for the P progression than the Q progression.

The only predicted states of O_2^+ which are about 18 volts removed from the ground state of O_2 are the $\sigma_g\pi_u^4\pi_g^2$, $^4\Sigma_g^-$ and $^2\Sigma_g^-$ states. It thus seems reasonable that the $PQR\cdots$ bands are approaching one of these (probably $^4\Sigma_g^-$). The fact that ω_e and $x_e\omega_e$ for Q are close to their values in the upper state of the visible O_2^+ bands indicates that this state can probably be identified as the limit and thus it corresponds to the configuration $\sigma_g\pi_u^4\pi_g^2$, $^4\Sigma_g^-$.

Two other progressions labeled V and W were found in the region 700–670A. The analysis of these bands is uncertain. The bands in W appear to be double headed with the apparent exception of that at 144,450 cm^{-1}. A few strong isolated bands believed to belong to oxygen were found at 112,890, 122,350 and 141,820 cm^{-1}. The last band is extremely strong.

The configuration of normal O_2 is $\sigma_g^2\pi_u^4\pi_g^2$, $^3\Sigma_g^-$. The bands which go to the first ionization potential of O_2 are due to the excitation of a π_g electron. Those going to the excited Π states of O_2^+ are due to the excitation of a π_u electron and those going to the Σ states due to the excitation of a σ_g electron. Thus in the far ultraviolet absorption spectra of O_2 we have evidence of the excitation of all three types. Theoretically the low energy states of O_2^+ can be obtained in a very simple way by the removal of an electron from each of the outer orbits of O_2. This is apparently what actually happens in the far ultraviolet absorption spectra of oxygen.

While the data given in this paper are not as accurate as could be wished for, the authors believe it is the best that will be available for some time. The difficulties of working in this region are considerable and even with the high dispersion used here the $\Delta\nu/\Delta\lambda$ factor is so large that the accuracy of the measurements is limited considerably. However, it is significant that where the accuracy of the measurements is greatest (i.e., in the I, N and Q systems) the interpretation is followed most closely. The work yields very plausible term values for some of the electronic states of O_2^+ relative to the ground state of O_2. It also gives an insight into the nature of the far ultraviolet absorption spectra of molecules and their relations to the results of electron impact experiments. As this is a subject on which there is as yet little experimental data the work is considered valuable in this respect.

In conclusion the authors wish to thank Professor G. H. Dieke for his advice and encouragement and Professor R. S. Mulliken for much valuable criticism of the manuscript.

Deep Terms in the Isoelectronic Sequence V I to Cu VII

P. GERALD KRUGER, *Department of Physics, University of Illinois*
AND
HELEN T. GILROY, *Department of Physics, Cornell University*

(Received July 22, 1935)

By the use of constant second differences in the radiated frequencies from terms involving an electron transition to the ground state, it has been possible to identify the $3d^5\ {}^6S_{5/2}$ and $3d^4\ 4p\ {}^6P^\circ$ terms of this sequence. Ionization potentials cannot be computed because of the lack of completeness in the data on the first three members of the sequence.

THE spectra of this sequence have been studied previously by Helen T. Gilroy.[1] At that time certain lines in the Mn III, Fe IV and Co V spectra were classified as the $3d^5\ {}^6S_{5/2} - 3d^4\ 4p\ {}^6P^\circ_{7/2,\ 5/2,\ 3/2}$ transitions. It now appears that these classifications are wrong and that the ${}^6S_{5/2}$ term lies somewhat deeper than was previously reported.

The data, reported in this paper, on Mn III and Fe IV were obtained from spectrograms taken at Cornell University with a one and one-half meter normal incidence vacuum spectrograph; on Cr II, with a Rowland mounting grating. The wave-lengths for Cr II agree with those previously reported by Russell,[2] C. E. Moore[3] and others. For Co V, Ni VI and Cu VII the lines have been photographed with a twenty-one foot grazing incidence vacuum spectrograph at the University of Illinois.[4] A hot spark previously described[5] was used as the light source. Pure metals of Co, Ni and Cu were used as electrodes and the length of exposure varied from one to two hours.

In all members of this sequence except V I the deepest term is $3d^5\ {}^6S_{5/2}$ which combines strongly with $3d^4\ 4p\ {}^6P^\circ$ to give three very strong and characteristic lines which can be followed down the sequence readily. These lines were recognized as part of an isoelectronic sequence, on the spectrograms of Co, Ni and Cu because they appeared with other characteristic groups of lines on all these spectrograms, in such a way that the group arrangement on one spectrogram (Co) was exactly reproduced on another spectrogram (Ni) at shorter wave-lengths. The three strongest lines, forming what appeared to be a triplet, were picked out and plotted on a graph like that in Fig. 1. The graph was then extrapolated to Fe and the corresponding three lines found within 500 cm^{-1} of the predicted wave-length. A further extrapolation to Mn and Cr showed that the corresponding three lines in Cr were the $3d^5\ {}^6S_{5/2} - 3d^4\ 4p\ {}^6P^\circ$ of Cr II as classified by Russell.[2] This fixed the identity of the other lines of the sequence, as being the corresponding transitions in the more highly ionized ions. An extrapolation to V I predicts the corresponding radiation to be approximately 3000 cm^{-1}. Thus it is quite understandable that it has not been observed.

Table I gives the radiated frequencies of these lines and the first and second differences. The second differences of this table are compared with the second differences in other sequences involving similar electron configurations, in Table II.

The classified lines are given in Table III. Since these radiations are caused by transitions to the ground state, the values of ν in cm^{-1} in

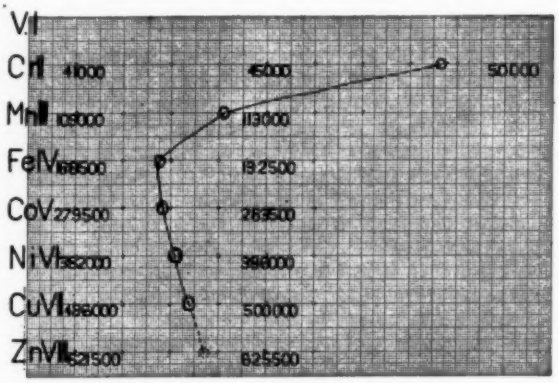

FIG. 1. Radiated frequencies, cm^{-1}, $3d^5\ {}^6S_{5/2} - 3d^4\ 4p\ {}^6P^\circ_{7/2}$

[1] Gilroy, Phys. Rev. **38**, 2217 (1931).
[2] Russell, Astrophys. J. **66**, 184 (1927).
[3] Moore, *Term Designations for Excitation Potentials*, Princeton University Observatory Publication (1934).
[4] Kruger, Rev. Sci. Inst. **4**, 128 (1933).
[5] Kruger and Shoupp, Phys. Rev. **46**, 124 (1934).

TABLE I. *Radiated frequencies (cm^{-1}) with first and second differences.*

ELEMENTS OF THE SEQUENCE	$3d^5\,{}^6S_{5/2}-3d^4\,4p\,{}^6P^\circ_{7/2}$	FIRST DIFFERENCE	SECOND DIFFERENCE
V I	(3,000)		
		(45,500)	
Cr II	48,633		(18,000)
		63,425	
Mn III	112,058		14,747
		78,172	
Fe IV	190,230		12,873
		91,045	
Co V	281,275		11,781
		102,826	
Ni VI	384,101		11,416
		114,242	
Cu VII	498,343		(11,500)
		(125,740)	
Zn VIII	(624,080)		

TABLE II. *Comparison of second differences.*

FIRST MEMBER OF THE ISOELECTRONIC SEQUENCE	ELECTRON CONFIGURATIONS	APPROXIMATE VALUE OF SECOND DIFFERENCE
Ne I	$2p^6-3p^53s$	30,000 cm^{-1}
Cl I	$3p^5-3p^44s$	11,000 cm^{-1}
A I	$3p^6-3p^54s$	11,000 cm^{-1}
K I	$3d\ -4p$	11,000 cm^{-1}
V I	$3d^5-3d^44p$	3,500 cm^{-1} [1]
		(new) 11,500 cm^{-1}
Ni I	$3d^{10}-3d^94p$	11,000 cm^{-1}
Pd I	$4d^{10}-4d^95p$	7,100 cm^{-1}

TABLE III. *Observed lines from transition to the deepest term in ions of the isoelectronic sequence V I to Cu VII.*

ELEMENTS OF THE SEQUENCE	INT.	λ (vac.)	$\nu(cm^{-1})$	COMBINATIONS $3d^5\,{}^6S_{5/2}-3d^4\,4p\,{}^6P^\circ$
V I		(33,330 A)	(3,000)	${}^6S_{5/2}-{}^6P^\circ_{7/2}$
		(34,610 A)	(2,889)	${}^6S_{5/2}-{}^6P^\circ_{5/2}$
		(35,600 A)	(2,809)	${}^6S_{5/2}-{}^6P^\circ_{3/2}$
Cr II	90	2,056.22	48,633	${}^6S_{5/2}-{}^6P^\circ_{7/2}$
	80	2,062.20	48,492	${}^6S_{5/2}-{}^6P^\circ_{5/2}$
	70	2,066.12	48,400	${}^6S_{5/2}-{}^6P^\circ_{3/2}$
Mn III	45	892.39	112,058	${}^6S_{5/2}-{}^6P^\circ_{7/2}$
	35	893.75	111,888	${}^6S_{5/2}-{}^6P^\circ_{5/2}$
	25	894.65	111,775	${}^6S_{5/2}-{}^6P^\circ_{3/2}$
Fe IV	100	525.68	190,230	${}^6S_{5/2}-{}^6P^\circ_{7/2}$
	75	526.28	190,013	${}^6S_{5/2}-{}^6P^\circ_{5/2}$
	60	526.60	189,897	${}^6S_{5/2}-{}^6P^\circ_{3/2}$
Co V	20	355.523	281,275	${}^6S_{5/2}-{}^6P^\circ_{7/2}$
	18	355.876	280,996	${}^6S_{5/2}-{}^6P^\circ_{5/2}$
	12	356.060	280,851	${}^6S_{5/2}-{}^6P^\circ_{3/2}$
Ni VI	400	260.348	384,101	${}^6S_{5/2}-{}^6P^\circ_{7/2}$
	300	260.591	383,743	${}^6S_{5/2}-{}^6P^\circ_{5/2}$
	250	260.713	383,564	${}^6S_{5/2}-{}^6P^\circ_{3/2}$
Cu VII	200	200.665	498,343	${}^6S_{5/2}-{}^6P^\circ_{7/2}$
	150	200.851	497,881	${}^6S_{5/2}-{}^6P^\circ_{5/2}$
	100	200.948	497,640	${}^6S_{5/2}-{}^6P^\circ_{3/2}$

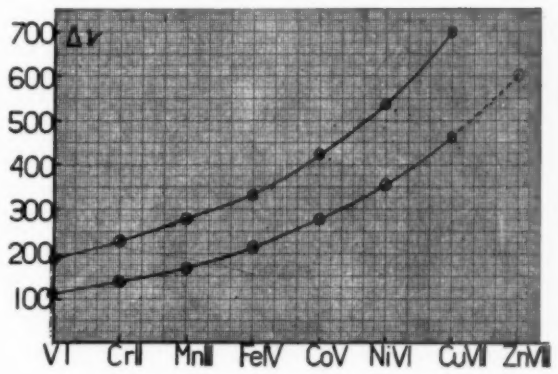

FIG. 2. $3d^4\,4p\,{}^6P^\circ_{7/2,\,5/2,\,3/2}$ term separations in cm^{-1}.

TABLE IV. *Splitting of ${}^6P^\circ$ terms for various ions of the sequence.*

	V I	Cr II	Mn III	Fe IV	Co V	Ni VI	Cu VII	Zn VIII
$\Delta\nu\ {}^6P^\circ_{7/2,\,5/2}$	111	141	170	217	279	358	462	(600)
$\Delta\nu\ {}^6P^\circ_{5/2,\,3/2}$	80	92	113	116	145	180	241	(320)
$\Delta\nu\ {}^6P^\circ_{7/2,\,3/2}$	191	233	283	333	424	538	703	(920)

column four are also the respective term values of the ${}^6P^\circ_{7/2,\,5/2,\,3/2}$ terms, when the ${}^6S_{5/2}$ is taken as zero. In the spectrum of Mn a group of lines near 50,000 cm^{-1}, reciprocal wave-length, appears to be the $3d^44s\ {}^6D-3d^44p\ {}^6P^\circ$ multiplet. Since this multiplet has not been located in the higher members of the sequence, the wave-lengths are not included in this report.

Since the data for Cr II and Mn III are so incomplete, it is not possible to extrapolate accurately the $(\nu/R)^{\frac{1}{2}}$ graph and obtain ionization potentials for the ions of this sequence. This may be done as soon as higher series members have been obtained in Mn III and its ionization potential well established.

Table IV and Fig. 2 show the increase in the splitting of the ${}^6P^\circ$ terms for the ions of this sequence. The smoothness of the curves gives added support to their correctness.

The study of these spectra, for the identification of other multiplets from the electron configurations $3d^5$, $3d^4\,4s$ and $3d^4\,4p$ in this sequence, is being continued.

The second author takes pleasure in thanking Professor R. C. Gibbs for the use of the facilities of the Cornell Physics Laboratory.

The Relative Energy of the $L\alpha$ Satellites Excited by Cathode Rays in the Atomic Number Range 47 to 52

F. R. HIRSH, JR., *Cornell University*

(Received August 3, 1935)

By a photographic method, the measurement of the integrated relative energy of the $L\alpha$ satellites, with respect to their parent $L\alpha_1$ line, has been extended from Ag(47) to Te(52). In this range the satellites decrease rapidly in relative energy with increasing atomic number. This is in substantial agreement with the new theory of Coster and Kronig.

INTRODUCTION

THE purpose of this paper is to report an extension of the measurements of the integrated relative energy for cathode-ray excitation of the $L\alpha$ satellites. The previous work[1] gave integrated relative energies from Zr(40) to Ag(47). The present work extends the measurements to Te(52).

X-ray satellites have been observed to occur within certain well-defined atomic number ranges.[2] The exact manner in which the integrated satellite energy changes with respect to the energy of the parent line, as we pass through the atomic number range of satellite occurrence, is of considerable interest and importance.

EXPERIMENTAL METHOD AND RESULTS

The $L\alpha$ lines of the elements from Ag(47) to Te(52) were recorded on Eastman IV–O Spectroscopic plates with a Siegbahn Vacuum Spectrograph. (A resolving power of about 3000 is attainable with this instrument at $\lambda = 4.0$A.) The Eastman IV–O plates are very fine grained, and, as a precaution further to minimize grain effects, Eastman D–76 Fine Grain Developer was used.

Microphotometric records of the $L\alpha$ lines of Ag(47) and Te(52) are shown in Fig. 1. These records were made by using the oscillation method previously described[3] and are noteworthy for their absence of "grain."

From these microphotometric records, density (intensity) plots were made as in the previous paper.[1] The density-exposure time curves for the wave-length range 4.0–5.4A have recently been studied[4] and a linear region, increasing in extent with increasing wave-length, is found to be present for all wave-lengths studied. The x-ray lines on all plates in the present work were exposed so as to have maximum densities lying within this linear region.

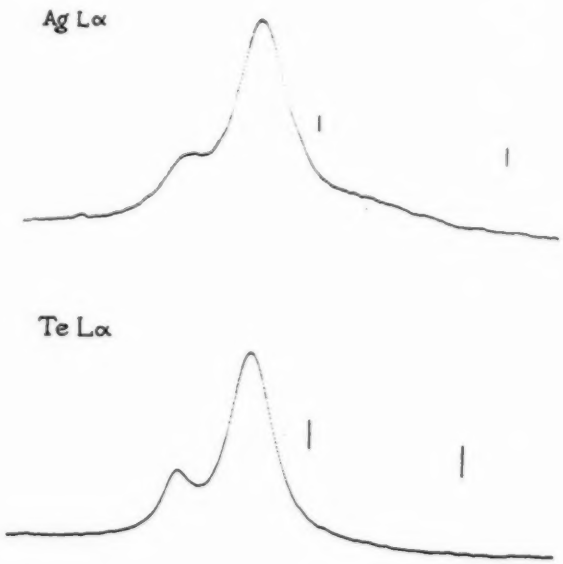

FIG. 1. Microphotometric records of the $L\alpha$ lines of Ag(47) and Te(52), excited by 20 kv electrons. Vertical lines indicate limiting wave-length positions between which satellites have been observed visually.

Fig. 2 shows density (intensity) plots made from microphotometer records. In these density plots the parent line, $L\alpha_1$, has been assumed to have the classical[5] shape and has been fitted with a curve having the proper relative energy, (as measured by areas), with respect to $L\alpha_2$.

[1] F. R. Hirsh, Jr. and F. K. Richtmyer, Phys. Rev. **44**, 955 (1933).
[2] F. K. Richtmyer, J. Frank. Inst. **207**, 353 (1929).
[3] F. K. Richtmyer and F. R. Hirsh, Jr., Rev. Sci. Inst. **4**, 353 (1933).
[4] F. R. Hirsh, Jr., J. Opt. Soc. Am. **25**, 229 (1935).
[5] A. Hoyt, Phys. Rev. **40**, 477 (1932).

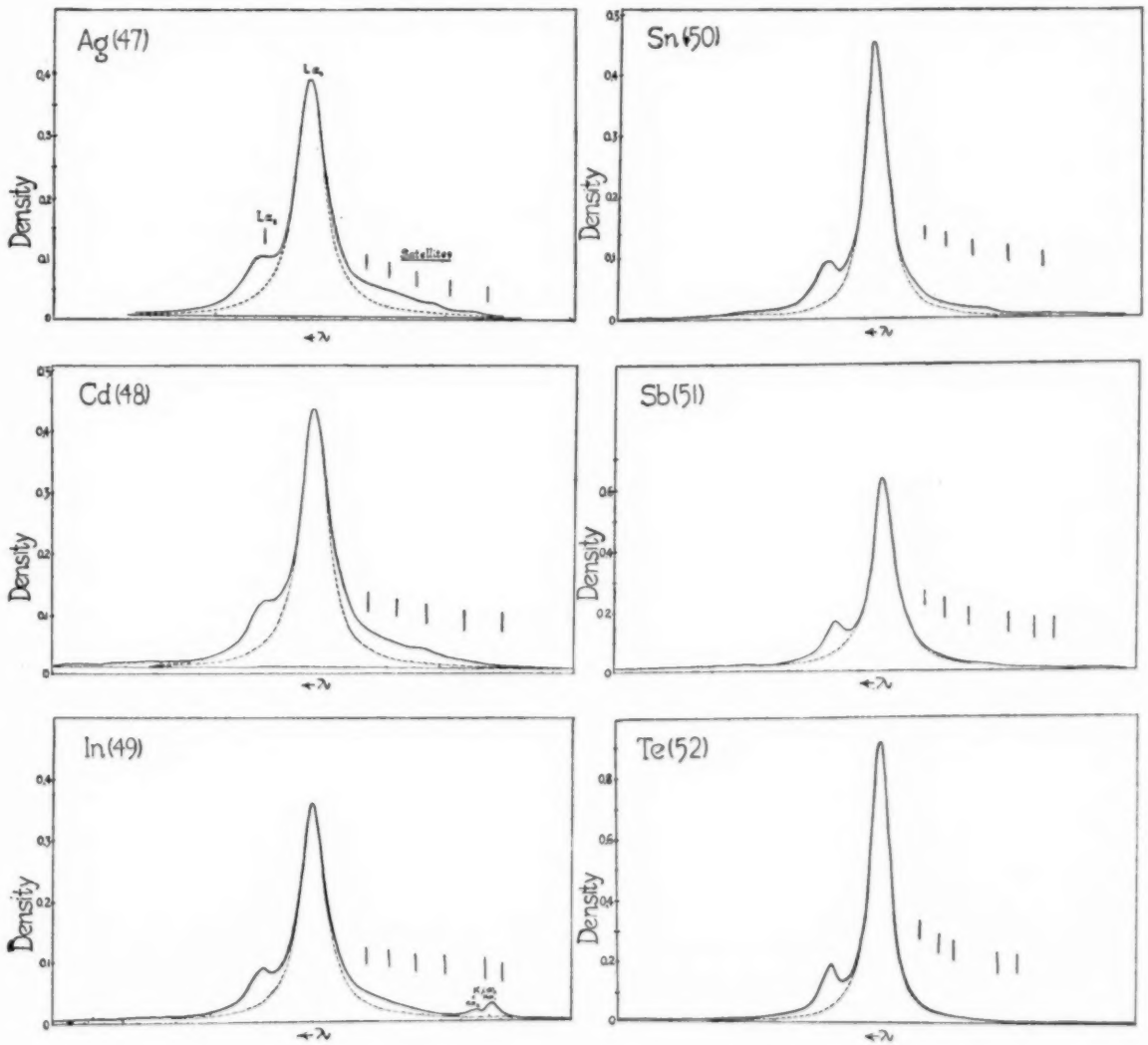

FIG. 2. Density, (intensity), plots of the $L\alpha$ lines of Ag(47) through Te(52) excited by 20 kv electrons. Vertical lines indicate positions at which satellites have been measured visually by others.

This assumption is reasonable since the $L\alpha_1$ line becomes symmetrical as we approach atomic number 52. At Te, (52) where the satellites are extremely faint, the asymmetry of $L\alpha_1$ has nearly vanished and the classical curve is seen to give a good representation of the line shape. All of the area between the classical curve and the short wave-length side of the $L\alpha$ line plot was designated as belonging to the satellite structure. This area divided by the area of $L\alpha_1$ gives the integrated relative energy of the group of satellites as shown in Table I.

The values given in Table I, column I are secured from the density plots in Fig. 2. A second set of spectrograms was made and independently analyzed to check these preliminary results (the data are given in Table I, column II). Both sets of data are plotted as the points surrounded by diamonds and squares in Fig. 3. The crosses are data previously reported.[1]

The full line of Fig. 3 rises to a maximum at atomic number 45, and falls off sharply to small values at atomic number 52. The broken curve[6] for the satellites of $L\beta_2$ shows a maximum at a higher atomic number than the maximum for

[6] A. W. Pearsall, Phys. Rev. **46**, 694 (1934).

the $L\alpha_1$ line curve. It is interesting to note that the $L\beta_2$ line first occurs at a higher atomic number than does $L\alpha_1$. Both the full and dashed curves of Fig. 3 fall off towards atomic number 52 in practically the same manner.

Conclusions

It is shown in Fig. 3 that the satellites of both $L\alpha_1$ and $L\beta_2$ fade out as we approach Te(52) from lower atomic numbers. Both of these parent lines, $L\alpha_1$ and $L\beta_2$, originate from electron transitions ending in the L_{III} shell. The theory, based on the Auger effect, recently advanced by Coster and Kronig[7] explains the disappearance of both the $L\alpha_1$ and $L\beta_2$ satellites near atomic number 52. This theory, furthermore, is in good agreement with other observations made in the Cornell X-Ray Laboratory. (For a discussion of these facts see the article[7] just referred to.)

The theory predicts:

(1) The vanishing of the $L\alpha_1$ and $L\beta_2$ satellites at about atomic number 53.

Table I.

Element	Atomic number	Integrated relative energy	
		I	II
Ag	47	0.155 *p*	0.330†
Cd	48	0.185	0.200
In	49	0.100	0.120
Sn	50	0.055	0.060
Sb	51	0.010	0.100*
Te	52	0.010	0.010

* High value because of uneven background on plate.
† Value from previous article (see reference 1).
p Dr. L. G. Parratt has very kindly checked with the two-crystal vacuum spectrometer, using a resolving power ~11,000, as obtained with "perfect" calcite crystals. Assuming the parent line is not of the classical shape, and drawing in freehand a "most reasonable" satellite background (foot of the parent line), he finds a total satellite intensity of 7 percent. Assuming the parent line is of the classical shape in an arbitrary region adjacent to the satellites, thus securing the constants and drawing in the background, he finds the value of 11 percent for the total satellite intensity. This is a fairly good check with the photographic value of 15.5 percent as given in Table I, column I. We are both agreed that no satisfactory analytical method of drawing in the parent line under the satellite structure, has been developed as yet. The photographic value of 15.5 is probably a low estimate, since the microphotometer record for Ag $L\alpha$ (see Fig. 1), is slightly lower on the short wave-length side. This would raise the estimate of 15.5 percent (shown as the square at $Z=47$ in Fig. 3), to a point considerably nearer the (full) curve for $L\alpha_1$.

[7] D. Coster and R. De L. Kronig, Physica **2**, 13 (1935).

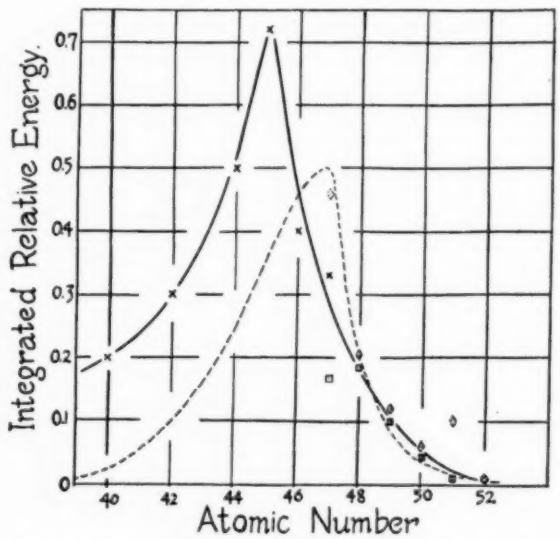

Fig. 3. Integrated relative energies of $L\alpha$ satellites plotted against atomic number. Full line plotted from data given in this article, and in a previous article.[1] Dashed curve is for relative energies of the satellites of $L\beta_2$.[6]

(2) The absence of any enhancement of the intensity of these satellites, due to Auger effects, between atomic numbers 53 and 74.
(3) The reappearance of these satellites above atomic number 74. (For the experimental facts see a recent paper by Kaufman.[8])

A crucial test of this new theory of Coster and Kronig would seem to lie in the comparison of the predicted behavior of the satellites of the lines $L\beta_1$, $L\gamma_1$ and $L\gamma_{2,3}$ according to this new theory, and the experimental facts concerning the satellites of these lines. Further discussion will appear in a later paper.

Acknowledgment

The author wishes to acknowledge Dean Richtmyer's continued interest in this work, and desires to express gratitude for permission to use certain apparatus granted Dean Richtmyer by the Heckscher research council of Cornell University.

[8] S. Kaufman, Phys. Rev. **45**, 385 (1934).

The Hyperfine Structure and Nuclear Magnetic Moment of Caesium I

L. P. GRANATH AND R. K. STRANATHAN, *Department of Physics, New York University, University Heights*

(Received July 16, 1935)

The hyperfine structure of the lines λλ8761, 4593, 4555, 3889 and 3877 of the arc spectrum of caesium were observed with a Fabry-Perot etalon. The interval factors for the $6^2S_{\frac{1}{2}}$, $6^2P_{\frac{1}{2}}$, $7^2P_{\frac{1}{2}}$, and $8^2P_{\frac{1}{2}}$ states were found to be 0.0767, 0.00925, 0.00329, and 0.0017 cm^{-1}, respectively. Assuming a nuclear spin of 7/2, the nuclear magnetic moments calculated from Goudsmit's formulas were 2.66, 2.38, 2.62, and 3.01 nuclear magnetons for the respective states.

INTRODUCTION

THE hyperfine structure of caesium was first investigated by Jackson,[1] but the accuracy of the work was not sufficiently great to warrant the calculation of magnetic moments from the more recently derived formulas.[2] Since that time several determinations have been made. The authors[3] obtained the hyperfine structure interval factor for the $6^2P_{\frac{1}{2}}$ state and from this calculated the nuclear magnetic moment, while Heydenburg[4] has obtained the separation factors of the $6^2P_{3/2}$ and $7^2P_{3/2}$ states from the polarization of resonance radiation. Jackson[5] has obtained the interval factors for the $6^2S_{\frac{1}{2}}$, $6^2P_{\frac{1}{2}}$, $6^2P_{3/2}$, $7^2P_{\frac{1}{2}}$ and $7^2P_{3/2}$ states.

The spin of caesium has been established as 7/2 by Kopfermann[6] from his work on the spark spectrum and by Cohen[7] from the atomic beam method.

This work is concerned with the determination of the interval factors of the $6^2S_{\frac{1}{2}}$, $6^2P_{\frac{1}{2}}$, $7^2P_{\frac{1}{2}}$ and $8^2P_{\frac{1}{2}}$ states, and the calculation of the corresponding nuclear magnetic moments.

APPARATUS AND METHOD

The arc spectrum of caesium was produced in a discharge tube of the type shown in Fig. 1. The caesium was obtained by heating a mixture of pulverized metallic calcium and caesium chloride in a glass tube sealed to the vacuum system. An inert gas, helium for the λ8761, both helium and argon for the λλ4593 and 4555 and argon for the λλ3877 and 3889 lines, was used to carry most of the discharge. Argon was necessary for the latter lines because the helium line at λ3888 was so close to the caesium doublets as to render microphotometering of the patterns impossible. The excitation was obtained by means of a 1500-volt d.c. generator. The voltage across the tube was lowered until the current was about 1/5 of that required to produce any observable reversal of the λ8521 ($6^2S_{\frac{1}{2}}-6^2P_{3/2}$) line which, under these conditions was about 0.2 ampere. The tube was cooled to a temperature of about 50°C by an air blast from a fan.

A special spectrograph was constructed with a lathe bed as a foundation. A 60° glass prism of index 1.75, a 76-cm focal length camera and a collimator from a Hilger constant deviation spectrograph were used in the construction. The advantage of this construction was its rigidity, all optical parts being mounted on the same foundation. The etalon was mounted between the collimator and the prism. Etalons of various sizes could be accommodated since the distance between prism and collimator was variable; and in addition all optical parts could be raised or lowered with respect to the lathe bed or to each other.

In order to eliminate changes in the optical system due to temperature fluctuations, the whole system, except the plateholder, was maintained at a constant temperature to within 0.1°C. It was important to adjust the etalon for parallelism at the same temperature at which it was to be used. This was accomplished by rotating the etalon stand until it came into line with light from a mercury arc which entered through a small window in the side of the constant temperature box.

[1] D. A. Jackson, Proc. Roy. Soc. **A121**, 432 (1928).
[2] S. Goudsmit, Phys. Rev. **43**, 636 (1933).
[3] L. P. Granath and R. K. Stranathan, Phys. Rev. **46**, 317 (1934).
[4] N. P. Heydenburg, Phys. Rev. **46**, 802 (1934).
[5] D. A. Jackson, Proc. Roy. Soc. **A147**, 500 (1934).
[6] H. Kopfermann, Zeits. f. Physik **73**, 437 (1932).
[7] V. W. Cohen, Phys. Rev. **46**, 713 (1934).

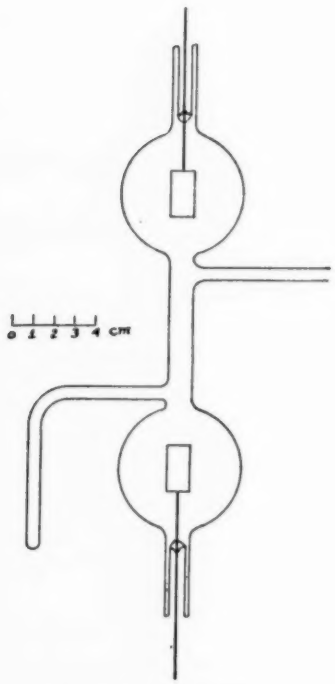

FIG. 1. Discharge tube.

For long exposures it was found necessary to eliminate changes in the index of refraction of air due to changes in atmospheric pressure. This was accomplished by placing the etalon in an aluminum chamber which could be made air tight. This chamber was used in photographing the λ8761 line which required an exposure time of about twelve hours. The separation of the components of this line is about 0.037 cm^{-1} and with a spacer of 2.5 cm, a change in pressure of 1 mm would cause the components to shift by 0.004 cm^{-1}. This is more than 1/10 the separation to be measured, consequently the pressure must be kept constant to better than this amount. This is impossible without the chamber, as the atmospheric pressure may vary by several millimeters during a twelve-hour exposure.

The etalon plates were of fused quartz and were silvered to provide a reflecting power of about 90 percent in the red. These silver surfaces were obtained by evaporating silver on the quartz surfaces in a vacuum. The reflecting power was measured by the method described by Childs.[8]

[8] W. H. J. Childs, J. Sci. Inst. **3**, 97, 129 (1926).

MEASUREMENTS

λ8761 ($6^2P_{1/2}-6^2D_{3/2}$)

This line was photographed with hypersensitized I P plates. It photographed as a doublet, the separation due to the $6^2D_{3/2}$ state being too small to be observed. The results of the measurements are given in Table I, where the order numbers do not refer to the order of interference but are numbered outward from the center of the Fabry-Perot pattern.

It will be seen that the values for orders 3 and 4 of plates 143 and 144 are noticeable lower than those for the first two orders. This is believed to be due to the microphotometer since it did not appear in plate 140, which was adjusted for each order to allow for the curvature in the pattern (due to the prism curvature). This was also borne out by the I/e widths which were found larger for orders 3 and 4.

The microphotometer traces did not fall to the clear plate level between the components. In order to correct for the mutual influence of the position of one component on the other, the patterns were drawn out to linear scales of intensity and dispersion. To obtain a linear scale of intensity, an intensity calibration was made on each plate by the use of a wedge-shaped slit. Spectral photographs of the light from a tungsten lamp were microphotometered and a curve of galvanometer deflections *versus* slit widths plotted. Since the intensity was proportional to the slit

TABLE I. *Measured separations of components of λ8761 of Cs I. Spacer 2.504 cm.*

PLATE	ORDER	MEASURED $\Delta\nu$ cm^{-1}	CORRECTED $\Delta\nu$ cm^{-1}	DEVIATION FROM AVERAGE
140	1	0.0341	0.0352	0.0002
	2	0.0335	0.0346	0.0004
	3	0.0337	0.0348	0.0002
	4	0.0339	0.0350	0.0000
143	1	0.0340	0.0351	0.0001
	2	0.0342	0.0353	0.0003
	3	0.0322	0.0353	0.0003
	4	0.0310	0.0341	0.0009
144	1	0.0357	0.0368	0.0018
	2	0.0334	0.0345	0.0005
	3	0.0320	0.0351	0.0001
	4	0.0315	0.0346	0.0004
		Average	0.0350	0.0004

width, this curve was equivalent to galvanometer deflections *versus* intensity. From this graph the galvanometer deflections on the pattern were transformed into a linear scale of intensity.

The center of the pattern was obtained by measuring the mean distance between corresponding points of similar components on either side of the center. These measurements were made for various intensity heights and the average of the various mean values taken as the center of the pattern. It was impossible to obtain, on one trace, more than one or two orders on both sides of the center, hence it was necessary to take several traces of the pattern, duplicating the end components. The distances from the center of the pattern to both sides of all components were measured for various galvanometer deflections. These distances were measured from small galvanometer deflections, in steps of 1 or 2 mm, to the maximum galvanometer deflection. Upon squaring these distances from the center, the linear dispersion of the pattern was obtained.

The centers of the components were then determined and the $\Delta\nu$ found by dividing the distance between components by twice the product of the spacer thickness and the distance between orders.

To correct for the influence of one component on the position of the other, each line was assumed to have a Doppler form. If the intensity at the center of the first component is A_1 and that at the center of the second A_2; and if X_0 is the distance between centers and X is the distance from the center of the component of intensity A_1 to any point on either curve, it follows that

$$I = A_1 e^{-aX^2} + A_2 e^{-a(X-X_0)^2},$$

where $a^{-\frac{1}{2}}$ is the width at $I = A/e$. The difference between X_0 and the distance between maxima of the plotted curves is the amount to be added to give the true separation. As a check, the correction was determined by finding two empirical curves which, when added together, gave the experimental pattern. The corrected intervals are shown in Table I.

Comparator measurements were made upon a plate taken with a one-cm spacer and the uncorrected interval found to be 0.034 cm^{-1}. Comparator measurements on plate 140 also checked the uncorrected values from the microphotometer traces.

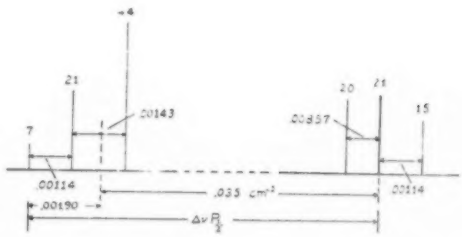

FIG. 2. Calculated pattern for the λ8761 line.

The average value of the corrected separation between centers of gravity of the lines is 0.035 cm^{-1} and this is probably accurate to less than 0.001 cm^{-1}.

To obtain the separation of the $6^2P_{\frac{1}{2}}$ state from this value, the influence of the $6^2D_{3/2}$ state must be considered. The ratio of the interval factors for the $6^2D_{3/2}$ and $6^2P_{\frac{1}{2}}$ states was calculated from the relation[2]

$$a = \Delta\nu l(l+1)g(I)/Z_i(l+\tfrac{1}{2})j(j+1)1838$$

where $Z_i(D_{3/2}) = 45$ and $Z_i(P_{\frac{1}{2}}) = 50$. This gave $a(D_{3/2})/a(P_{\frac{1}{2}}) = 0.03085$. By using a nuclear spin of 7/2, diagrams of the pattern were constructed similar to the one shown in Fig. 2 for several assumed values of the interval factor of the $6^2P_{\frac{1}{2}}$ state. The amount to be added to the measured value to obtain the separation of the $6^2P_{\frac{1}{2}}$ state was noted in each case. The quantity to be added was found to be 0.002 cm^{-1}. The value of the $6^2P_{\frac{1}{2}}$ separation was then $0.035+0.002=0.037 \pm 0.001$ cm^{-1}. This gives an interval factor of 0.00925 ± 3 percent. The proper values for Z_i are not well established; however, since Z_i appears only as a very small correction to the interval, a large error in it would produce an extremely small error in the interval factor.

λ4555($6^2S_{1/2}-7^2P_{3/2}$) and λ4593($6^2S_{1/2}-7^2P_{1/2}$)

These lines were investigated by using two spacers and silver surfaces on the etalon plates of about 90 percent reflecting power for these wavelengths. Eastman process plates were used and the exposure time ranged from 10 to 40 minutes for tube currents of 0.08 to 0.10 ampere. The lines appeared as doublets, the separation due to

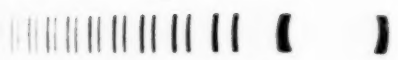

FIG. 3. Photograph of λ4593 and λ4555.

FIG. 4. Microphotometer trace of λ4555.

the $7^2P_{3/2}$ and $7^2P_{1/2}$ states being too small to be observed. A photograph of one of the patterns and a microphotometer trace are shown in Figs. 3 and 4. The $\Delta\nu$'s were calculated in a manner similar to that described for the λ8761 line, except that no intensity calibration was necessary and it was not necessary to plot the measured pattern.

The results of the measurements of the microphotometer traces are given in Tables II and III.

The observed separation is different for the two lines by 0.0079 cm^{-1}, this difference being due to the splitting of the 7^2P states. To obtain the interval factor for the $7^2P_{1/2}$ state from the observed data, diagrams were constructed as shown in Fig. 5 for various assumed values of the interval factor for the $7^2P_{1/2}$ and $7^2P_{3/2}$ states. These diagrams show that a small quantity must be added to the $6^2S_{1/2}$ separation to obtain the measured separation of the λ4593 line, and another small quantity must be subtracted from

TABLE II. *Measured separations of components of λ4555 of Cs I.*

PLATE	SPACER (cm)	$\Delta\nu$ (cm^{-1})	DEVIATION FROM FINAL AVERAGE
172	1.024	0.3029	0.0003
		.3029	.0003
		.3034	.0002
		.3030	.0002
		.3032	.0000
		.3033	.0001
		.3033	.0001
		.3032	.0000
		.3032	.0000
		Ave. 0.3032	
173	1.024	0.3036	0.0004
		.3034	.0002
		.3041	.0009
		.3033	.0001
		.3027	.0005
		.3034	.0002
		.3036	.0004
		.3036	.0004
		.3037	.0005
		.3035	.0003
		Ave. 0.3035	
235	0.9974	0.3034	0.0002
		.3031	.0001
		.3030	.0002
		.3030	.0002
		.3031	.0001
		.3033	.0001
		.3027	.0005
		.3029	.0003
		.3022	.0010
		.3022	.0010
		Ave. 0.3029	0.0003

Final average $\Delta\nu = 0.3032 \pm 0.0003$ cm^{-1}

TABLE III. *Measured separations of components of λ4593 of Cs I.*

PLATE	SPACER (cm)	$\Delta\nu$ (cm^{-1})	DEVIATION FROM FINAL AVERAGE
235	0.9974	0.3111	0.0000
		.3116	.0005
		.3116	.0005
		.3116	.0005
		.3117	.0006
		.3118	.0007
		.3117	.0006
		.3115	.0004
		.3115	.0004
		.3113	.0002
		Ave. 0.3115	
170 *A*	1.024	0.3101	0.0010
		.3107	.0004
		.3110	.0001
		.3110	.0001
		.3121	.0010
		.3119	.0008
		.3109	.0002
		.3103	.0008
		.3107	.0004
		.3111	.0000
		Ave. 0.3110	
170 *B*	1.024	0.3111	0.0000
		.3111	.0000
		.3103	.0008
		.3112	.0001
		.3109	.0002
		.3108	.0003
		.3106	.0005
		.3107	.0004
		Ave. 0.3108	0.0004

Final average $\Delta\nu = 0.3111 \pm 0.0004$ cm^{-1}

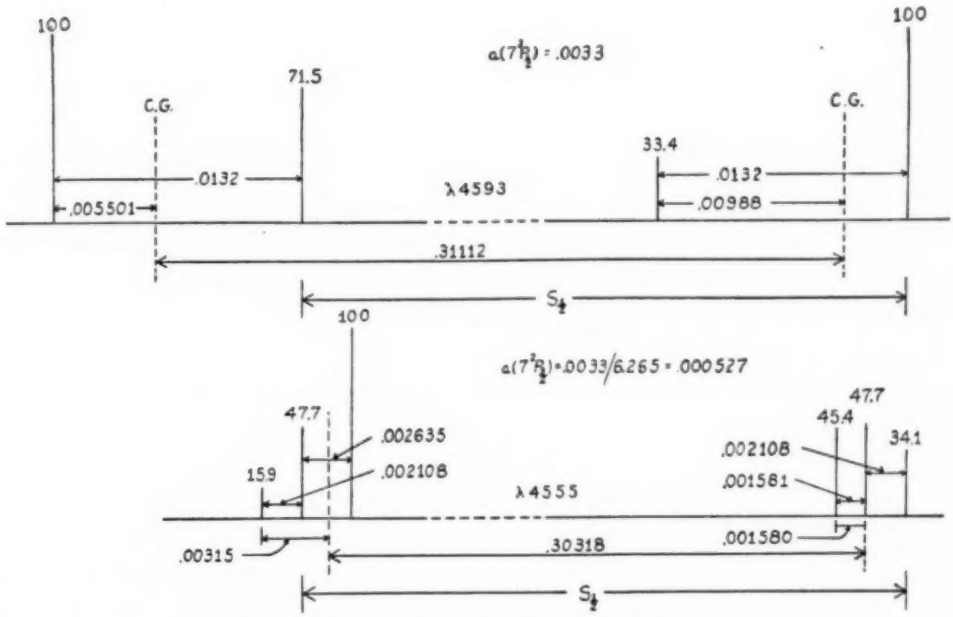

FIG. 5. Calculated pattern of λ4593 and λ4555.

the $6^2S_{\frac{1}{2}}$ separation to obtain the observed separation of the λ4555 line. The quantities to be added in one case and subtracted in the other were plotted against the respective interval factors as shown in Fig. 6. Next the ratio of the interval factors of the $7^2P_{\frac{1}{2}}$ and $7^2P_{3/2}$ states was calculated from the formula

$$g(I)=aZ_i j(j+1)(l+\tfrac{1}{2})\lambda 1838/\Delta\nu l(l+1)K$$

for $Z_i=55$, 51 and 45. For a given Z_i and a particular $a(P_{\frac{1}{2}})$ the difference in separation between the λ4593 and the λ4555 was calculated. This quantity is designated by $\Delta Sp_{\frac{1}{2}}-\Delta Sp_{3/2}$. It was plotted against various assumed values of the $7^2P_{\frac{1}{2}}$ interval factor with $Z_i=55$, 51 and 45.

This graph is shown in Fig. 7 and from it, that interval factor for the $7^2P_{\frac{1}{2}}$ state was selected which corresponded to the measured value of $\Delta Sp_{\frac{1}{2}}-\Delta Sp_{3/2}(0.0079\pm0.0004\ \text{cm}^{-1})$. From the graph, the corresponding $7^2P_{\frac{1}{2}}$ interval factor using $Z_i=49.5$ is $0.00329\pm0.00017\ \text{cm}^{-1}$. This Z_i was calculated from fine structure data. To see the dependence of $a(7^2P_{\frac{1}{2}})$ on Z_i, it was determined for $Z_i=55$ and a value of 0.00336 obtained.

In constructing the above diagrams, it was assumed that the calculated ratio of intensities is the same as was actually present in the radiation. This seems valid since all lines were photographed under conditions such that the λ8521 line exhibited no reversal. The "*f* values"[9] of the λ4500 and λ3800 lines are about 1/60 and 1/10,000 that of the *f* value for the λ8521 line and the reversal expected in these lines would be extremely small. The conclusion is also verified by the fact that the ratios of the intensities of the components of the λλ4555, 4593, 3877 and 3889 lines were as expected from theory.

The separation of the $6^2S_{\frac{1}{2}}$ state was obtained from the observed separation of the λλ4555 and 4593 lines. Taking $a(7^2P_{\frac{1}{2}})=0.00329\pm0.00017$ cm^{-1} and referring to Fig. 6, it is found that $\Delta S_{\frac{1}{2}}$ is the measured separation of λ4593 minus 0.00436 ± 0.00020 or $0.3067\pm0.0004\ \text{cm}^{-1}$. This gives an interval factor of $0.0767\pm0.0001\ \text{cm}^{-1}$ for the $6^2S_{\frac{1}{2}}$ state.

λ3889($6^2S_{1/2}-8^2P_{1/2}$) and λ3877($6^2S_{1/2}-8^2P_{3/2}$)

These lines were also observed as doublets. The exposure times were from 1 to 8 hours using Eastman 33 plates, a tube current of from 0.3 to 0.5 ampere, and reflecting powers of

[9] S. A. Korff and G. Breit, Rev. Mod. Phys. **4**, 471 (1932).

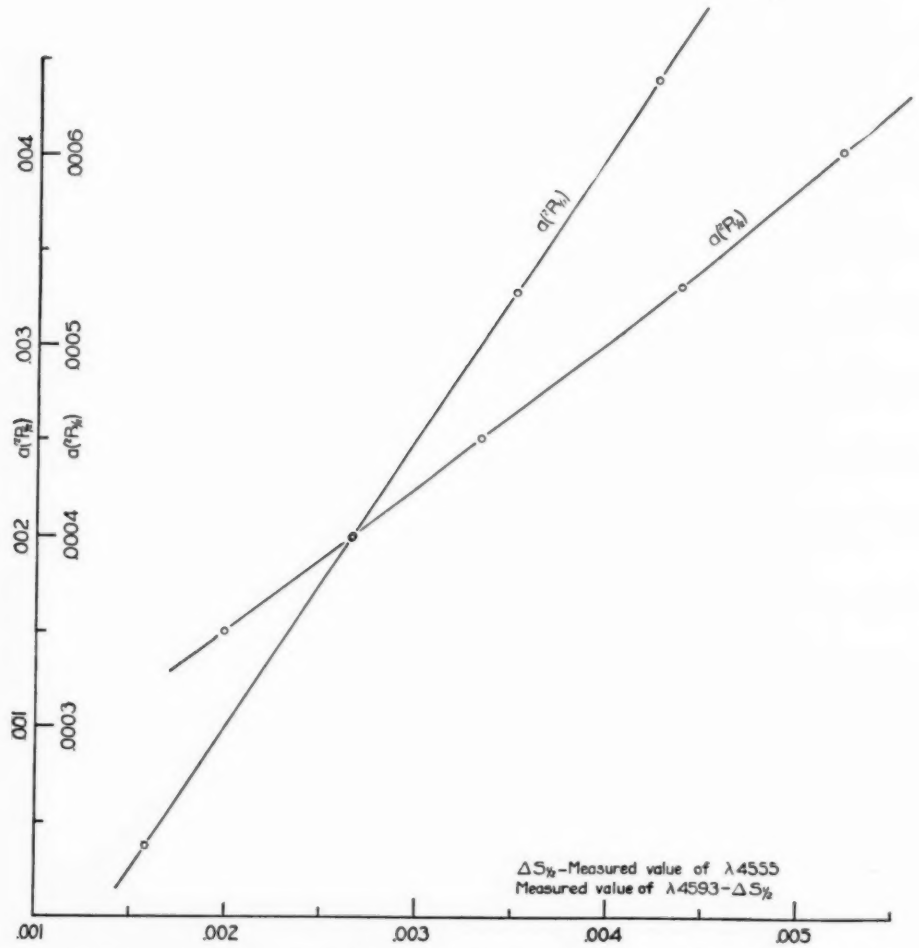

FIG. 6. Difference between centers of gravity and $\Delta 6^2S_{\frac{1}{2}}$ plotted against $a(P_{\frac{1}{2}})$ and $a(P_{3/2})$.

about 80 percent for these wave-lengths. The results of the measurements are given in Table IV.

These measurements are not considered as accurate as those for the 4500 lines. Due to the weak intensity it was necessary to use coarse grained plates which did not microphotometer as well as the process plates. The lines were wider due to the larger tube current and also due to lower resolving power in this region. On only a few plates was the intensity sufficient to obtain usable microphotometer traces, consequently most of the measurements were obtained by use of a comparator.

The interval factor for the $8^2P_{\frac{1}{2}}$ state was obtained from the measurements in the same manner as was described for the $7^2P_{\frac{1}{2}}$ state and was found to be 0.0017 ± 0.0003 cm^{-1}.

TABLE IV. *Measured separation of components of λλ3877 and 3889 of Cs I.*

INSTRUMENT	PLATE	SPACER	NUMBER OF ORDERS MEASURED	$\Delta\nu$ (cm^{-1})
		λ3877		
Microphotometer	228	0.9974	9	0.3058
Comparator	200	.9974	12	.3062
"	231	.9974	18	.3052
"	241	.9974	16	.3051
				Ave. 0.3056±0.0006
		λ3889		
Microphotometer	226	0.9974	9	0.3099
Comparator	230	.9974	18	.3091
"	209	1.024	14	.3104
"	229	.9974	8	.3094
				Ave. 0.3097±0.0007

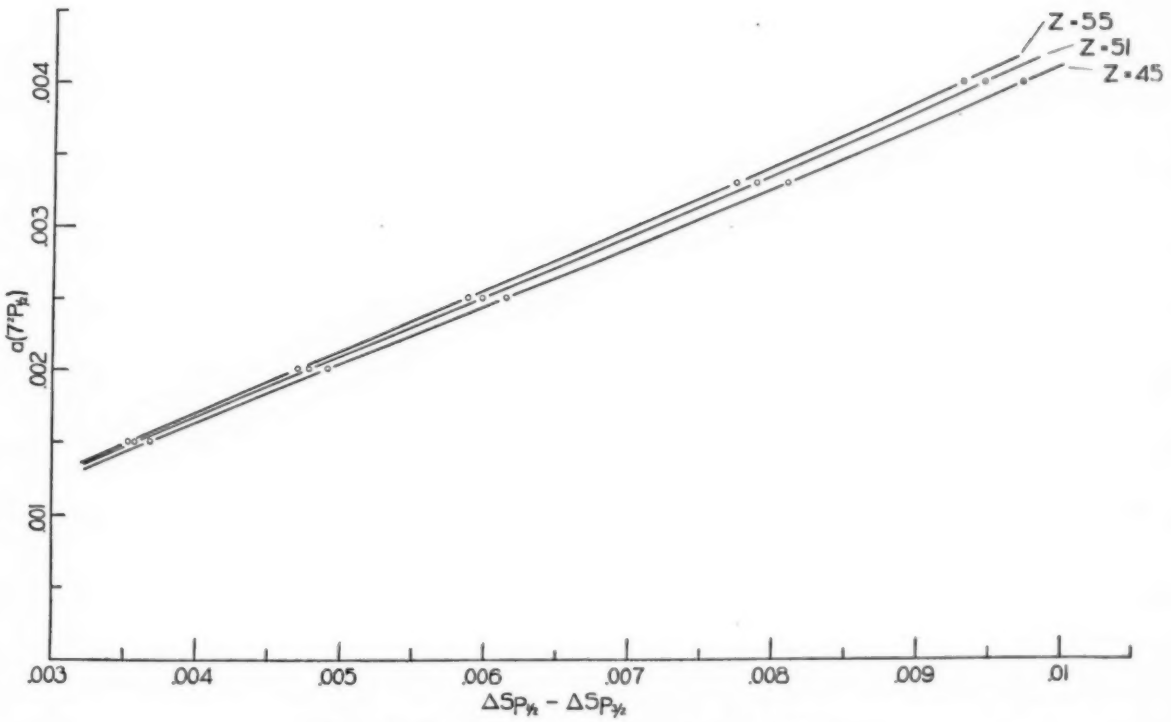

FIG. 7. $a(P_1)$ plotted as a function of $\Delta SP_1 - \Delta SP_{3/2}$.

CONCLUSION

The "g values" and hence the nuclear magnetic moments were calculated from Goudsmit's formulas, using the measured interval factors, the Z_i values for the P states as calculated from fine structure data and the corresponding relativity corrections. The results of these calculations are shown in Table V.

The percentage error has been given for the interval factors only, since the formulas available, at present, for the calculation of the magnetic moments may be in error by a magnitude comparable to the experimental error.

TABLE V. *Calculated g values and nuclear magnetic moments of Cs I.*

STATE	INTERVAL FACTOR (cm^{-1})	% ERROR	Z_i	$g(I)$	NUCLEAR MAGNETIC MOMENT
$6^2S_{\frac{1}{2}}$	0.0767	0.2	55	0.76	2.66
$6^2P_{\frac{1}{2}}$	0.00925	3	49.5	0.68	2.38
$7^2P_{\frac{1}{2}}$	0.00329	5	49.5	0.75	2.62
$8^2P_{\frac{1}{2}}$	0.0017	20	48.5	0.86	3.01

It is of interest to compare these results with those obtained by Heydenburg[4] from polarization of resonance radiation. He obtains a value of 0.00142 ± 5 percent for $a(6^2P_{3/2})$ and 0.000486 ± 3 percent for $a(7^2P_{3/2})$. By using his values for the $^2P_{3/2}$ states and the authors' values for the $^2P_{\frac{1}{2}}$ states the ratio $a(6^2P_{\frac{1}{2}})/a(6^2P_{3/2}) = 6.52 \pm 5$ percent and the ratio $a(7^2P_{\frac{1}{2}})/a(7^2P_{3/2}) = 6.80 \pm 5$ percent. The theoretical value of this ratio is 6.5 for $Z_i = 55$ or 6.265 for $Z_i = 51$.

It appears that the most probable value of $g(I)$ is between 0.68 and 0.75 and that it is the same for all the states considered within the limit of experimental error.

In conclusion the authors wish to express their appreciation to Professors G. Breit, and A. C. G. Mitchell for many helpful suggestions; and to the National Research Council for aiding this work with a research grant.

The *E* Band System of Calcium Hydride

WILLIAM W. WATSON AND ROBERT L. WEBER, *Sloane Physics Laboratory, Yale University*

(Received August 5, 1935)

The *E* band system of CaH at 4900A is shown to be the $\Delta v=0$ sequence of a $^2\Pi\rightarrow{}^2\Sigma$ transition, the lower state being the normal $^2\Sigma^+$ state. Quantum analysis gives for the *E*, $^2\Pi$ state $B_0=4.2844$, $D_0=-2.16\times10^{-4}$, $A=9.3$, $\gamma=+0.230$ for $K<20$, $\omega_0=1248.6$ and $\omega_e x_e=21.8$. The large γ-constant, its changing value for the higher rotational levels and other relations are indications of strong interaction between the *E* state and other near-lying CaH states. Spin- and Λ-doubling relations are discussed.

A BAND system near 4900A due to the CaH molecule was reported by B. Grundström[1] to represent a transition *E*, $^2\Pi\rightarrow N$, $^2\Sigma^+$, but he was unable to get a spectrogram at high dispersion having sufficient intensity to make analysis possible. It was noted that the bands possessed *P*, *Q*, and *R* branches, the *Q* branch being very compressed. This indication of an equilibrium internuclear distance for the upper electronic state, *E*, about that of the normal state, *N*, together with the ν_0 of 20,400 cm^{-1}, made it seem probable that the potential curves for the *D*, $^2\Sigma^+$ and *E*, $^2\Pi$ states intersected in the region of the low vibrational levels of the *D* terms, thereby producing the observed perturbations in the latter terms. We have obtained spectrograms of this *E* system with good intensity in both the second and third orders of our 21-foot grating in a stigmatic mounting. We present below the main features of the quantum analysis of these bands.

The light source was a 220-volt d.c. arc carrying 3 amperes between a water-cooled copper cathode and an anode of metallic calcium in an atmosphere of hydrogen at about 7 cm of Hg pressure. With Eastman Hypersensitive Panchromatic plates, the exposure time in the second order was 4 hours. To get better resolution

[1] B. Grundström, Zeits. f. Physik **69**, 235 (1931) and **75**, 302 (1932).

TABLE I. *Assignment of frequencies for the 4900A E, $^2\Pi\rightarrow N$, $^2\Sigma^+$ (0,0) CaH band (cm^{-1} units).*

K''	P_1	Q_1	R_1	P_2	Q_2	R_2
2					20390.34	20415.98
3		20393.82	20428.87	20365.74	91.36	25.87
4	20361.19	94.44	37.77	57.78	91.74	35.01
5	52.85	95.11	46.84	49.91	92.14	44.25
6	44.81	95.84	56.00	42.29	92.75	53.28
7	37.36	96.37	65.25	34.51	93.21	62.46
8	29.05	97.01	74.65	26.94	93.83	71.83
9	22.52	97.83	84.09	19.67	94.44	81.15
10	15.34	98.70	93.50d	12.20	95.11	90.56
11	08.27	99.57	502.86	05.10	95.84	99.84
12	01.41	400.52	12.37	298.09	96.68	509.01
13	294.55	01.65	21.84	91.17	97.41	18.47
14	87.66	02.45	31.29	84.30	98.26	27.74
15	81.33	03.37	40.61	77.67	99.16	36.94
16	74.63	04.28	49.90	71.05	400.00	46.04
17	68.26	05.36	59.15	64.48	00.90	55.26
18	61.57	06.14	68.28	57.90	01.65	64.23
19	55.57	07.17	77.35	51.67	02.45	73.11
20	49.13	07.67	86.12	44.74	03.37	81.79
21	42.90	08.69	94.90	38.68	04.08	90.40
22	36.75	09.37	603.51	32.65	04.48	98.53
23	30.73	09.94	11.54	26.35	05.36	607.00
24	24.35	10.62	19.66	19.97	06.14	14.90
25	18.25		27.49	13.67		22.55
26	12.10		34.98	07.18		29.92
27	05.99		42.06	00.91		37.03
28	199.79			194.69		43.81
29	92.44			88.08		
30				81.40		

of the closely-spaced Q branch lines, a third-order spectrogram was obtained, exposing 12 hours.

This band spectrum is typical of systems arising from transitions between two electronic states having almost identical rotational B constants. Only the $\Delta v=0$ sequence is present, the (0,0) band being by far the most intense band. The rotational lines in the P and R branches are uniformly spaced for some distance from the band origins, while the Q branch lines are very closely and uniformly spaced for the same range of quantum numbers. Sharply at $K'=19$ in the (0,0) band, however, this regularity of spacing ceases, the subsequent rotational levels are perturbed, and the Q branches form definite heads.

Table I contains quantum assignments for the lines of the (0,0) band. The agreement of the $R(K-1)-P(K+1)$ combination differences with those of the other known CaH system proves that the lower state of these E bands is the normal $^2\Sigma^+$ state. Q branch assignments have been based on Λ-doubling considerations. It was apparent early in our work of analysis that the upper electronic state is a case b $^2\Pi$ level with the ratio A/B somewhere in the range 0 to 4. No satellite branches are observed. The average deviations of the lower state combination differences from those of the other CaH system would somewhat favor the labeling of the set of branches proceeding from the high frequency side of the origin as P_2, Q_2 and R_2. But since the $\Delta_2T_1''(K)$ and $\Delta_2T_2''(K)$ values differ only slightly, and since theory indicates that for $^2\Pi$ states having an A/B between 0 and $+4$ $T_1(K')>T_2(K')$, we designate these the P_1, Q_1 and R_1 branches.

For computation of the rotational energy constants for the $^2\Pi$ state the values of the $\Delta_1T_1'(J+\frac{1}{2})$ and $\Delta_1T_2'(J+\frac{1}{2})$ differences—the averages for the d and c levels in each case—are computed in the usual manner. Both of these sets divided by $2K+2$ may, when plotted against K, be well represented by a single curve,

TABLE II. *Constants of the E, $^2\Pi$ state of the CaH molecule.*

$B_0=4.2844$	$A=9.3$
$D_0=-2.16\times10^{-4}$	$\gamma=+0.230$ for $K<20$
$p_0=+0.052$	$\omega_e=1248.6$
$q_0=+0.017$	$\omega_e x_e=21.8$

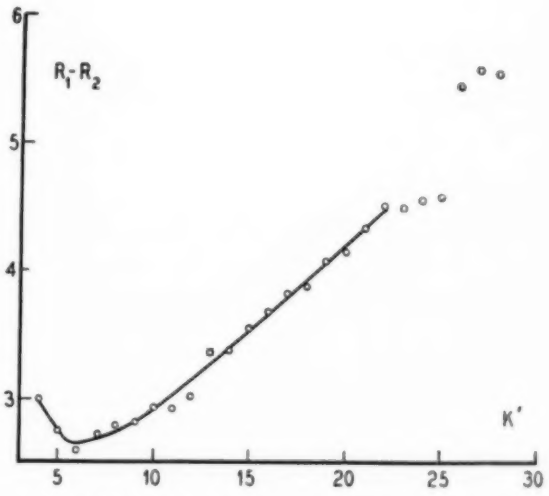

FIG. 1. $R_1(K)-R_2(K)$ frequency separations. Note the existence of the minimum at $K'=6$.

thus indicating that for $K>5$ the contributions of the terms containing the A and γ-coupling constants are negligible. This semigraphical method yields the values of B_0 and D_0 given in Table II. Calculations with the $\Delta_2T'(J)$ differences give for the d levels alone practically these identical values.

The accurate determination of the coupling constants A for the L^*S^* interaction and γ for the S^*K^* interaction for a case b $^2\Pi$ state with an abnormally large γ which is apparently not constant for the entire range of K values is not a simple matter. The variation of the doublet intervals $T_1'(K)-T_2'(K)$ with K should give these constants, for[2]

$$T_1'(K)-T_2'(K)=\Delta\psi(A,\Lambda,K')+\gamma'(K'+\tfrac{1}{2}),$$

the exact form of $\psi(A,\Lambda,K)$ to be determined by application of the Hill and Van Vleck energy term formula. These doublet intervals are obtained from the values of the doublet separations for any branch, such as those of the R branch plotted in Fig. 1, plus the known doublet intervals $\gamma''(K''+\frac{1}{2})$ for the normal $^2\Sigma$ state. We find this calculation to be rather unsatisfactory, however, both because of algebraic difficulties and because of an apparent variation of γ with K. This attempt at strict application of the Hill and Van Vleck formula does indicate that $5<A<10$ and that $\gamma\sim0.3$. Although the

[2] R. S. Mulliken, Rev. Mod. Phys. **2**, 110, 506 (1930); **3**, 142 (1931).

approximation[3] to the Hill and Van Vleck formula which yields the relation

$$T_1'(K)-T_2'(K)=[A\Lambda^2/K(K+1)+\gamma](K+\tfrac{1}{2})$$

is not expected to apply when the ratio A/B is so far from the value 0, we find that an equation of this form with $A=9.3$ and $\gamma=+0.230$ quite accurately gives the doublet intervals of Fig. 1 up to $K=20$. We therefore take these values as the approximately correct ones for the coupling constants of this E state.

The size of the γ is indicative of large interaction with other near-lying CaH levels, largely, perhaps, those of the D state whose $v=0$ level lies but 2135 cm^{-1} above the origin of this E band. In view of the violent perturbations encountered in these terms, the changing value of γ which we note for the higher K levels is not surprising.

Fig. 2 is a plot of the Λ-doubling in this $^2\Pi$ state. In sign, relative position and magnitude these curves are about what one would expect for a $^2\Pi$ state of this character. These values of $\Delta\nu_{1dc}(J)$ and $\Delta\nu_{2dc}(J)$ yield the constants $p_0=+0.052$ and $q_0=+0.017$ upon application of the well-known Λ-doubling formulas.[4] It is not to be expected, however, that a relation of "pure precession" should hold between this state and a single other CaH state.

The Q_1 and Q_2 branches of the (0,0) band form

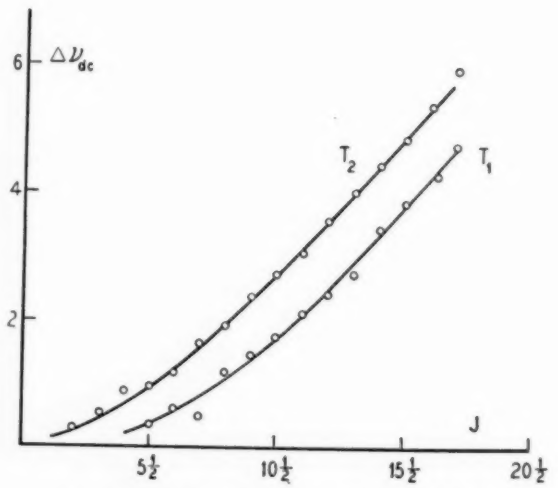

FIG. 2. Λ-doubling in the E, $^2\Pi$ state of CaH.

heads at 20,410.60 and 20,406.11, respectively. A similar pair of fainter heads for the (1,1) band occur at 20,337.16 and 20,333.65, while corresponding Q branch heads of the (2,2) band lie at 20,258.66 and 20,254.30. Assuming the small interval between the origin and Q head to be the same for each of these bands, one can compute the vibrational constants for this $^2\Pi$ state given in Table II. Just as for the D state,[1] the relation $D=4B_0^3/\omega_0^2$ which holds accurately for the normal state fails to hold for this E state. This fact indicates again the existence of strong perturbing influences from neighboring CaH levels.

[3] Reference 2, p. 508.
[4] R. S. Mulliken and A. Christy, Phys. Rev. **38**, 87 (1931).

NOVEMBER 1, 1935 PHYSICAL REVIEW VOLUME 48

Photoelectric Properties of Pure and Gas-Contaminated Magnesium*

R. J. CASHMAN AND W. S. HUXFORD, *Department of Physics, Northwestern University*
(Received August 19, 1935)

The present study is a continuation of an earlier investigation by the authors on the effects of gases on the photoelectric sensitivity of magnesium. A method for purifying magnesium by multiple distillations is described. The threshold characteristic of all gas-free surfaces obtained by successive distillations is found to lie at 3430±20A. The threshold value at 5100A, previously ascribed to pure magnesium, is now definitely attributed to magnesium contaminated by hydrogen. The effects of oxygen are further investigated in detail, a very slight dosing giving rise to a maximum excursion of the long wave limit to about 5700A. Calculations show that the formation of polar molecules on the magnesium surface will account for the threshold shift observed when hydrogen or oxygen is present.

* This paper was presented at the meeting of the Am. Phys. Soc., Minneapolis, June 21 and 22, 1935; Phys. Rev. **48**, 475A (1935).

IN a previous report by the authors[1] on the photoelectric properties of magnesium it has been shown that layers of this metal deposited in vacuum exhibit rapid changes in sensitivity when slight traces of air or oxygen come in contact with the surface. Pure nitrogen had no effect on the emission except when a glow discharge was set up in the gas, so that the sensitization caused by air was attributed solely to the oxygen contained in it. These results appeared to account rather well for the large discrepancies between thresholds for magnesium reported by many investigators in the past 15 or 20 years, but left unconfirmed recent values obtained for metal supposedly gas-free and in the pure state. The investigation was continued in the hope that with new refinements in the technique of purification and degassing of the metal completely gas-free layers could be obtained. This anticipation has been achieved with respect to the elimination of traces of gas which affect the photoelectric sensitivity of magnesium. In addition the investigation includes a detailed study of the surface structure of the metal when activated by contact with oxygen or hydrogen.

Gas-Free Surfaces of Magnesium Formed by Multiple Distillation

An extended study of magnesium surfaces prepared by single distillations of the metal indicated the presence of traces of residual gases too small to be detected by pressure-measuring devices. A search was undertaken to discover what gases are easily absorbed and probably, therefore, easily retained by the condensed layers. It was found that heated magnesium absorbed large volumes of hydrogen upon cooling. This observation was not in agreement with the work of Mrs. M. R. Andrews[2] but was in accord with observations of Hanawalt,[3] who found that large volumes of hydrogen were evolved by ordinary specimens of magnesium when they were heated. A more recent publication by Reimann[4] gives a detailed account of the "clean-up" of hydrogen by magnesium.

It is our experience that a condensed surface formed by rapid sublimation of magnesium is always contaminated with gas. A study of the photo-emission from layers deposited by slowly subliming the metal in successive distillations showed that the gas which is evolved during this time is hydrogen, although the sample had not been previously exposed to the gas. A subsequent slight contamination of such surfaces with hydrogen results in a definite and reproducible shift of the threshold, indicating a sensitization arising solely from the action of this gas upon the pure metal. Moreover, the maximum excursion of the threshold so obtained agrees exactly with the threshold at 5100A previously obtained[1] for magnesium layers which had not been specially treated to remove the hydrogen.

The method of successive distillations involves slow vaporization of a considerable quantity of magnesium in an auxiliary chamber in which a portion of the metal as it condenses is collected on a gas-free molybdenum or tantalum plate. At low gas pressures appreciable dispersal gettering does not occur if the vaporization is carried out very slowly. If the collecting plate is close to the vaporizing sample, the deposit on it is thicker than the layers formed at larger distances on the walls of the glass bulb. It is obvious that these latter layers of larger area will remove by contact gettering the major portion of hydrogen gas evolved during the process.[5] The hydrogen absorbed per gram of magnesium collected on the plate will be small by comparison to that absorbed per gram of metal condensed on the walls of the bulb. The plate is then removed to a second chamber, and the process repeated, the magnesium being again collected on a second movable plate.

An extension of the study in which condensed layers of magnesium were deposited by a single distillation showed that under certain conditions effectively gas-free layers may be formed. The magnesium specimen is first given a very slow progressive heating while the tube is still on the pumps. After several hours and at the time when noticeable sublimation has begun the tube is sealed off. A coating is then formed by very

[1] R. J. Cashman and W. S. Huxford, Phys. Rev. **43**, 811 (1933).
[2] Quoted by Dushman, Rev. Mod. Phys. **2**, 381 (1930).
[3] Hanawalt, Dow Chemical Co. Private communication.
[4] Reimann, Phil. Mag. **16**, 673 (1933).

[5] Reimann, reference 4, found that one hydrogen molecule out of every 1.5×10^6 which impinge upon the surface of magnesium is absorbed at room temperature.

slow sublimation. This coating is gas-contaminated but subsequent coatings formed in the same way show the emission characteristics of pure magnesium.

Experimental Photo-Cells; Outgassing Treatment

It is well known that if the temperature of an evacuated glass bulb containing magnesium is increased to a point where sublimation of the metal is noticeable (about 400°C) a reaction occurs between the glass and the magnesium, and a brown or black deposit forms along the inner wall. It is necessary because of this reaction to develop other methods of distillation so that the glass is never heated to a high temperature while in contact with magnesium.

The first type of tube used for the study of multiply distilled surfaces is shown in Fig. 1.

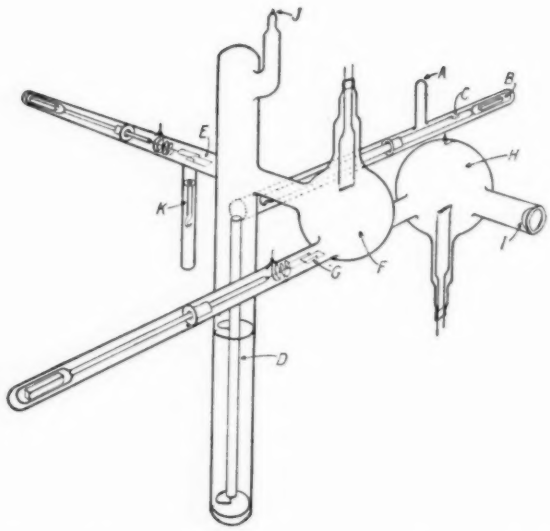

Fig. 1. Diagram of tube used for study of multiply distilled surfaces of magnesium. *A*, side tube for admitting magnesium; *B*, iron armature sealed in Pyrex tube; *C*, movable tube containing magnesium; *D*, molybdenum tube 35 cm long, 7 mm diameter; *E*, molybdenum plate 1.8 cm ×1 cm×5 mil; *F*, 300 cm³ flask containing 13-mil spiral tungsten filament; *G*, molybdenum plate, 1.8 cm×1 cm ×5 mil; *H*, 300 cm³ flask containing 13-mil tungsten filament; *I*, thin Pyrex window 0.01 mm thick; *J*, side tube connection to pump; *K*, side tube for admitting gas, tip broken by an iron armature enclosed in glass.

Since the tube contained several metal parts, extreme care had to be exercised in outgassing. Following the usual cleaning of glass and metal parts the tube was sealed to a two-stage mercury diffusion pump containing two liquid-air traps. An oven at a temperature of 550°C surrounded the tube for a period of 10 days. During this time the long molybdenum tube *D* was heated to 2000°C many times with an induction furnace, and the other metal parts were subjected to a vigorous heat treatment by electron bombardment.

At the end of 10 days dried tank-nitrogen was allowed to fill the system and the vertical side tube *A* was broken off for the purpose of admitting the magnesium. Through the courtesy of the Dow Chemical Company, magnesium was secured which had been especially purified by fractional distillation in an evacuated iron tube. The specimens were better than 99.9 percent pure and contained traces of iron and aluminum only. About 3 grams of the metal were introduced into the inner Pyrex tube *C*.

Another week of outgassing followed. An auxiliary oven maintained at a temperature of 340°C was mounted around the side arm containing the magnesium. The remainder of the tube was kept at 550°C as before. During the final stages the metal parts were given a thorough heat treatment. Magnesium was finally introduced into the vertical tube *D* by moving the tube *C* into position by electromagnetic control. A slight tapping of the tube caused the pieces to fall into the vertical tube.

The magnesium was slowly heated in successive stages with the induction furnace. The coil of the furnace was slowly raised and the magnesium repeatedly distilled and condensed until a mirror-like coating formed at the top of the outer glass tube. The chamber was sealed off from the vacuum system at this point, following which the molybdenum plates were heated to the point where vaporization of the molybdenum began. It was believed that any residual gas would be effectively removed by the "gettering" action of the condensed magnesium and molybdenum.

Magnesium was again vaporized from the bottom of tube *D* and allowed to condense on plate *E*. This plate was moved to bulb *F* where a very gradual heating of the filament caused some of the magnesium to sublime and condense on plate *G*. Sensitivity plots were obtained both for coatings formed in this manner and for coatings formed on the wall of bulb *H*.

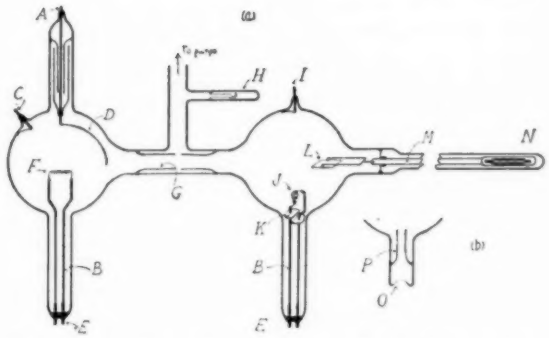

FIG. 2. Diagram of second type tube used for study of multiply distilled surfaces of magnesium. (a) *A*, highly insulated anode; *B*, nickel leads; *C*, contact to cathode; *D*, tungsten wire, makes contact with plate during electron bombardment; *E*, tungsten wire seals; *F*, 13-mil spiral tungsten filament 1 cm² area; *G*, Pyrex shields; *H*, tube for admitting gas; *I*, contact to cathode; *J*, 13-mil cone-shaped spiral tungsten filament for vaporizing magnesium; *K*, nickel plates to prevent magnesium from going down neck; *L*, tantalum plate 1.8 cm×1 cm×5 mil; *M*, Pyrex rod; *N*, iron armature. (b) *O*, thin Pyrex window (one on each bulb perpendicular to (a); *P*, Pyrex shield.

Another tube possessing the advantages of a minimum number of metal parts and high electrical insulation is shown in Fig. 2. Only two distillations were possible but each deposit could be studied individually. A third tube contained simply a tungsten spiral filament inside of which the magnesium sample was placed, and layers were deposited on the glass walls in a single slow distillation.

MEASURING EQUIPMENT

The photoemission was measured with an FP 54 Pliotron amplifier. With a Leeds and Northrup high sensitivity galvanometer in the plate circuit, currents as small as 2×10^{-16} ampere were measurable.

Light was resolved with a Gaertner quartz monochromator, a 68-watt linear spiral tungsten filament ordinarily serving as the light source. Qualitative observations were made in the range 2000 to 2800A with iron and mercury arcs.

RESULTS

Work function of pure magnesium

The composite curve of Fig. 3 shows typical total emission plots obtained with the three tubes. Ordinates have not been reduced to unit light intensity, but have been adjusted so that the maximum current is the same for all tests. Fig. 4 illustrates how small traces of gas remaining in a tube following the sealing off process may affect the emission from the first deposit of magnesium. All later deposits in this bulb, and all layers formed in the other two types of cells, both for magnesium surfaces formed on molybdenum or tantalum plates and on the walls of the Pyrex bulbs, are in excellent agreement and fix the threshold at 3430A, approximately, corresponding to a work function of 3.60 volts.

When illuminated with resolved light from a tungsten filament the emission from these pure magnesium surfaces was so small that the total available sensitivity of the amplifying circuit was required to obtain readable deflections. Under these circumstances it was not possible to obtain the energy distribution of the resolved light and apply Fowler's method for determining the true work function. A consideration of the finite range of wave-lengths passing the slit of the monochromator leads to an estimated error of ±20A in the apparent threshold determinations.

Work functions for tantalum and molybdenum

An excellent opportunity for measuring the photoelectric work functions of tantalum and

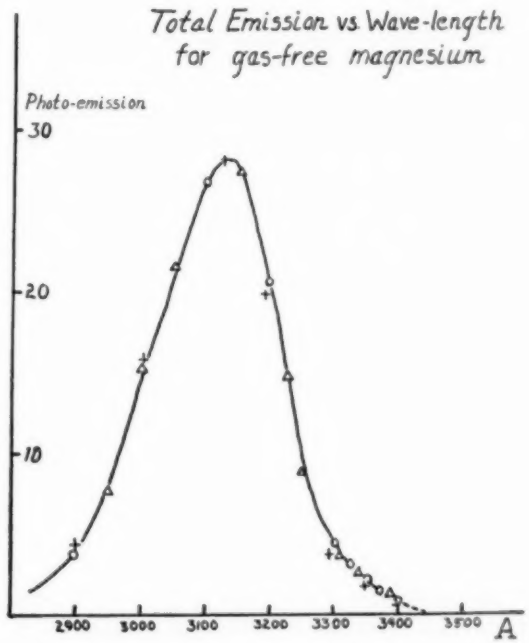

FIG. 3. Composite curve showing results from three cells.

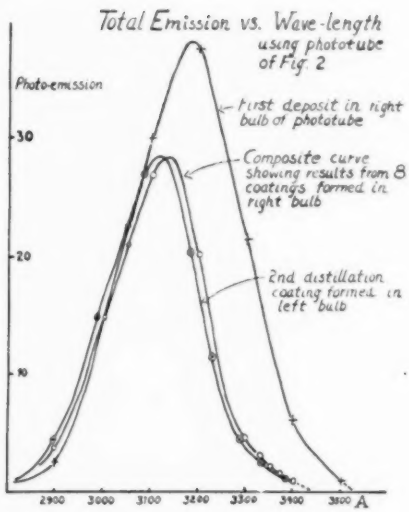

FIG. 4. Curves showing the "clean-up" of residual gases in a tube following the sealing off process.

molybdenum was provided by the multiple distillation tubes. By using the full sensitivity of the amplifier and taking the last observable reading as the approximate value of the threshold, a value of 3000A (4.12 volts) was obtained for molybdenum and 3050A (4.05 volts) for tantalum. DuBridge and Roehr[6] obtained 4.15 volts for molybdenum and Cardwell[7] obtained 4.10 volts for tantalum.

Hydrogen on magnesium

Samples of hydrogen were obtained by heating specimens of ordinary magnesium in vacuum and from an outside tank supply. In the latter case the hydrogen was allowed to flow through a calcium chloride drying tube, a liquid-air trap, a small capillary tube onto a glowing platinum spiral and through another liquid-air trap before introduction into the photo-cell.

Results when using either source for the gas showed an immediate increase in sensitivity and a shift of the threshold from 3430 to 5100A. Pressures of hydrogen ranging from about 10^{-6} or lower to 10^{-1} mm of Hg produced the same shift in the threshold. Fig. 5 shows the effect of admitting different amounts into the cell. The first trace of gas gave rise to a selective maximum at about 4100A and a threshold of 5100A. Pumping practically removed the maximum and produced

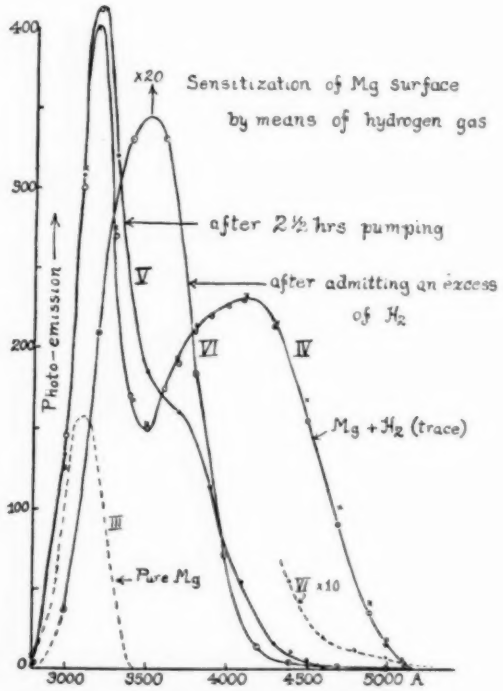

FIG. 5. Effect of hydrogen on magnesium.

a shift in the threshold to about 4700A. An added dose, however, gave the characteristic value at 5100A, but the maximum either disappeared or was masked by the large increase in sensitivity over the range 2800–5100A. Pumping again caused the threshold to recede to 4700A.

The above phenomenon was observed several times, the presence of a trace of hydrogen in the cell giving rise to a threshold at 5100A whereas the absence of the trace gives the value 4700A. Finally a small amount of gas was admitted and caused to dissociate by means of a glow discharge. The threshold again receded from 5100 to 4700A and a rapid "clean-up" of the gas took place. When the magnesium was distilled in the *presence* of hydrogen a characteristic threshold at 5100A always appeared.

These results indicate that at least two definite equilibrium conditions may exist at the surface under the action of hydrogen, one of which is characterized by a threshold at 4700A and is probably due to the effect of atomic hydrogen alone, and the other of which gives rise to a threshold at 5100A and is probably due to both atomic and molecular hydrogen. These results are discussed in more detail later.

[6] DuBridge and Roehr, Phys. Rev. **42**, 52 (1932).
[7] Cardwell, Phys. Rev. **38**, 2041 (1931); **47**, 628 (1935).

It was possible to obtain the energy distribution of the resolved light in the region near 5100A and consequently Fowler's theory could be applied to an activated surface at room temperature. The experimental points were found to fit the theoretical curve and the threshold was shifted from the apparent value 5100A to the true value at 5040A. Others[8] have obtained similar checks on the theory using activated surfaces so that it seems established that the theory may now be applied to homogeneous activated surfaces as well as clean surfaces.

Oxygen on magnesium

Considerable difficulty was encountered in obtaining pure oxygen. Spectroscopic examination of samples prepared in various ways generally indicated the presence of minute traces of hydrogen and carbon monoxide. A method was finally developed by which oxygen was obtained from mercuric oxide by heating.

The oxygen passed through a liquid-air trap to a jet, from which it streamed against a glowing platinum spiral and through another liquid-air trap to the photo-cell. A spectroscopic analysis with exposure times as long as 15 hours revealed only the presence of oxygen. At room temperatures the mercuric oxide evolved no oxygen so that a controllable heater provided a convenient means of obtaining very small traces of the gas.

The sensitization and final desensitization of a magnesium surface by oxygen is shown in the curves of Fig. 6. The initial sensitization occurred at a pressure of 10^{-7} mm of Hg or less. The maximum shift in the threshold toward the red was from 3430 to about 5700A (see curve III). Further exposure produced a decrease in sensitivity and a recession of the threshold toward the violet. Pumping, however, brought the threshold back to 5700A. As long as the gas pressure was small it was found that this phenomenon could be repeated.

Finally oxygen was allowed to flow slowly into the cell. As the threshold receded into the ultraviolet, curves IV, V, VI and VII were taken. The procedure was to set the monochromator at different wave-lengths as quickly as possible and determine the corresponding emission currents. Since the sensitivity was continually changing the curves are only rough approximations. Eventually the threshold receded to a value below 2000A and pumping the tube failed to restore the sensitivity.

Oxygen and hydrogen on magnesium

If a layer of magnesium is laid down in the presence of slight traces of hydrogen and oxygen in the tube, remarkable increases in sensitivity and decreases in work function may be observed. The response to unresolved light may be as high as 10^6 times the response of the pure layer, and the corresponding threshold has been found as far out as 7000A. The *yield* to white light, however, is very small when compared with ordinary commercial caesium oxide cells.

Discussion of Results

These experiments show that the threshold 5100A obtained previously by the authors[1] is characteristic not of pure magnesium but of magnesium contaminated with hydrogen. In the early work sufficient time was not spent during the heating and vaporizing period. It is now obvious that when hydrogen and magnesium come off together from a specimen of the metal at a rapid rate, dispersal gettering occurs and a condensed layer containing both elements will be formed.

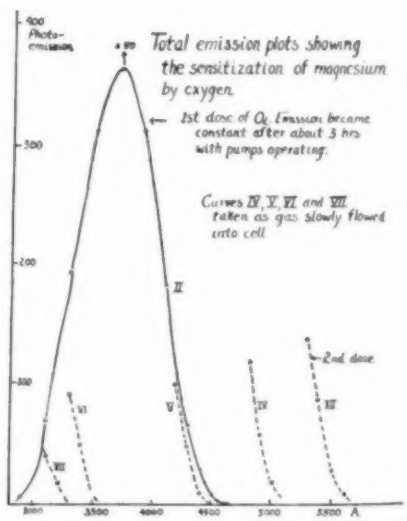

FIG. 6. Effect of oxygen on magnesium.

[8] DuBridge, Phys. Rev. **46**, 339A (1934) (sodium on nickel); Jamison, unpublished results (thoriated tungsten).

On the other hand, the constancy and reproducibility of the threshold 3430A, obtained from surfaces formed by repeated distillation and very slow sublimation following the methods given above, provide convincing evidence that the layers are gas-free. The result is in good agreement with the values 3400A obtained by Déjardin and Schwegler[9] and 3300A, obtained by Kenty,[10] for pure magnesium surfaces.

That the discordant results obtained by other investigators arise from contamination by hydrogen or oxygen, or both, is shown by the gas study. All the published values fall within the limits set by the present work, which range from 2000A or less for heavily oxidized magnesium to 7000A, the threshold observed when magnesium is distilled in the presence of traces of hydrogen and oxygen. The high photoelectric efficiency for magnesium reported by de Laszlo[11] (1 electron per 100 quanta at 3130A) as compared to the low value found by Déjardin and Schwegler[9] (1 electron per 25,000 quanta at 3130A) may be attributed to activation by hydrogen or oxygen, since the sensitivity at 3130A has been increased several hundred-fold by the authors through application of traces of these gases.

Effect of oxygen on other metals

Oxygen has the effect of increasing the work function of electronegative metals, the most noted example being that of tungsten.[12] Others[13] have obtained similar results for gold, silver, palladium, platinum, tantalum and molybdenum. For the more electropositive metals, however, most observers report a sensitization by small traces of oxygen. Olpin[14] and Selenyi[15] have produced shifts in the threshold of sodium of about 1000A toward the red. Koller[16] and others have sensitized caesium with oxygen. Renschler and Henry[17] have lowered the work functions of uranium, calcium and thorium by exposing these elements to traces of oxygen whereas heavy dosing completely destroyed all photoelectric activity.

Interpretation of results for magnesium

Calculations based on the Sommerfeld model for the electrons in a metal show that changes in the inner work function, W_i, under the action of absorbed gases, are too small to account for the large changes in work function observed. It is believed that the phenomena are due to changes in the character of the surface of the metal, presumably by the formation of an electric double layer and hence the observed results are attributed to changes in the outer work function, W_a.

To account on a classical basis for the observed decrease in work function when a sparse distribution of atoms of an alkali or alkali earth metal are deposited on an electronegative metal base such as tungsten, Langmuir, Becker, Suhrmann, De Boer and others have assumed an electric double layer, formed by + ions of the electropositive material and their images in the metal underneath. If the ionization potential of the adsorbed particle is much higher than the work function of the base metal experiments have shown that the work function is increased.

Thus in our experiments an adsorbed hydrogen molecule (ionization potential, 16 volts) or an adsorbed oxygen molecule (ionization potential, 12.5 volts) certainly would not be expected to give up an electron to the magnesium undercoating (work function, 3.60 volts). If dissociation of the molecules takes place the ionization potentials of the resulting atoms are still too high (13.6 volts for O and 13.5 volts for H). Even if one assumes that magnesium atoms in some way detach themselves from the metal, get on top of the adsorbed gas layer and a portion become positive ions (ionization potential 7.61 volts) the work function should vary continuously with the number of adsorbed molecules, a conclusion in agreement with the oxygen experiments, but not the hydrogen experiments.

In order to account for the observed results on a classical basis we may assume that polar molecules are formed at the surface between magnesium atoms and atoms of the gas. This

---

[9] Déjardin and Schwegler, Comptes rendus **196**, 1585 (1933).
[10] Kenty, Phys. Rev. **44**, 891 (1933).
[11] de Laszlo, Phil. Mag. **13**, 1171 (1932).
[12] Langmuir, J. Am. Chem. Soc. **38**, 2221 (1916); Warner, Proc. Nat. Acad. Sci. **13**, 56 (1927).
[13] Hughes and DuBridge, *Photoelectric Phenomena* (McGraw-Hill, 1932), p. 78.
[14] Olpin, Phys. Rev. **36**, 251 (1930).
[15] Selenyi, *Photoelectric Cells and Their Application* (Sir Isaac Pitman and Sons, 1929), p. 25.
[16] Koller, Phys. Rev. **36**, 1639 (1930).
[17] Renschler and Henry, Phys. Rev. **47**, 807A (1935).

assumption seems reasonable since O_2 or H_2 possess no permanent dipoles and under the influence of van der Waals forces alone at the surface would not have any dipoles induced in them. On the other hand nonhomonuclear molecules as a rule possess permanent dipoles. By making assumptions as to the orientation and number per cm², the value of the dipole for the different molecules is calculated below, and the results indicate the correct order of magnitude when compared to similar molecules.

For hydrogen on magnesium the threshold shift from 3430 to 4700A is attributed to the formation of a single layer of MgH molecules on the surface having a positive component of the dipole outward from the metal and the number per cm² the same as the number of Mg atoms per cm² at the surface. The experiments indicate that this surface layer of molecules is permanent and any hydrogen which diffuses into the metal must come from the outside. The second shift from 4700 to 5100A obtained when traces of hydrogen are admitted is attributed to induced dipoles in weakly adsorbed hydrogen molecules. An equilibrium condition must then exist at the surface between molecules coming in from the outside, molecules leaving the surface outwardly and molecules or atoms diffusing into the interior.

The change in potential experienced by an electron in going through an electric double layer is $\Delta\varphi = 4\pi NP$, where N is the number of dipoles per cm² and P the dipole moment. By taking 1.59A as the radius of the magnesium atom (from crystal structure data) the number of MgH molecules per cm² is assumed to be

$$N_{MgH} = (1.59 \times 2 \times 10^{-8})^{-2} \text{ per cm}^2.$$

If 4700A (2.62 volts) is the threshold corresponding to this maximum surface coverage, the value for $\Delta\varphi$ is $3.60 - 2.62 = 0.98$ volt or 3.3×10^{-3} e.s.u. Assuming that all of the normal component of the dipole contributes to the change in work function,

$$P_{MgH} = \frac{\Delta\varphi}{4\pi N} = \frac{3.3 \times 10^{-3}}{4\pi(1.59 \times 2 \times 10^{-8})^{-2}}$$

$$= 0.26 \times 10^{-18} \text{ e.s.u.}$$

The maximum shift in the threshold of magnesium from 3430 to 5700A when exposed to oxygen is assumed to be due to the formation of a single layer of MgO molecules oriented with a positive component of the dipole outward from the metal. The final desensitization in which the threshold recedes to a value below 2000A is attributed to a thick coating of MgO, the emitting layer being characteristic of this compound and not of magnesium.

If it is assumed that the number of MgO molecules per cm² is the same as the number of magnesium atoms per cm² of surface, similar assumptions and calculations as were made above lead to the value

$$P_{MgO} = 0.38 \times 10^{-18} \text{ e.s.u.}$$

In like manner the shift of the threshold of magnesium from 3430 to 7000A when exposed to traces of oxygen and hydrogen is assumed to be due to the formation of a single layer of MgOH molecules. The value of the dipole moment of this molecule, using similar assumptions, becomes

$$P_{MgOH} = 0.51 \times 10^{-18} \text{ e.s.u.}$$

The magnitudes of these dipole moments fall within the range of measured values of the moments of several nonhomonuclear molecules for which experimental data exist. If there is appreciable deformation of the molecules adsorbed on the surface their dipole moments may differ somewhat from the measured values for the same molecules in the gas state. The agreement in order of magnitude of the moments calculated from the change in photoelectric threshold and those of similar molecules measured by other methods, provides considerable evidence for the existence of nonhomonuclear molecules on the surface of magnesium contaminated with certain gases.

Disintegration of Lithium by Deuterons

T. W. BONNER* AND W. M. BRUBAKER, *Kellogg Radiation Laboratory, California Institute of Technology*

(Received August 21, 1935)

The energy distribution of the neutrons from the disintegration of lithium by 0.85 MEV deuterons has been determined by the method of recoil protons in a high pressure cloud chamber. The results of the experiment indicate that the neutrons come from the two reactions

$_3Li^7+{}_1H^2\rightarrow 2{}_2He^4+{}_0n^1$; $_3Li^7+{}_1H^2\rightarrow {}_4Be^8+{}_0n^1$.

The neutrons from the first reaction (95 percent of the disintegrations) have a continuous energy distribution, while the neutrons from the second reaction (5 percent of the disintegrations) are nearly homogeneous, with a maximum energy of 13.3±0.5 MEV. From these data, the mass of $_4Be^8$ was calculated to be 0.3±0.75 MEV greater than that of two alpha-particles.

WHEN lithium is bombarded by deuterons, the following nuclear reactions are known to occur:

$$_3Li^6+{}_1H^2\rightarrow 2{}_2He^4; \quad (1)$$
$$_3Li^6+{}_1H^2\rightarrow {}_3Li^7+{}_1H^1; \quad (2)$$
$$_3Li^7+{}_1H^2\rightarrow 2{}_2He^4+{}_0n^1. \quad (3)$$

The first two of these reactions have been investigated by Lawrence,[1] Dee and Walton,[2] Oliphant, Kinsey and Rutherford,[3] and by Cockcroft and Walton.[4] The emission of neutrons when lithium is bombarded by deuterons was first reported by Crane, Lauritsen and Soltan.[5] Experiments done with the separated isotopes of $_3Li^6$ and $_3Li^7$ by Oliphant, Shire and Crowther[6] have shown that the disintegration products had been attributed to the proper isotope.[7] Oliphant, Kempton and Rutherford[8] have determined the energies of the alpha-particles liberated in reaction (3).

The purpose of the experiment described below was to investigate the energy distribution of the neutrons liberated in the disintegration of lithium by 0.85 MEV deuterons. In particular, we were interested in determining the maximum energy of the neutrons, and in investigating the probability of the transformation of $_3Li^7$ into $_4Be^8$ according to the reaction

$$_3Li^7+{}_1H^2\rightarrow {}_4Be^8+{}_0n^1. \quad (4)$$

There is evidence that $_4Be^8$ is formed in other disintegrations. Kirchner and Neuert[9] proposed the reaction

$$_5B^{11}+{}_1H^2\rightarrow {}_4Be^8+{}_2He^4$$

and Crane and Lauritsen[10] suggested that the γ-rays emitted when lithium is bombarded with protons may indicate the formation of Be^8 by capture.

We have already published, in a Letter to the Editor[11] a preliminary report of the evidence for the formation of $_4Be^8$ in the disintegration of lithium by deuterons.

Experimental Procedure

In previous papers[12] we have described our method of determining neutron energies by observing recoil proton tracks in a high pressure cloud chamber filled with methane. We can measure a track approximately 8.8 cm long in our chamber; hence, when the chamber is operated at an expanded pressure of 14.7 atmospheres it will stop a particle which has a range of 126 cm in air. In the present experiment, we have altered our procedure due to the very long ranges (over 190 cm in air) of the recoil protons projected by neutrons released in the disintegration of lithium. We placed a sheet of mica of 114 cm air equivalent across the center of the chamber in a plane perpendicular to a line drawn to the target. With this apparatus a series of runs were made in which we were able to investigate the range interval of approximately 125 cm to 240 cm, or the energy interval of 10.5 MEV

* National Research Fellow.

[1] Lawrence, Phys. Rev. **44**, 55 (1933).

[2] Dee and Walton, Proc. Roy. Soc. **A141**, 733 (1933).

[3] Oliphant, Kinsey and Rutherford, Proc. Roy. Soc. **A141**, 722 (1933).

[4] Cockcroft and Walton, Proc. Roy. Soc. **A144**, 704 (1934).

[5] Crane, Lauritsen and Soltan, Phys. Rev. **44**, 692 (1933).

[6] Oliphant, Shire and Crowther, Nature **133**, 377 (1934).

[7] We might also expect to observe neutrons from the reaction $_3Li^6+{}_1H^2\rightarrow {}_2He^4+{}_2He^3+{}_0n^1$ which appears to be exothermic by 1.3 MEV, but apparently this mode of disintegration is quite improbable.

[8] Oliphant, Kempton and Rutherford, Proc. Roy. Soc. **A149**, 406 (1935).

[9] Kirchner and Neuert, Physik. Zeits. **35**, 293 (1934).

[10] Crane and Lauritsen, Phys. Rev. **47**, 420 (1935).

[11] Bonner and Brubaker, Phys. Rev. **47**, 973 (1935).

[12] Brubaker and Bonner, Rev. Sci. Inst. **6**, 143, (1935); Phys. Rev. **47**, 910 (1935).

1A 1B

FIG. 1. Recoil protons in the cloud chamber when operated at 14.7 atmospheres pressure.

2A 2B

FIG. 2. Photographs of recoil protons which penetrate the mica sheet in the center of the chamber. On *A* there is a proton of range 123 cm, which made a collision with a proton near the end of its range. The recoil proton in *B* which goes through the mica had a range of 168 cm.

to 15.3 MEV. With a sheet of mica of 58 cm air equivalent, we investigated the energy interval of 8.4 MEV to 11.2 MEV, and with no mica in the chamber we covered the interval 2.2 to 8.4 MEV. Because the tracks of the lower energy protons were too short to be observed at a pressure of 14.7 atmospheres, two more series of runs were made. In one of these we used methane at a pressure of 2.67 atmospheres, and in the other we used hydrogen at a pressure of $\frac{1}{2}$ atmosphere.

We measured only those proton tracks which made angles less than 8° with a line drawn to the center of the source. A proton projected at an angle of 8° by a neutron gets 98.1 percent of its energy, so recoil protons which are projected at angles less than 8° have essentially the same energy as the incident neutrons. Our previous work on the neutrons from beryllium[12] has shown that the number of tracks caused by scattered neutrons which appear to be in this angular interval is very small.

The ranges of the recoil protons were computed from the track lengths and the calculated stopping power of the gas and the mica sheet.[13] These proton ranges were then converted into proton energies by the range-velocity curve of Mano.[14] A correction has been applied to the data of each run to compensate for the unequal probabilities of observing tracks of different lengths in the chamber. This was particularly important when the mica sheet was used.

The effect of the small amount of proton contamination in the deuteron ion beam was examined by making a control run in which the bombarding ions were protons. There were less than 1/200 as many recoil protons photographed as when deuterons were used, which indicates that the proton impurity could not have been responsible for more than 1/2000 of the observed neutrons. In test runs which were made when the lithium chloride target was replaced by a brass one, less than 1/200 as many recoil protons were photographed. The few tracks which were observed were probably due to the reaction

$$_1H^2+{}_1H^2\rightarrow{}_2He^3+{}_0n^1.$$

However, in the present experiment the number of neutrons obtained from the bombardment of the absorbed deuterium on the target is so small that it is unimportant.

Results

We have taken a total of 19,600 sets of stereoscopic photographs on which there were approximately 60,000 recoil protons. Examples of such photographs of the recoil protons are given in Figs. 1 and 2. From these photographs we have measured the ranges of 1550 recoil protons which were projected in nearly the forward direction (0°–8°). The energy distribution of these recoil protons is given in Fig. 3. The curve includes data from five overlapping series of runs which were fitted together as shown. In the lower energy portion of the curve, the number of tracks in a given 0.4 MEV interval was only about half of the number indicated.

The upper curve of Fig. 3 gives the distribution of recoil protons but not necessarily the distribution of the primary neutrons. A variation in the neutron-proton collision area with energy would make the neutron distribution curve differ from the proton curve.[15] It is well known that the collision area increases as the energy of the neutrons decreases. In order to obtain the neutron distribution curve, we have taken into account the experimental variation of collision area with neutron energy as found by Bonner[16] and Dunning.[17] The collision areas[18] used were: $E\approx 0, \sigma=31\times10^{-24}$; $E=1.2$ MEV, $\sigma=5.8\times10^{-24}$; $E=2.1$ MEV, $\sigma=3.2\times10^{-24}$; $E=5$ MEV, $\sigma=1.68\times10^{-24}$. Thus we get the dotted curve of Fig. 2, which we believe to be the approximate form of the neutron distribution curve. It exhibits a broad maximum near 2.1 MEV; this indicates that the most probable energy of the

[13] The gas in the chamber was 85.1 percent CH_4, 13.5 percent C_2H_6, and 1.4 percent N_2. The corresponding stopping powers were 0.86 for methane, 1.52 for ethane, and 0.99 for nitrogen. The stopping power of the mica was computed in the usual manner, using the value 1.43 mg sq. cm equivalent to one cm air.

[14] G. Mano, J. de phys. et rad. **5**, 628 (1934).

[15] Any change with energy in the angular distribution of neutron-proton collisions would also alter the neutron distribution curve from the one shown.

[16] T. W. Bonner, Phys. Rev. **45**, 601 (1934).

[17] J. R. Dunning, Phys. Rev. **45**, 586 (1934); Dunning, Pegram, Fink and Mitchell, Phys. Rev. **47**, 970 (1935).

[18] Because of differing geometrical conditions the absolute values of the target areas obtained by Bonner and Dunning were not the same, so all of Bonner's data have been multiplied by the factor 2.3 to give the same cross section as Dunning for 5 MEV neutrons.

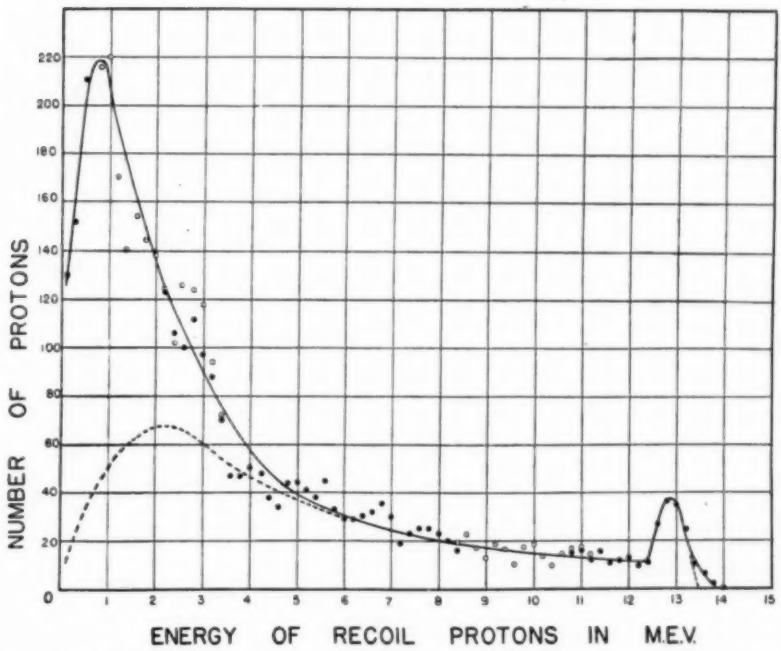

FIG. 3. The energy distribution of the recoil-protons (upper curve) primary neutrons (dotted curve).

neutrons released in the disintegration of lithium by deuterons is approximately 2.1 MEV. The mean energy under the neutron curve is 3.9 MEV.

It is possible to correlate this mean neutron energy with the mean energy of the alpha-particles which are produced in the same disintegration. Oliphant, Kempton and Rutherford[8] obtained the distribution-in-range of the alpha-particles with a differential counter, which counts the number of particles in the range interval between x and $x+\Delta x$. The corresponding energy interval, ΔE, is not a constant but is a function of x. Hence, when their data are transformed to equal energy intervals and plotted, it appears as in the curve of Fig. 4, which exhibits a maximum near 6.8 MEV. The mean energy under this curve is approximately 5.0 MEV. If we rather arbitrarily add 0.2 MEV to this value to compensate for the depth of the counting chamber, we have 5.2 MEV as the mean alpha-particle energy, in which case the mean energy of the two alpha-particles is 10.4 MEV. When this is added to the mean neutron energy of 3.9 MEV, we get 14.3 MEV for the kinetic energy appearing after the disintegration. These results were taken from two different experiments; in one of these the bombarding energy was 0.2 MEV and in the other it was 0.85 MEV. While we are uncertain as to how much of the bombarding energy appears in the respective disintegration products, we have estimated that 0.3 MEV should be subtracted if we wish to represent the case of zero bombarding energy in both cases. This calculation gives 14.0 MEV as the energy released in the disintegration. Considering the uncertainties in the mean energies of the disintegration particles, this result checks as well as could be expected with the value of 14.6 ± 0.25 MEV found by Oliphant, Kempton and Rutherford.[8]

MASS OF $_4Be^8$

The recoil proton distribution curve, Fig. 3, shows a pronounced hump near 13 MEV, which

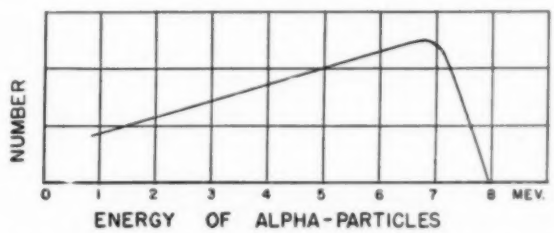

FIG. 4. The energy distribution of the alpha-particles (data of Oliphant, Kempton and Rutherford for oscillograph kicks greater than 1 cm, replotted in equal energy intervals).

we have interpreted as being due to the transformation of $_3Li^7$ into $_4Be^8$ and a neutron, as postulated in reaction (4). The area under the hump is approximately 5 percent of the area under the entire curve; this indicates that $_4Be^8$ is formed in 5 percent of the disintegrations.

As the neutrons were observed at right angles to the incident deuterons, the energy of disintegration, Q, is given by

$$Q=9/8E_N-3/4E_H,$$

where E_N is the neutron energy and E_H is the energy of the incident deuteron. The extrapolated maximum neutron energy is 13.4 ± 0.5 MEV. Because Mano's range-velocity curve is for mean and not extrapolated range, we have subtracted 0.1 MEV from our extrapolated energy. Using a neutron energy of 13.3 MEV and a bombarding energy of 0.85 MEV, we find that $Q=14.3\pm0.5$ MEV. From the value of 14.6 ± 0.25 MEV found by Oliphant, Kempton and Rutherford for the energy of disintegration into two alpha-particles and a neutron, we calculate the mass of $_4Be^8$ to be 0.3 ± 0.75 MEV greater than that of two alpha-particles. A recalculation of Kirchner's mass of $_4Be^8$ with Bethe's new isotopic scale[19] gives a mass just equal to that of two alpha-particles. Recently, Oliphant, Kempton and Rutherford[20] have shown that $_4Be^8$ is formed according to the reactions $_4Be^9+{}_1H^1\rightarrow{}_4Be^8+{}_1H^2$; $_4Be^9+{}_1H^2\rightarrow{}_4Be^8+{}_1H^3$ and find a mass of $_4Be^8$ which is 0.2 MEV greater than that of two alpha-particles. The present evidence seems strongly to indicate the existence of a $_4Be^8$ nucleus with a mass slightly greater than that of two alpha-particles, although a mass equal to or less than that of two alpha-particles cannot be excluded at the present time.

We wish to thank Professor C. C. Lauritsen for valuable suggestions made during the progress of this work, and the Seeley W. Mudd Fund for its financial support.

[19] H. A. Bethe, Phys. Rev. **47**, 633 (1935).
[20] Oliphant, Kempton and Rutherford, Proc. Roy. Soc. **A150**, 241 (1935).

NOVEMBER 1, 1935 PHYSICAL REVIEW VOLUME 48

On the Nuclear Moments of Lithium, Potassium, and Sodium[1]

MARVIN FOX AND I. I. RABI, *Columbia University*
(Received August 7, 1935)

The atomic beam method of "zero moments" was applied to the measurement of the nuclear spin and hfs separation of the normal $^2S_{\frac{1}{2}}$ state of Li^7. The experimental arrangement was such that the precision obtained was about 1 percent. It was verified that the nuclear spin was 3/2, and the hfs separation was measured to be 0.0268 ± 0.0003 cm^{-1}. By using the modified Goudsmit formula the nuclear magnetic moment was calculated to be 3.20 nuclear magnetons compared with the value of 3.28 calculated from hyperfine structure measurements on the $^3P_0-{}^3S_1$ group (λ5485) of $(Li^7)^+$ by Breit and Doerman using wave functions. The same method applied to potassium and sodium yielded hfs separations of 0.0154 ± 0.0002 and 0.0596 ± 0.0006 cm^{-1}, respectively, which lead to nuclear magnetic moments of 0.397 and 2.08 nuclear magnetons. With another arrangement of the apparatus yielding higher resolution than was previously obtained it was possible to set the value of 5/2 as an upper limit for the spin of the K^{41} nucleus. With the same arrangement applied to lithium it was found that the nuclear spin of Li^6 is 2/2 or greater and that the magnetic moment of the nucleus is of the order of magnitude of that of the deuteron.

INTRODUCTION

THE hyperfine structure of the $(Li^7)^+$ spectrum and the band spectra of the Li_2^7 molecule have been studied by a number of investigators.[2] The band spectra results have yielded a value of $3/2\ h/2\pi$ for the nuclear spin of Li^7, which is consistent with the results

[1] A preliminary report on the spin and magnetic moment of Li^7 was given at the Washington meeting of the Am. Phys. Soc. Fox, Millman and Rabi, Phys. Rev. **47**, 801 (1935).

[2] Schüler, Zeits. f. Physik **66**, 431 (1930); Harvey and Jenkins, Phys. Rev. **35**, 789 (1930); Güttinger and Pauli, Zeits. f. Physik **67**, 743 (1931); Goudsmit and Inglis, Phys. Rev. **37**, 328 (1931); Granath, Phys. Rev. **42**, 44 (1932); Ladenburg and Levy, Zeits. f. Physik **88**, 449 (1934).

obtained from the hyperfine structure studies.* The hyperfine structure measurements were made on the $^3P_0-{}^3S_1$ group (λ5485) of Li^+. The separations were large enough to yield very precise values, from which the magnetic moment of the Li^7 nucleus has been calculated with the theory of Breit and Doerman,[3] to be 3.28 nuclear magnetons. The hyperfine structure of the levels of neutral Li^7 is not suitable for spectroscopic study. In view of the probable importance of an accurate knowledge of nuclear moments, particularly those of the lighter elements, in connection with a theory of nuclear structure, these experiments were undertaken with the object of measuring accurately the hfs separation of the normal $^2S_{1/2}$ state of the Li^7 atom. For experiments of this type the method of "zero moments" by using atomic beams[4] is most suitable. The results of the experiments to be described will allow a comparison of the theory of Breit and Doerman, which depends on the calculation of wave functions, with the semi-empirical theory of Goudsmit[5] and Fermi and Segrè.[6] Since in experiments of this type the precision is equally good for large and small hfs separations, it was considered desirable to measure also the hfs separations of the normal states of K^{39} and Na^{23} with a view toward obtaining greater precision than was obtained in previous experiments. In addition it was hoped that some information about the nuclear spins and hfs separations of the normal states of Li^6 and K^{41} would be obtained.

The experimental method involved is fully described in recently published papers.[4]

Apparatus

The apparatus, shown schematically in Fig. 1, which had been previously used to investigate the nuclear moments of the principal isotopes of potassium,[4] was modified to attain greater precision. A new duralumin field block supporting two wires of twice the diameter of those in the field block used in the potassium work was constructed. This resulted in a decrease of the ratio of the gradient to the field by one-half. If Δy is the error in measuring the distance between the atomic beam and the field wires, then

$$\frac{\partial H/\partial y}{H}\Delta y=\frac{\Delta H}{H}$$

and consequently there is a gain in precision in reducing the ratio of the gradient to the field. There is, of course, a corresponding reduction in resolution which was partly compensated for by using narrower beams. There is an additional gain in precision due to the fact that the field and the gradient become more uniform over the height of the beam with an increase in the size of the wires. The height of the beam was limited to 1.5 mm and the beam passed along the field wires at a distance of a few hundredths of a mm from the surface. The collimating slit was 0.012 mm and the oven slit was 0.010 mm.

Procedure

The procedure is similar to that followed in the work on potassium.[4] The temperature of the oven was raised to about 600°C over a period of three hours and then stabilized. Before any magnetic field was impressed a plot was made of the intensity of the beam with respect to the position of the detector. We shall refer to this plot as the shape of the original beam. The end of the field block toward the detector was then moved a measurable distance until a one-mil filament mounted at a measured distance from the surface of the wires at this end of the block was exactly in the center of the original beam. With this "stopping filament" so situated, the beam pattern at the position of the detector shows a minimum of intensity at the center of the original beam and maxima on either side of this shadow cast by the stopping filament. The collimating slit having been set by means of a telescope at a measured distance from the surface of the wires at the end of the field block toward the oven, the position of the beam with respect to the wires was then known. The collimating slit was then moved a measured distance either toward or away from the field block so that the stopping filament no longer intercepted the beam, and this new

* Some slight doubt has been cast upon this result by the studies of Ladenburg and Levy whose results indicate a nuclear spin of 5/2.

[3] Breit and Doerman, Phys. Rev. **36**, 1262 (1930).

[4] Cohen, Phys. Rev. **46**, 713 (1934); Millman, Phys. Rev. **47**, 739 (1935).

[5] Goudsmit, Phys. Rev. **43**, 636 (1933).

[6] Fermi and Segrè, Zeits. f. Physik **82**, 729 (1933).

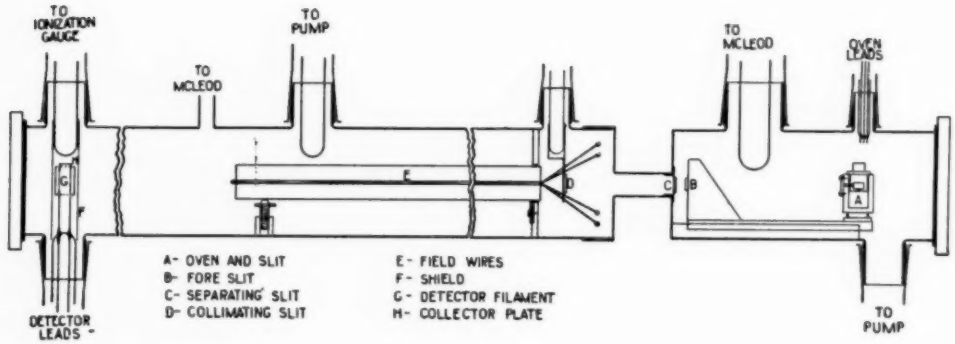

FIG. 1.

position of the beam with respect to the field wires was known precisely. This procedure (unlike that followed in the potassium work where the stopping filament was burned out after being set in the position where it intercepted the beam) was followed so that the stopping filament was always available for resetting the position of the beam with respect to the field wires. Measurements were made with the beam passing between the stopping filament and the wires and also with it passing on the side of the filament away from the wires. The apparatus was taken apart several times and the stopping filament was set at different distances from the surface of the field wires and at different positions along the field block near the detector end. After reassembling the apparatus, the collimating slit was set by means of a calibrated telescope at a measured distance from the surface of the field wires independently for each run. In this way the possibility of a systematic error in the position of the beam was greatly reduced.

Runs were made with lithium, potassium, and sodium in the oven separately and also with mixtures of potassium and lithium present. In the cases where a mixture was in the oven, the temperature of the oven was first raised to the working temperature for potassium and measurements were made. When the potassium was finally boiled off completely (after a few hours), the temperature was raised to the lithium working temperature and measurements again were made. The results of such measurements gave not only very precise values for the hfs separations of potassium and lithium, in agreement with values obtained from runs taken on each element separately, but also precise ratios of their hfs separations.

DISCUSSION OF PRECISION

The precision of our measurements does not depend on a knowledge of the temperature of the oven, on the distribution of velocities of the atoms in the beam, or on an accurate knowledge of the original beam shape. There are four factors which affect the precision:

(1) The determination of the ammeter reading of the current in the field wires at which the intensity of the "zero moment" peak is a maximum. In making this determination the current was varied in small steps and the resulting intensities were recorded. It was found that the ammeter readings corresponding to the determinations of the maximum intensities did not differ amongst themselves by more than 1/3 percent for a particular setting of the beam position. As numerous readings were taken the errors arising from this source could hardly exceed 1/5 percent.

(2) The conversion of the ammeter readings to current. This depended on the calibration of the shunt used and on the reading of a potentiometer measuring the potential difference across the shunt. The shunt resistance was measured with a Kelvin double bridge and was found to agree with the factory calibration to about 1/5 percent. The standard cell used with the potentiometer was checked against a factory calibrated standard. The currents carried by the shunt were always considerably below the rated capacity.

(3) The effect of stray magnetic fields. This was eliminated by making a determination of the current at which the intensity of the "zero moment" peak is a maximum with the magnetic field in one direction and repeating with the magnetic field reversed.

(4) The determination of the position of the beam with respect to the field wires, from which the effective magnetic field traversed by the beam can be calculated. This involves the measurement of a number of geometric

quantities and constitutes the largest source of error in the experiment. The beam was located with respect to two points along the length of the wires, i.e., the collimating slit and the stopping filament, in the manner described above. The field wires were examined for uniformity of cross section and were found to be circular and uniform to within 0.003 mm, the average diameter being 4.767 mm. The duralumin block which supports the wires was examined for straightness by stretching a No. 40 copper wire along its surface so as to be taut, and measuring the distance between this wire and the surface of the block with a microscope. The microscope axis was vertical so that any sag in the wire had no effect on the measurements. This examination showed the block to be straight to 0.004 mm. In addition, a point to point plot of the straightness of the wires after being mounted in the block was made by using a "last word" indicator calibrated to 1/10,000 in., and this plot showed that the wires were straight to within 0.005 mm. A further correction to the effective magnetic field corresponding to the maximum intensity of the "zero moment" peak involves the effects of the ends of the wires where the field and the gradient vary considerably from their values in the central portions of the field. Because of the great length of the field (61.1 cm) compared with the distance between the wire centers 0.4895 cm), this correction is easily made, and serves to lower the effective magnetic field by about 1/2 percent. The total error involved in the determination of the geometry mentioned above we estimate to be about 1 percent.

Results

Li^7

As typical of the agreement between results obtained from different runs, the following is a list of values obtained for the effective magnetic field at which the Li^7 atoms with total magnetic quantum number $m=-1$ have a zero moment: 143.0, 143.1, 143.1, 143.4, 143.2, 143.4, 143.2, 143.2, 143.3 gauss. The precision of our results as indicated by the agreement between these values is not real, however, because of the systematic errors in the measurement of the position of the beam relative to the field wires.

It was verified that the nuclear spin of the Li^7 atom is $3/2\ h/2\pi$ as is readily seen from Fig. 2(A). The hfs separation of the normal $^2S_{1/2}$ state is calculated to be 0.0267 ± 0.0003 cm^{-1}. With the formulae of Goudsmit[5] as modified by Fermi and Segrè,[6] the magnetic moment of the Li^7 nucleus is calculated to be 3.20 nuclear magnetons. In view of the nature of the theory involved in this result, it is in very satisfactory agreement with the value of 3.28 calculated by Breit and Doerman.[3]

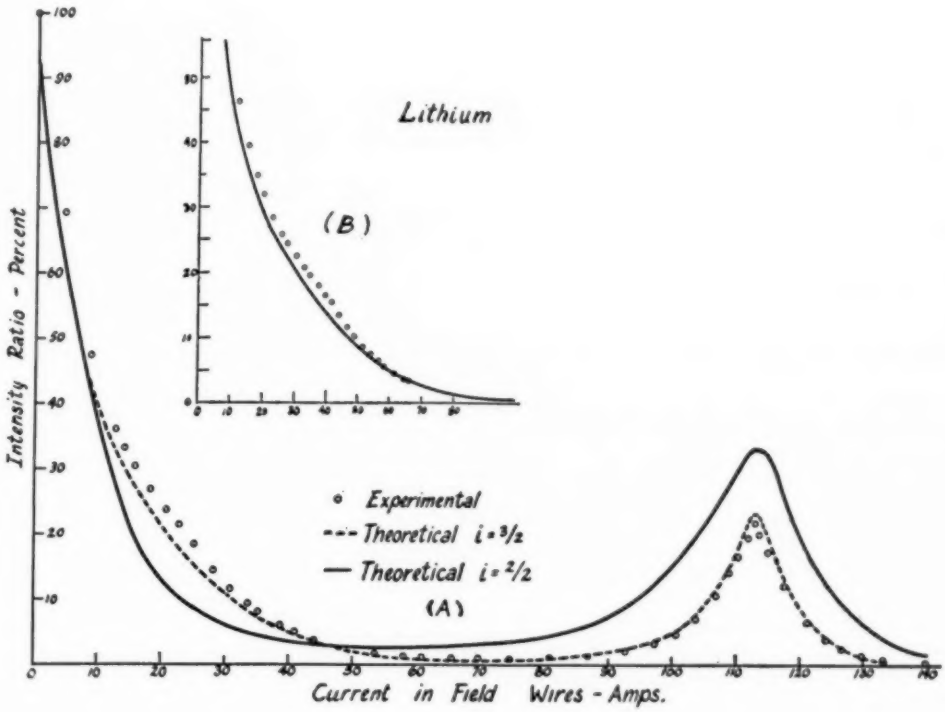

FIG. 2.

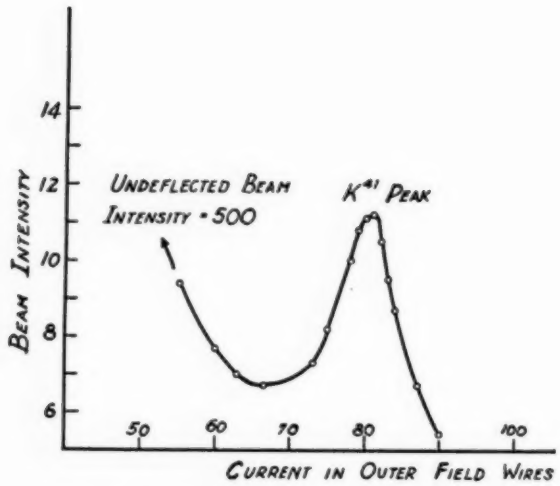

FIG. 3. Four-wire system current ratio 5 : 2.

K^{39}

The hfs separation of the normal $^2S_{1/2}$ state of K^{39} was measured to be 0.0154 ± 0.0002 cm^{-1}, from which the magnetic moment is calculated to be 0.397 nuclear magnetons.

Na^{23}

For Na^{23} the hfs separation of the normal $^2S_{1/2}$ state was measured to be 0.0596 ± 0.0006 cm^{-1}, which is somewhat higher than the value of 0.0583 cm^{-1} obtained by Granath and Van Atta,[7] but in excellent agreement with the result of 0.059 cm^{-1} of Jackson and Kuhn.[7a] Since our experimental result yields an independent measurement of the $^2S_{1/2}$ separation, it can be used in connection with the hyperfine structure measurements of the separations $\delta P_{1/2}-\delta S_{1/2}$ and $\delta P_{3/2}-\delta S_{1/2}$ independent of the cosine law of interaction between the nuclear spin and the total electronic angular momentum. When such calculations are made, the results for the hfs separations of the $^2P_{1/2}$ and the $^2P_{3/2}$ states do not agree with the results of Granath and Van Atta. However the precision of the spectroscopic measurements is not sufficiently good to attach great significance to this disagreement. The nuclear magnetic moment for Na^{23} is calculated to be 2.08 nuclear magnetons. This value may be compared to the value of 2.55 which would be obtained with the Fock wave functions as applied by Wills and Breit[8] and Shoupp, Bartlett and Dunn.[9]

K^{41}

In addition to the experiments described, further experiments on K^{41} and Li^6 were undertaken using the field block used by Millman in the potassium work. By increasing the ratio of the currents in the two sets of wires, the ratio of the gradient to the field was increased to about 15, thus resulting in higher resolution. This enabled us to resolve the "zero moment" peak due to K^{41} more clearly than was done in Millman's work as is shown in Fig. 3. Calculation shows that the background intensity due to the K^{39} atoms is about 1/4 percent of the intensity of the original beam, so that practically all of the intensity of the peak is due to K^{41}. Since the intensity of the peak is of the order of 2 percent of the original beam intensity, the nuclear spin of the K^{41} atom is not likely to be greater than 5/2.

Li^6

It is seen in Fig. 2(A) that the experimental points lie very close to the theoretical curve everywhere except in the region where the current in the field wires is in the neighborhood of 20 amperes. This region of the intensity *versus* magnetic field curve was examined under higher resolution and the departure of the experimental

[7] Granath and Van Atta, Phys. Rev. **44**, 935 (1933).
[7a] Jackson and Kuhn, Proc. Roy. Soc. **A148**, 335 (1935).
[8] Wills and Breit, Phys. Rev. **47**, 704 (1935).
[9] Shoupp, Bartlett and Dunn, Phys. Rev. **47**, 705 (1935).

points from the theoretical curve was more pronounced as is seen in Fig. 2(B). The resolution was not good enough to actually resolve a peak due to Li^6 but it can be assumed, as was originally done with the unresolved peak due to K^{41}, that the discrepancy between the experimental and theoretical intensities is due to an unresolved "zero moment" peak of Li^6. It follows from this that the nuclear spin of Li^6 is 2/2 or greater, and that the ratio of the magnetic moments of the two isotopes of lithium, μ_6/μ_7, can be put between the limits of 0.15 and 0.25, the value depending on the spin of Li^6. If a spin of 2/2 is assumed the magnetic moment of the Li^6 nucleus is calculated to be of the order of magnitude of that of the deuteron.

We are much indebted to Dr. Sidney Millman and other workers in the molecular beam laboratory for their able assistance in the course of these experiments.

NOVEMBER 1, 1935 PHYSICAL REVIEW VOLUME 48

Positive and Negative Thermionic Emission from Molybdenum

H. B. WAHLIN AND J. A. REYNOLDS, *University of Wisconsin*

(Received August 9, 1935)

The positive and negative thermionic emission for molybdenum has been investigated. The electron work function has been found to be 4.17 volts and that of the positive ion 8.35 volts. The positive ion emission has been shown to agree with the Saha theory of ion formation to within the experimental limits of error.

IT has been shown by Smith[1] and by Wahlin[2] that when molybdenum is heated to a sufficiently high temperature, positive ions of the metal itself are emitted. The temperature variation of this ionic current has been studied by Smith[1] and by Barnes[3] with differing results. Smith, following the analysis used by Bridgman[4] in his derivation of the Richardson equation, has derived a positive ion thermionic equation which for molybdenum takes the form:

$$\log_{10} i + 0.453 \log_{10} T + 2.7 \quad 10^{-4}T = -\varphi_{0+}e/2.303kT + C, \quad (1)$$

neglecting any effect of the surface heat of charging. From this equation he computed φ_{0+} to be 6.33 volts. Barnes using the same equation obtains a value of 8.17 volts.

Because of these discordant results it was thought worth while to repeat the experiment with better outgassing conditions than have been used hitherto.

The thermionic tube used was one with a single guard ring and a U type filament. The tube, the potentials used and the outgassing treatment were similar to those described in a study of the positive ion emission from columbium by Wahlin and Sordahl.[5]

Extreme care was exercised in the baking and heating process to eliminate alkaline impurities as far as possible. The baking of the tube was continued for at least 500 hours with the filament at a temperature of about 1700°K and the furnace at a temperature of 450°C. The heat treatment of the filament was then continued at a temperature of 1900°K with occasional flashing to 2100°K or higher until a value for the electron work function, as measured at intervals from a Richardson plot, did not vary with heat treatment for at least 200 hours. After the baking and heat treatment the pressure remained lower than 3×10^{-8} mm when the filaments were varied over the temperature ranges used.

Three disappearing filament optical pyrometers were used in measuring the temperatures. These were calibrated in the usual manner by sectoring up and down from the gold point and then checked against the palladium point. None

[1] L. P. Smith, Phys. Rev. **35**, 381 (1930).
[2] H. B. Wahlin, Phys. Rev. **34**, 164 (1929).
[3] L. L. Barnes, Phys. Rev. **42**, 491 (1932).
[4] P. W. Bridgman, Phys. Rev. **27**, 173 (1926).
[5] Wahlin and Sordahl, Phys. Rev. **45**, 886 (1934).

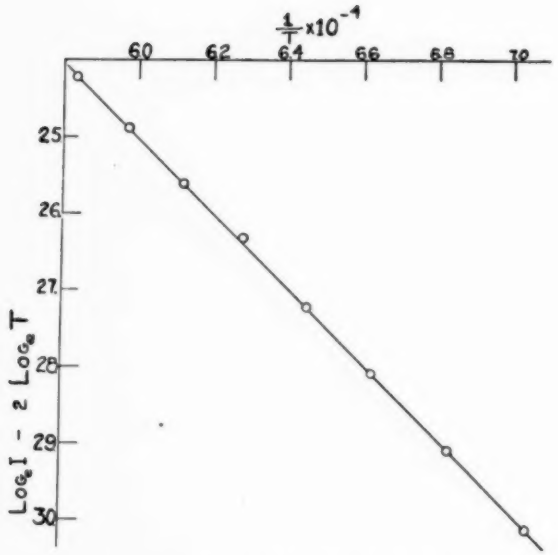

FIG. 1. Richardson plot for electrons.

were found to be as much as 1° in error at this temperature.

The emissivity used in calculating the true temperatures is the constant value 0.382 determined by Whitney.[6]

ELECTRON WORK FUNCTION

Two samples of pure molybdenum 1 mm wide and 0.05 mm thick, obtained from the Fansteel Company gave values for the electron work function of 4.17 volts with a constant $A = 51$. These values were reached after 600 hours of heat treatment and did not change with further degassing up to 1100 hours at temperatures as given above. Fig. 1 shows a Richardson plot for one of these samples. A strip of the metal, of the same dimensions, kindly furnished by Dr. W. E. Forsythe was mounted in the tube after being rolled cold to a uniform thickness. This was given the same initial heat treatment as the others and after about 600 hours gave a work function of 4.25 volts. This value rose with further degassing and flashing to a final value of 4.38 volts in fair agreement with the value found by Dushman. The A for this specimen was found to be 175 amp.$\cdot$cm$^{-2}\cdot$degrees^{-2}. Flashing up to 2600°K did not change this value. A sample of the Fansteel specimen was then mounted after having been cold rolled lightly. This specimen gave a terminal value of 4.30 volts with $A = 96$ amp.$\cdot$cm$^{-2}\cdot$degrees^{-2}.

Whether or not in the rolling process some impurity was introduced could not be determined. A spectroscopic analysis of the specimens failed to reveal any difference. There is a possibility as has been pointed out to the writer by Dr. W. P. Jesse that due to the cold rolling certain crystal faces may come up parallel to the surface of the strip and that these may persist with heat treatment in a vacuum. If this is the case, the difference in the specimens may be due to a difference in the crystalline orientation. However, since the first two specimens gave the most reasonable values for A, it is probable that 4.17 volts represents more nearly the correct value for a pure polycrystalline molybdenum surface. This value, furthermore, is in good agreement with the photoelectric and thermionic value (4.15) obtained by DuBridge and Roehr.[7]

If one assumes a roughness factor for the well outgassed molybdenum surface of 1.25 the true value of the experimental A is 41.0. The deviation of this value from the theoretical 120 is probably due to a temperature variation of the electron work function. Reimann[8] has computed this temperature variation on the assumption that it is due to a change in the zero-point energy of the electrons caused by a change in the number density of the free electrons; this change being due entirely to the expansion of the metal. From his calculation he estimates that the experimental A should be in the neighborhood of 41. However, with the present uncertainty in the roughness factor, the agreement with the determined value may be fortuitous.

POSITIVE ION EMISSION

After steady conditions as indicated by the electron work function study had been obtained, the potential was reversed and the positive ion variation with temperature obtained within the temperature range 2150°K to 2630°K. The currents at low temperatures were measured with a quadrant electrometer and those at high temperatures by means of a sensitive galvanometer.

Fig. 2 shows plots of the log $i+f(T)$ against

[6] L. V. Whitney, Phys. Rev. **48**, 458 (1935).

[7] DuBridge and Roehr, Phys. Rev. **42**, 32 (1932).

[8] A. L. Reimann, Nature **133**, 833 (1934).

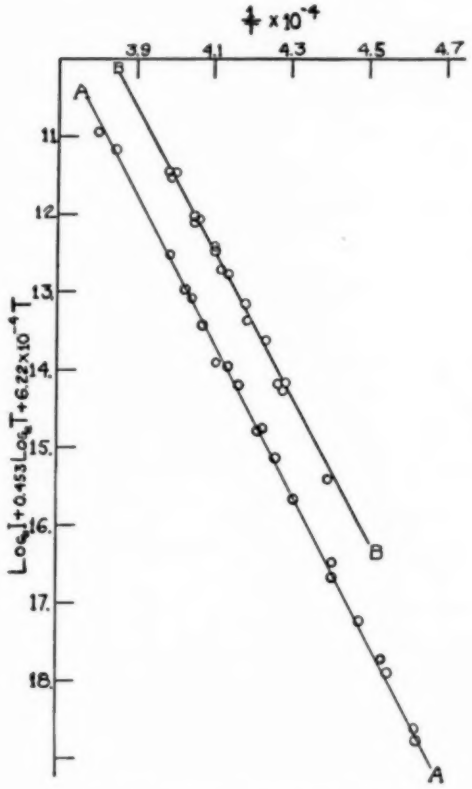

FIG. 2. Richardson plot for positive ions.

$1/T$ for the positive ion current, using Smith's equation. As will be noticed the curves are linear within the limits of experimental error over the entire temperature range. Barnes' plots show a definite curvature thus indicating the presence of an ionic impurity. Curve A is the plot for a specimen with electron work function of 4.17 volts and curve B for one with an electron work function of 4.38 volts.

The positive ion work function computed from the slope of these curves is 8.3 volts for curve A and 8.21 for curve B. These values are only slightly higher than the value found by Barnes (8.17 volts). This would seem to indicate that the impurity which acted to produce the curvature in his results did not greatly affect the slope at the higher temperatures. The points on the two curves in Fig. 2 represent data taken intermittently over a period of at least 100 hours of flashing and heat treatment. No progressive change in the current at a given temperature could be noticed during this time. One can conclude therefore that a steady condition had been reached.

It is to be noted that the positive ion current from the specimen with the higher electron work function is greater than the other by a factor of nearly 3. At first it was thought that this was due to the presence of an impurity ion but a mass spectrograph analysis failed to reveal the presence of a measurable amount of any such contamination.

The difference is, however, readily explainable on the basis of the difference in the electron work functions of the two specimens. Moon[9] has shown that according to the Langmuir-Kingdon-Saha theory of positive ion emission from hot metals, the following relation should hold.

$$n_p/n_a = \sigma_p/\sigma_a \exp -11{,}600(U-\varphi_-)/T, \quad (2)$$

where n_p and n_a are the rates of evaporation of positive ions and neutral atoms, respectively, σ_p and σ_a are the statistical weights of the two, U is the ionization potential and φ_- the electron work function.

If we assume that n_a is independent of φ_- within the limit of experimental error, we see on taking the ratio of two equations with different electron work functions, that everything except the ratio of the n_p's, the difference in the electron work functions and the temperature, drops out. This is on the assumption that the abnormally high value of A observed for the high work function specimen is due to some other cause than simply a temperature variation in φ_- and that this temperature variation is the same for both specimens. Taking this ratio we see that with the observed difference of 0.2 volt the ratio of the + ion currents should be 2.6 at 2300°K. This agrees within the limits of error with the experimental ratio particularly in as much as the exponent is very sensitive to a small error in φ_-.

In Table I, the computed and observed ratios

TABLE I. *Observed and computed values of* n_p/n_a.

$1/T\ 10^4$	OBSERVED RATIO	COMPUTED RATIO
4.0	1.89	1.82
4.2	1.94	1.88
4.4	1.97	1.94

[9] P. B. Moon, Proc. Camb. Phil. Soc. **28**, 490 (1932).

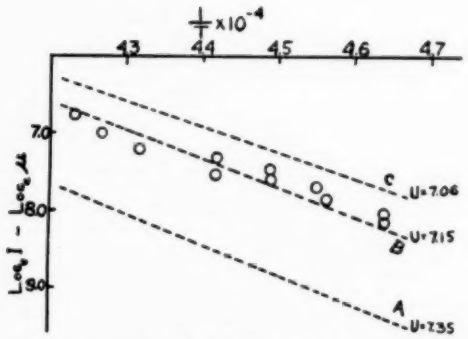

FIG. 3. Comparison of Langmuir-Saha equation with experiment.

for two samples with electron work functions of 4.17 and 4.30 volts are given for three values of $1/T$.

This variation of the positive ion current with φ_- shows, incidentally, that a stable condition giving a constant electron work function is essential for an accurate determination of the positive ion work function.

In order to compare Eq. (2) more directly with the experimental results it is convenient to write it in the form:

$$i_p/\mu = e/m\sigma_p/\sigma_a \exp -11{,}600 \times [U-(\varphi_{0-}+\alpha T)]/T. \quad (3)$$

Where α is the temperature coefficient of φ_-. This according to the discussion of the electron work function given above reduces to

$$i_p/\mu = e/m\sigma_p/\sigma_a 2.9 \exp -11{,}600(U-\varphi_{0-})/T, \quad (4)$$

where i_p is the positive ion current/cm², μ is the loss of mass/cm² per sec. and e/m is the specific charge for molybdenum.

Unfortunately the ionization potential of molybdenum is not known with sufficient accuracy to make a good comparison of this equation with experiment possible. Bacher and Goudsmit[10] give a value of 7.35 volts for U and Catalan and Magariaga[11] in a more recent determination give a value of 7.06 ± 0.03 volts. The estimated error in this determination may, however, be too low. An earlier estimate by Catalan[11] yielded a value of 7.15 volts.

Fig. 3 shows a plot of $\log i_p - \log \mu$ against $1/T$ for the above equation with a statistical weight of 6 for the ion and 7 for the neutral atom where the statistical weight is taken as $2j+1$. φ_{0-} is here taken as 4.17 volts. Curve A is with $I=7.35$ volts. Curve B with $I=7.15$ and C with a value of 7.06 volts. The points are experimental, using evaporation data obtained in this laboratory by Mr. E. R. Piore and which will be published soon. The temperature range used in the plot is limited by the range of temperature used in obtaining the evaporation data.

As may be seen from the above plot the experimental data definitely favor an ionization potential of 7.15 volts. In order to agree with the 7.06 value the ratio of i_p/μ would have to be increased by a factor of 1.4. There is of course an uncertainty in the 2.9 factor but it does not seem likely from the value for the constant A given above that this can be 40 percent in error.

If in Eq. (3), we substitute

$$\mu = Bf(T) \exp -11{,}600H/T, \quad (5)$$

where H is the heat of evaporation of neutral atoms in volts, we get

$$i_p = Cf(T) \exp -11{,}600(U+H-\varphi_{0-})/T.$$

This is essentially the form of Smith's equation (Eq. (1)) and we see that $\varphi_{0+}=U+H-\varphi_{0-}$. Piore's vapor pressure data give $H=5.75$ volts computed from the slope of the Jones-Langmuir-Mackay[12] vapor pressure equation. With $U=7.15$ volts and φ_{0-} as 4.2 volts the value of φ_{0+} should be 8.7 volts. The average of all the experimentally-determined values is 8.35 volts. The lack of agreement may be due to a combination of a number of possible errors. There is an uncertainty of approximately 1/10 volt in the determined value of φ_{0+} and a somewhat greater possible error in H. In addition there is an uncertainty in the temperature factor in Eq. (1) due to the neglect of the effects of the surface heat of charging which might influence the experimental value of φ_{0+} appreciably. For the present, therefore, we must conclude that the agreement between the computed and experimental values of the positive ion work functions is as good as can be expected.

[10] Bacher and Goudsmit, *Atomic Energy States.*

[11] Catalan and Magariaga, Anales soc. espan. fis. y. quim **31**, 707 (1933).

[12] Jones, Langmiur and Mackay, Phys. Rev. **30**, 201 (1927).

Theory of Pressure Effects of Foreign Gases on Spectral Lines

HENRY MARGENAU, *Sloane Physics Laboratory, Yale University*

(Received August 5, 1935)

The chief aim of the considerations presented is to contribute to the understanding of the effects of high pressures of foreign gases upon the shape and the position of a spectral line. A formal distinction is made between statistical and impact distributions, and the former is calculated in closed form for an interaction law of the type $\Delta\nu = -\alpha/r^6$. The distribution (Eq. (7a)) is a special case of Pearson's curves. Next the relation between the statistical and the true distribution is examined from a fundamental point of view which illuminates the character of the approximations made in the various theories of pressure broadening. Finally, by the use of a simplified procedure, approximative expressions are developed for the entire intensity distribution within the line, probably valid for pressures around 20 atmos. An expression (Eq. (18)) capable of graphical integration, is given which represents the true distribution for lower pressures. The theoretical results are compared with experimental data. Some concrete conclusions: the shift of the maximum is nearly proportional to the pressure of the perturbing gas at low pressure, proportional to its square at high pressures. The transition occurs at a pressure for which the impact half-width $\approx$ the shift of the statistical maximum. (About 20 atmos. for $K-N_2$, 50 atmos. for $Hg-N_2$.) At pressures up to $\approx$20 atmos. the impact width determines the shift of the intensity maximum, the latter being at low pressures far greater than the shift of the statistical maximum. Half-widths are also proportional to approximately the first power of the pressure at low, to the second power at high pressures. At pressures up to $\approx$10 atmos., the half-width is about twice the shift of the maximum. The shift is a function of the temperature as well as the pressure.

THE interesting features of a spectral line broadened by pressure of foreign gases are its width, the shift of its frequency maximum, and its peculiar asymmetry. It is not difficult to explain all these facts in descriptive physical terms, attributing each to a separate characteristic phenomenon. Thus it is customary to ascribe the cause of the increased width in some way to the lack of phase coherence, produced by the perturbing atoms, of the waves emitted or absorbed; the frequency shift is linked to the fact that the average energy of the levels between which a transition occurs is changed as a consequence of perturbations; the asymmetries, finally, are regarded as due to the different and in general irregular statistical weights of the various transitions of slightly different frequencies.

Theories dealing with the problem at hand are not entirely in harmony because they emphasize different aspects of it. The oldest and simplest theory is that of Lorentz, which explains, with considerable success, the width of the line on the assumption that impacts suddenly interrupt the radiation process. Weisskopf[1] has adapted this theory to the problem of continuous collisions, obtaining essentially the result of Lorentz but on physically more plausible grounds. We shall later return to it. For the present it suffices to state that, since random interruptions necessarily produce symmetrical spreading of frequencies, this method is inadequate for handling shifts and asymmetries while dealing correctly with line widths.

The present writer has attacked the problem from much the opposite standpoint.[2] Neglecting entirely the width of the line which results from the incoherence of the phases, a statistical theory was developed in which the intensity of any frequency between ν and $\nu+d\nu$ within the spectral line is considered proportional to the time interval during which the optically active atom is capable of emitting a frequency of this range. On this basis one obtains spectral distribution curves[3] which resemble closely the experimental ones observed at very high pressures, while correspondence at low pressures fails completely. The reason for this will later be clear. Moreover, the statistical theory in question yields correctly and very simply the mean frequency, $\bar{\nu}$, of the broadened line. This mean frequency is strictly proportional to the relative density of the perturbing gas. Experimentally, however, it is not the mean frequency but the maximum frequency which is measured. Yet in discussing agreement with observation, $\bar{\nu}$ has

[1] V. Weisskopf, Zeits. f. Physik **75**, 287 (1932); Physik. Zeits. **34**, 1 (1933).

[2] H. Margenau, Phys. Rev. **40**, 387 (1932).

[3] H. Margenau, Phys. Rev. **43**, 129 (1933).

been compared with the experimental $\nu_{max.}$ because, since the exact distribution of frequencies was not known, $\bar{\nu}$ and $\nu_{max.}$ were expected to behave similarly. This procedure, however, is fundamentally wrong, as the correct calculation of the statistical distribution will show. Curiously, however, for low pressures the expectation happens to be nearly right.—The considerations of Kulp[4] are essentially identical with those just outlined.—Any statistical theory of pressure broadening misses the important part of the line width at low pressures, as was already found, but not clearly understood, in reference 2. In a sense, it may be said to be complementary to Weisskopf's theory. Only at high pressures does the width of the statistical distribution agree with the observed line width.

A complete theory which comprises both aspects, the statistical distribution as well as that resulting from incoherence of phases, must be based upon a Fourier analysis of the varying electric moment of the radiating atom, as was emphasized by Weisskopf[1] and by Lenz.[5] The last author has treated the problem starting with this theoretically rigorous procedure. His results are notable inasmuch as they are impeccable in the range for which they hold, but, due to unavoidable analytical approximations this range is unfortunately small. Lenz claims validity for his results only up to pressures of 1 atmosphere. Furthermore, the calculatory details of his method are so unperspicuous that it is impossible to estimate the error which his treatment entails at higher pressures, where the characteristic features of the line can be more easily observed experimentally. The results of the method to be presented in this paper agree substantially with those of Lenz within the limits of validity of the latter.

Recently, Kuhn[6] has made a number of observations exhibiting some of the defects of the statistical theory of broadening sketched above. In particular he finds, on the basis of interesting plausibility arguments, that the intensity maximum should vary as the square of the pressure. His work also involves the suggestion that to each point of the statistical distribution curve should be assigned an intrinsic diffuseness. This can be done, however, only if the statistical distribution is known. The results to be obtained presently confirm, in part, Kuhn's expectations, though with quantitative modifications. They will also show how the fact that the maximum of the statistical distribution varies as the square of the relative density falls in line very naturally with observations on the shift of the intensity maximum.

For the sake of definiteness we shall continue to use the term statistical distribution (German *Häufigkeitsverteilung*) in the sense previously outlined, and refer to the spreading of frequencies due to incoherence of phases (Weisskopf's *Stossverbreiterung*) as impact broadening. Strictly speaking, the two effects cannot be separated either physically or mathematically, yet we shall treat them in this paper formally as distinct. The first step will be to obtain and discuss an approximation to the statistical distribution of frequencies in closed form (§1), the next to exhibit the relation between the statistical and the true distribution (§2). It will then be necessary to modify the former distribution by incorporating the effect of impact broadening (§3) and finally to compare the results with experiments. (§4).

§1. The Statistical Distribution

For the forces causing the displacement of energy levels as a result of interactions with foreign perturbers we may refer to London's[7] papers. His theory is applied in detail to the present problem in reference 2, where the numerical magnitude of these forces is also roughly computed. If a stationary perturber (foreign atom or molecule) is a distance r from the optically active atom, the frequency which the latter emits or absorbs differs from the normal frequency by an amount

$$\Delta\nu = -\alpha/r^6 + R, \tag{1}$$

where α is a constant and R a series of even inverse powers of r beginning with r^{-8}. At reasonably large distances, in most cases probably for $r > 10^{-7}$ cm, R may be neglected against

[4] M. Kulp, Zeits. f. Physik **79**, 495 (1932).
[5] W. Lenz, Zeits. f. Physik **80**, 423 (1933).
[6] H. Kuhn, Proc, Roy. Soc. **A18**, 987 (1934).
[7] F. London, Zeits. f. Physik **63**, 245 (1930); Zeits. f. physik. Chemie **B11**, 222 (1930).

α/r^6. Closer in there follows a range in which R becomes appreciable, and for still smaller distances of separation $\Delta\nu$ increases in general. In the analytical work in this section we shall ignore R. The error introduced thereby is considerable for higher pressures and requires discussion; as a preliminary guide we recall that at a pressure of 1 atmos. the mean distance between atoms is 3.3×10^{-7} cm. The choice of a modified law $\Delta\nu=-\alpha'/r^p$ to begin with would be of doubtful utility, for it would falsify the entire distribution curve, while the procedure here adopted will produce the maximum at the correct place, even for moderately high pressures ($\sim$10 atmos.), introducing errors for greater frequencies only. Also, the choice here made permits the evaluation of the distribution in closed form. It should be remarked that, as long as Eq. (1) holds, the contributions to $\Delta\nu$ of the different perturbers are additive. The density of emitting or absorbing atoms is taken to be very small.

Let us assume uniform distribution of the perturbers in phase space, and measure all frequencies from the position of the line at zero pressure. Then, if the statistical distribution is denoted by $I'(\nu)$ and r_i is the distance of the ith perturber from the emitting atom, the total number of perturbers being n, and the volume V,

$$I'(\nu)d\nu=(4\pi/V)^n\int\cdots\int_{d\nu}r_1^2r_2^2\cdots r_n^2dr_1\cdots dr_n. \quad (2)$$

The integration here extends over the range of r's in which

$$\nu-\frac{d\nu}{2}<-\sum_i\frac{\alpha}{r_i^6}<\nu+\frac{d\nu}{2}. \quad (3)$$

By inserting a Dirichlet factor which has the value 1 in the range (3) and vanishes outside we can transform (2) to read

$$I'(\nu)d\nu=\frac{1}{\pi}\left(\frac{4\pi}{V}\right)^n\int\cdots\int r_1^2r_2^2\cdots r_n^2dr_1\cdots dr_n\int_{-\infty}^{\infty}d\rho\frac{\sin(\frac{1}{2}\rho d\nu)}{\rho}e^{-i\nu\rho+i\alpha\rho\Sigma(1/r_i^6)}, \quad (4)$$

where now the r-integrations may be taken over all accessible configuration space. In this expression we have changed the sign of α, which is equivalent to measuring ν in the direction of decreasing frequencies. All shifts will thus conveniently appear with a positive sign although they are really negative. In (3) we shall now assume that $d\nu\to0$ which simplifies the sine-factor; we then split off the integration over the r's and write $e^{i\alpha\rho/r^6}$ in the form $1-(1-e^{i\alpha\rho/r^6})$, obtaining

$$I'(\nu)=\frac{1}{2\pi}\left(\frac{4\pi}{V}\right)^n\int_{-\infty}^{\infty}d\rho e^{-i\nu\rho}\left\{\int[1-(1-e^{i\alpha\rho/r^6})]r^2dr\right\}^n. \quad (5)$$

Consider now the term in { }. The integration is to be carried from some smallest distance of approach r_1, to the maximum distance of separation d, which may be related to the total volume by: $4\pi d^3/3=V$. But in integrating r^2dr we are permitted without appreciable error to use 0 as the lower limit, and in integrating the remainder we may replace the upper limit by ∞ because of the behavior of the integrand. If we integrate from 0, as we shall do, we are committing an error whose effect we must later investigate. With this understanding,

$$\int[1-(1-e^{i\alpha\rho/r^6})]r^2dr=\frac{V}{4\pi}\left(1-\frac{4\pi V'}{V}\right),$$

where we have used the abbreviation

$$V'=\int_0^\infty(1-e^{i\alpha\rho/r^6})r^2dr.$$

In raising this quantity to the nth power we allow the volume of the gas to increase indefinitely while maintaining $n_1=n/V$ constant. Then

$$\lim_{n\to\infty}(1-4\pi n_1V'/n)^n=e^{-4\pi n_1V'},$$

and (5) takes the form[8]

$$I'(\nu)=(1/2\pi)\int_{-\infty}^{\infty}d\rho e^{-i\nu\rho}e^{-4\pi n_1V'(\rho)}. \quad (6)$$

We now proceed to evaluate V'. After substitution of x for $\alpha\rho/r^6$ and one partial integration

[8] I am indebted to Professor Lars Onsager for showing me a mathematically more elegant way of obtaining this equation. The presentation here chosen is less abstract.

this becomes

$$V'(\rho)=\frac{(\alpha\rho)^{\frac{1}{2}}}{3}\int_0^\infty\left(\frac{\sin x}{x^{\frac{1}{2}}}-i\frac{\cos x}{x^{\frac{1}{2}}}\right)dx$$

$$=\frac{(2\pi\alpha\rho)^{\frac{1}{2}}}{6}(1-i).$$

When this is substituted into (6) there results an expression which is easily evaluated. The most convenient procedure is to change the integrand in (6) to real form by writing

$$\int_{-\infty}^{\infty}=\int_{-\infty}^{0}+\int_0^\infty,$$

and then taking for the variable of integration in the first integral $-\rho$ instead of ρ. The limits will then be 0 and ∞ for both integrals and the integrands if added, become real. The result is

$$I'(\nu)=\frac{1}{\pi}\int_0^\infty\exp\left[-\frac{2\pi}{3}n_1(2\pi\alpha\rho)^{\frac{1}{2}}\right]$$

$$\cos\left(\nu\rho-\frac{2\pi}{3}n_1(2\pi\alpha\rho)^{\frac{1}{2}}\right)d\rho.$$

This integral is known; it is of the form

$$\int_0^\infty e^{-px}\cos(x^2-px)xdx \quad \text{with} \quad x=(\nu\rho)^{\frac{1}{2}}$$

and reduces to the function

$$I'(\nu)=\tfrac{2}{3}\pi\alpha^{\frac{1}{2}}n_1\nu^{-\frac{1}{2}}\exp(-(4/9)\pi^3\alpha n_1^2/\nu). \quad (7)$$

Henceforth we shall use the abbreviation $\lambda=\frac{2}{3}\pi\alpha^{\frac{1}{2}}n_1$, so that (7) becomes

$$I'(\nu)=\lambda\nu^{-\frac{1}{2}}e^{-\pi\lambda^2/\nu}. \quad (7a)$$

This distribution is plotted in Fig. 1, where ν is measured in units $\pi\lambda^2$.

The maximum of (7) comes at

$$\nu_{\max.}=\tfrac{2}{3}\pi\lambda^2=(\tfrac{2}{3}\pi)^3\alpha n_1^2. \quad (8)$$

It varies with the square of the relative density of perturbers as was predicted by Kuhn[6] (only his numerical coefficient is in error by a factor ~ 1.35). His conclusion that for large ν the distribution should behave essentially like $\nu^{-\frac{1}{2}}$, based on the supposition of single impacts, is also verified by (7). The exponential factor in this expression represents the effect of the cooperation of several perturbers in producing the intensity at a given frequency. The half-width of (7) is given by $1.85\pi\lambda^2$ and is therefore also proportional to n_1^2.

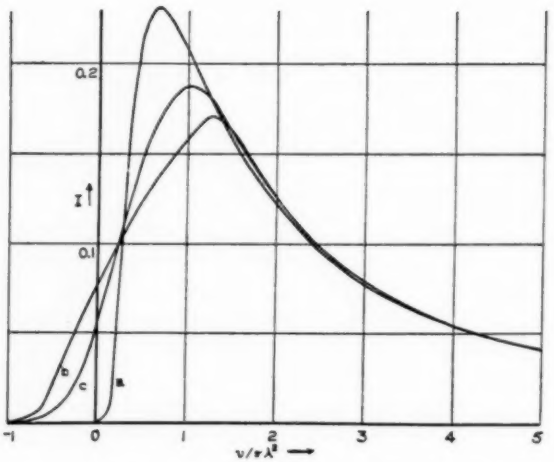

FIG. 1. (a) Statistical distribution $I'(\nu)$; (b) Eq. (21), with $\omega=2\pi\lambda^2$; (c) Eq. (23), with $\omega=2\pi\lambda^2$. Abscissae are in units $\pi\lambda^2$; the area under each curve is unity.

Before we consider to what extent the statistical distribution now derived can be expected to be reproduced in experiments, let us investigate it more critically. The law used for the energy interaction (Eq. (1)) with the neglect of R is certainly too simple. To use round numbers which indicate the order of magnitude of the various effects, $\Delta\nu$ will fall first more rapidly than assumed as we pass from 10A inward, then less rapidly, and at smaller distances it will rise. Indeed, from about 5A inward no encounters are possible. Also, at such close distance, additivity of the perturbing effects ceases to be valid. One may therefore expect that those portions of the distribution curve (7) which correspond to single impacts at distances between about 5 and 10A are incorrect. But here the curve can sometimes be modified very simply by considering the effects of single impacts alone, although we feel that the use of a law of the form $\Delta\nu=\alpha' r^{-p}$ will be inadequate for that purpose.

If, in the region of single impacts, that is, for frequencies which cause the exponential factor in (7) to be nearly 1, $\nu=f(r)$ where $f(r)$ may contain several parameters, then the intensity at frequency ν is given by

$$I(\nu)d\nu=\text{const.}\int_{d\nu}r^2dr, \quad \text{whence}$$

$$I(\nu)=[\varphi(\nu)]^2d\varphi/d\nu. \quad (9)$$

Here $\varphi(\nu)$ is written for the solution $r=\varphi(\nu)$ of $\nu=f(r)$. In some cases, (9) is given directly by experiment, and $f(r)$ can then be determined empirically.

Next, we must estimate the consequences of carrying the integration in all the way into the origin. Physically this means that we are including in (7) the contribution of very large frequencies at distances of approach inferior to the collision diameter, which in reality do not occur. It is clear that they will modify the tail of the distribution law which, in (7), is too long. As a result of their inclusion, the first moment of (7) does not exist, whereas the true statistical distribution has a mean (which is equal to $n_1\Delta\bar{\nu}$, $\Delta\bar{\nu}$ being the space average, calculated for a single perturber, over the true $\Delta\nu$ in place of (1); $\Delta\bar{\nu}$ as given by (1) diverges).

An upper limit for the error thus introduced may be found as follows: If we wish to cut off the integration at the lower limit r_1 we must replace V' in (6) by the function

$$\int_0^\infty(1-e^{i\alpha\rho/r^6})r^2dr+\int_0^\infty(e^{i\alpha\rho/r^6}-e^{i\rho F(r)})r^2dr,$$

where $F(r)=\alpha r^{-6}$ for $r>r_1$, but vanishes if $r<r_1$. The first integral is the old V'. Now the second integrand in this expression cannot be greater, in absolute value, than 2, hence the entire second integral has an absolute value $\leqq 2r_1^3/3$. If this is added to V' in (6) $I'(\nu)$ is multiplied by $e^{\pm(8\pi/3)n_1r_1^3}$. The exponent here is twice the number of perturbers contained, on the average, in the excluded volume. Hence, if we take r_1 to be $\sim$5A, the error in (7) cannot be greater than a few percent even for the largest frequencies considered at pressures about 1 atmos. For higher pressures, this upper limit of error grows very rapidly and is not a good index for the approximation involved.

To estimate the actual error we rely on physical considerations. We know that the true statistical distribution must give practically zero intensities for $\nu>\nu_1=\alpha/r_1^6$. The ratio $\nu_1/\nu_{\max.}$ is independent of α, the strength of interaction; it is about 10^4 for relative density unity, 10 for relative density 30 (again taking $r_1\sim$5A). In the latter case, Eq. (7) predicts an intensity about 1/10 maximum at ν_1; hence at smaller frequencies we can say that the error due to the present cause is smaller than 10 percent of the maximum. The position of the maximum, however, should not be very strongly in error even at relative densities 30.

Some caution is also necessary in applying single-impact considerations to the tail of the distribution curve. Even at $\nu=10\nu_{\max.}$ the error in neglecting the exponential factor in (7) amounts to more than 10 percent. It will be seen, however, (cf. §3), that for pressures of a few atmospheres the maximum of $I'(\nu)$ has practically nothing to do with the maximum of the experimental distribution.

It may be of theoretical interest to remark that the frequency at which the area under the curve $I'(\nu)$ is divided into two equal parts lies at $4.34\pi\lambda^2$. Statisticians will observe that $I'(\nu)$ represents a certain type of Pearson's distribution function. In a previous paper[3] an attempt was made to evaluate this function graphically, but it was not obtained in closed form. The constants in this section are so chosen that $\int_0^\infty I(\nu)d\nu=1$, and I' must be regarded as zero for $\nu<0$, although analytically it assumes complex values in that range.

§2. Relation Between Statistical and True Distribution

When an atom emits or absorbs light of constant amplitude but varying frequency $\nu(t)$, the intensity distribution in the spectral line is accurately given by the Fourier analysis of its electric moment $e^{2\pi i\int_0^t\nu(\tau)d\tau}$; that is, if $I(\nu')$ is the intensity associated with a fixed frequency ν' and $J(\nu')$ the corresponding amplitude,

$$I(\nu')=|J(\nu')|^2,$$

where

$$J(\nu')=\int dt\exp\{-2\pi i\nu' t\}\exp\{2\pi i\int_0^t\nu(\tau)d\tau\}.$$

Hence

$$I(\nu')=\int\int dt_1dt_2\exp\{2\pi i[\int_0^{t_1}\nu(\tau)d\tau-\int_0^{t_2}\nu(\tau)d\tau+\nu'(t_2-t_1)]\}. \quad (10)$$

The two integrations for which no limits are stated extend over the entire time during which the process of radiation occurs, and this interval may be taken to be infinite since we are not at

present interested in natural line widths. After substitution of the variable x for (t_2-t_1) (10) takes the form

$$I(\nu')=\int dt\int dx \exp\{2\pi i[\nu' x-\int_0^x \nu(\tau)d\tau]\}. \quad (11)$$

Up to this point the analysis is straightforward, but from here on approximative methods must be adopted in the solution of any concrete problem. Two main procedures have been employed.

The first is based on a Taylor expansion of the varying phase:

$$\int_0^x \nu(\tau)d\tau=\nu_{x=0}\cdot x+\dot{\nu}\frac{x^2}{2}+\cdots$$

$$=\nu(t)x+\dot{\nu}(t)\frac{x^2}{2}+\cdots. \quad (12)$$

If here all terms but the first are disregarded and the result is substituted in (11), the integral over x in this expression becomes a δ-function which is 0 whenever $\nu(t)\neq\nu'$. The element dt is the time during which the frequency is $\nu(t)$, and is proportional to the statistical weight $I'(\nu)$ which was calculated in §1 for the problem of broadening by foreign gases. Hence to this approximation (11) simply reduces to

$$I(\nu')=\int I'(\nu)d\nu\delta(\nu-\nu')=I'(\nu').$$

This observation shows clearly in what sense the statistical distribution is in error: the second integral in (11) is not really a δ-function but has a finite width. The true distribution can be obtained from the statistical one by "diffusing" each ordinate of $I'(\nu)$ in the proper manner.

The second procedure referred to is the method of impact broadening due to Lorentz and Weisskopf.[1] Its meaning can also be most clearly understood in view of Eq. (11), for it amounts to an evaluation of this equation by substituting a δ-function for dt and by using a distribution of finite width for the factor of dt. In detail, one puts $dt=\delta(\nu-\nu'')d\nu$, and with respect to the remainder of (11) one makes the simple assumption that $\nu(\tau)=\nu$, a constant in time within the interval $-T\leqq\tau\leqq T$ and zero outside. The frequency distribution is then that of an interrupted wave train of duration $2T$, i.e.,

$$I(\nu')=\int\delta(\nu-\nu'')d\nu\int_{-T}^{T}e^{2\pi i(\nu'-\nu)x}dx$$

$$=\sin[2\pi(\nu'-\nu'')T]/\pi(\nu'-\nu'').$$

If this last result is averaged over all emission times $2T$ with the correct weight factor, the familiar "dispersion" curve (cf. reference 1) is obtained. Weisskopf's treatment differs from that of Lorentz by its method of computing the mean time of uninterrupted emission (or absorption).

In the next section we shall make an attempt at combining the two procedures now outlined, using for dt the statistical distribution, and some suitable diffusing function for the remainder. The success of the impact theories would recommend the use of a dispersion curve for this purpose. But in choosing a diffusing function we must, unfortunately, be guided by considerations as to what functions allow the analysis to be carried through. Some idea of the true nature of this function may be obtained, however, by reverting to Eq. (12).

Suppose we retain the first two terms of the expansion. Since in the case of a single perturbation $\dot{\nu}$ is proportional to the speed with which the molecules move, the second term is inappreciable at sufficiently low temperatures. The statistical distribution, as is well known, must therefore agree with the true one at very low temperatures.—On introducing (12) in (11) the integration over x leads to

$$\int_{-\infty}^{\infty}e^{2\pi i(\nu'-\nu)x-\pi i\dot{\nu}x^2}dx=\left(\frac{1}{2\dot{\nu}}\right)^{\frac{1}{2}}(1-i)e^{i\pi(\nu'-\nu)^2/\dot{\nu}}. \quad (13)$$

$\dot{\nu}$ is the time rate at which the frequency varies as the result of the combined action of all perturbers; it cannot in general be calculated by considering single impacts alone. It will depend on ν as well as on the pressure of the perturbing gas and on its temperature. For the present let us assume it to vary so slowly with ν that the width of (13) can be computed by treating it as constant. The real part of (13) is

$$\left(\frac{1}{2|\dot{\nu}|}\right)^{\frac{1}{2}}\left[\cos\frac{\pi(\nu'-\nu)^2}{|\dot{\nu}|}+\sin\frac{\pi(\nu'-\nu)^2}{|\dot{\nu}|}\right]. \quad (14)$$

The imaginary part is of no interest since it disappears in the next integration in (11). The

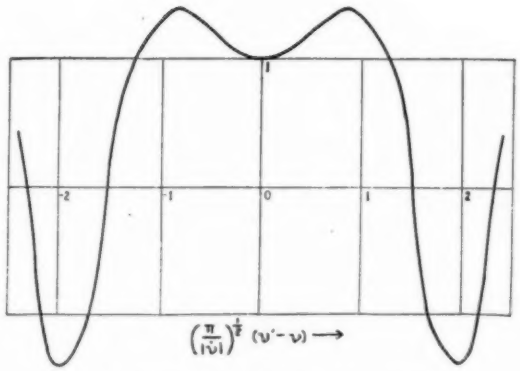

FIG. 2. Graph of the function (14).

function (14) is plotted in Fig. 2, where the unit $(|\dot{\nu}|/\pi)^{\frac{1}{2}}$ is employed in measuring $\nu'-\nu$. Its width ω is given by $(\pi/|\dot{\nu}|)^{\frac{1}{2}}\omega\approx 2$, hence

$$\omega\approx 2(|\dot{\nu}|/\pi)^{\frac{1}{2}}. \tag{15}$$

A crude estimate of the factors upon which this width depends can be obtained by calculating an average of the quantity $|\dot{\nu}|^{\frac{1}{2}}$ over all perturbers. The ith perturber will contribute

$$[\,|(dv_i/dr_i)v_i\cos(r_i\bar{v}_i)|\,]^{\frac{1}{2}}.$$

Upon averaging over velocities and directions of motion of the foreign atoms this becomes $c(\bar{v})^{\frac{1}{2}}|dv_i/dr_i|^{\frac{1}{2}}$. c is some numerical constant which we do not care to determine. We now take the origin of all frequencies at the unperturbed position of the spectral line so that ν is identical with the $\Delta\nu$ of Eq. (1). The term under the radical will then be $6\alpha/r_i^7$. In summing over all perturbers we use the method of statistical mechanics:

$$\sum_i |dv_i/dr_i|^{\frac{1}{2}}=4\pi n_1\int(6\alpha/r^7)^{\frac{1}{2}}r^2dr,$$

beginning the integration with some suitable smallest value r_1. Collecting these results we find for the average in question

$$\text{Ave}\;|\dot{\nu}|^{\frac{1}{2}}=Cn_1(\alpha\bar{v})^{\frac{1}{2}}, \tag{16}$$

where C, a constant, has the dimension $L^{-\frac{1}{2}}$. This expression depends but little on the choice of r_1.

It is of interest to compare this impact width with that calculated by Weisskopf. According to his theory

$$\omega=\text{const.}\;\bar{v}n_1\rho^2,$$

where $\rho=\text{const.}\;(\alpha/\bar{v})^{1/5}$. Thus

$$\omega=\text{const.}\;n_1\alpha^{2/5}\bar{v}^{3/5}. \tag{17}$$

The difference in the exponents of α and $\bar{v}$ in (16) and (17) is unimportant, for both expressions are only approximately true. The superiority of Weisskopf's treatment lies in its greater simplicity and in the opportunity which it offers for evaluating the constant. The point to be noticed is that ω varies linearly with the relative density of the perturbing gas. In making use of these results later we can take the constant in question from experiment.

§3. Modification of the Statistical Theory by Inclusion of Impact Broadening

In the present section we shall calculate (11), but with the use of a highly simplified distribution function representing the effect of impact broadening. The half-width of the function will be given by (16) or (17). The form of the diffusing function suggested both by experiment and theory would be of the dispersion type:[9]

$$w(x)=(\omega/2\pi)/(x^2+\tfrac{1}{4}\omega^2),$$

so that the modified distribution becomes:

$$I(\nu)=\int_{-\infty}^{\infty}w(x-\nu)I'(x)dx \tag{18a}$$

$$=\frac{\omega}{2\pi}\int_{-\infty}^{\infty}\frac{I'(x)dx}{(x-\nu)^2+\omega^2/4}, \tag{18}$$

I' being given by (7) for a large range of pressures. (18) could be computed graphically and should agree well with the observed intensity distributions. In this procedure, ω can be taken either from (17) or from the experimental half-width of the line at small pressures; it should be allowed to increase slowly with ν across the line since large perturbations are accompanied by larger values of $|\dot{\nu}|^{\frac{1}{2}}$ (cf. Eq. (15)). The value of $I(\nu)$ for two limiting cases can be determined at once. If $-\nu\gg\omega\gg\pi\lambda^2$, that is, for the extreme blue wing of the spectral line, $I(\nu)$ varies nearly as $1/\nu^2$, i.e., it behaves like the dispersion curve.

[9] The constants are so chosen that ω represents the half-width and $w(x)$ is normalized to 1.

On the other hand, if $\nu \gg \omega$, (18) takes on the features of $I'(\nu)$. At the extreme red side of the line the true distribution should therefore approach the statistical one.

We shall not attempt to calculate (18); for some general features of the true distribution can probably be recognized by using simpler trial functions for $w(x)$. Let us first make the assumption that the impact breadth diffuses all frequencies within a range ω in a uniform manner, allowing ω for the present to be a function of ν. This assumption is likely to be better than the second one whose consequences we will investigate, namely that $w(x)$ is a triangle function which confers much greater weight upon the center than upon the "wings" of the impact distribution. Before proceeding with the work we write down some transformations of certain integrals which occur, and which the reader can readily verify.

$$\int_a^b I'(x)dx = \lambda \int_a^b x^{-\frac{1}{2}} e^{-\pi\lambda^2/x} dx$$
$$= \phi((\pi\lambda^2/a)^{\frac{1}{2}}) - \phi((\pi\lambda^2/b)^{\frac{1}{2}}). \quad (19)$$

ϕ is Gauss' integral

$$\phi(x) = 2/\pi^{\frac{1}{2}} \int_0^x e^{-y^2} dy;$$

we recall that $\phi(\infty) = 1$. Finally,

$$\int_a^b x I'(x)dx = 2\lambda\{b^{\frac{1}{2}} e^{-\pi\lambda^2/b} - a^{\frac{1}{2}} e^{-\pi\lambda^2/a}$$
$$+ \pi\lambda[\phi(\pi\lambda^2/b)^{\frac{1}{2}} - \phi(\pi\lambda^2/a)^{\frac{1}{2}}]\}. \quad (20)$$

1. Uniform diffusion

In accordance with the first assumption, $w(x)$ will be taken to be the constant $1/\omega$ in the range $-\omega/2 \leqq x \leqq \omega/2$, thus ensuring correct normalization. Then

$$I(\nu) = \int_{-\infty}^{\infty} w(x-\nu) I'(x)dx = \frac{1}{\omega} \int_{\nu-\omega/2}^{\nu+\omega/2} I'(x)dx.$$

Here it must be remembered that $I'(x)$ is zero for negative x. Hence, in view of (19),

$$I(\nu) = \frac{1}{\omega}\left[\phi\left(\frac{\pi\lambda^2}{\nu-\omega/2}\right)^{\frac{1}{2}} - \phi\left(\frac{\pi\lambda^2}{\nu+\omega/2}\right)^{\frac{1}{2}}\right]. \quad (21)$$

If the argument of ϕ becomes imaginary, ϕ is to be replaced by 1. In Fig. 1 is shown a graph of this function for $\omega = 2\pi\lambda^2$, the same for all values of ν. The maximum is, of course, less steep and is shifted with respect to that of $I'(\nu)$. There is now an appreciable intensity at negative ν-values.

The position of the maximum of $I(\nu)$ is in general easily obtained by differentiating (21) with respect to ν, treating ω as a function of ν. An interesting and sufficiently significant result is obtained, however, if again we take ω to be constant. The maximum, occurring at ν_0, is then given by

$$I'(\nu_0 + \omega/2) = I'(\nu_0 - \omega/2), \quad (22)$$

as is directly seen from the equation preceding (21). According to (22) ν_0 can be determined by the simple graphical procedure of finding where the $I'(\nu)$ curve has a horizontal width ω. The mean of the two abscissae defining this width is ν_0.

Now suppose that $\omega \gg \pi\lambda^2$, which is the case up to pressures of several atmospheres, as will be shown in the next section. Then, since $I'(\nu)$ rises very rapidly at $\nu = 0$, the point bounding the range of width ω on the left lies practically at $\nu = 0$, the limit on the right is about ω, and $\nu_0 \sim \omega/2$. This is true regardless of the precise behavior of $I'(\nu)$ for large ν. We see that ν_0 in this case bears very little relation to the maximum of $I'(\nu)$. Moreover, since ω varies linearly with n_1, ν also does. At low pressures the shift of the observed maximum is thus entirely occasioned by the increasing impact width of the line. If this explanation is correct the shift should roughly correspond to one-half of the half-width, as will be shown to be the case empirically.

In case $\omega \ll \pi\lambda^2$, which prevails for high pressures because λ^2 increases with n_1^2, ν_0 coincides with the maximum of I', and hence varies with n_1^2. The region in which the linear law gradually changes into the square law is given by $\omega \approx \pi\lambda^2$.

The actual shape of the line cannot be expected to be rendered accurately at all by (21) for the former case $\omega \gg \pi\lambda^2$. For the reverse condition, lack of agreement of (21) with observation, if found, should be attributed mainly to the faults of I' previously discussed.

2. Diffusion by a triangle function

To see the effect of the particular diffusing function chosen upon the distribution of intensities it seemed well

to try one other choice:

$$w(x)\begin{cases} 0 & \text{if } x<-\omega/2 \\ (4/\omega^2)(x+\omega/2) & \text{if } -\omega/2\leqq x<0 \\ (4/\omega^2)(\omega/2-x) & \text{if } 0\leqq x<\omega/2 \\ 0 & \text{if } x>\omega/2 \end{cases}$$

w represents an isosceles triangle with base ω and area 1. If this is substituted in (18a) with x everywhere replaced by $(x-\nu)$, the result is

$$I(\nu)=\frac{4}{\omega^2}\int_{\nu-\omega/2}^{\nu}\left(\frac{\omega}{2}-\nu+x\right)I'(x)dx + \frac{4}{\omega^2}\int_{\nu}^{\nu+\omega/2}\left(\frac{\omega}{2}+\nu-x\right)I'(x)dx.$$

The integrals can be evaluated by the use of (19) and (20), yielding finally

$$I(\nu)=\frac{4\pi\lambda^2}{\omega^2}\left[2G\left(\frac{\pi\lambda^2}{\nu}\right)^{\frac{1}{2}}-G\left(\frac{\pi\lambda^2}{\nu+\frac{\omega}{2}}\right)^{\frac{1}{2}}-G\left(\frac{\pi\lambda^2}{\nu-\frac{\omega}{2}}\right)^{\frac{1}{2}}\right]. \quad (23)$$

The function G is defined as follows:

$$G(x)=\frac{\phi(x)}{x^2}+2\phi(x)+(2/\pi^{\frac{1}{2}})e^{-x^2}/x.$$

The procedure must be modified somewhat when $\nu<\omega/2$, for then the arguments of some of the G's become imaginary. Closer inspection shows that when this happens the corresponding $G(x)$ is to be replaced by $(2+1/x^2)$. We shall not reproduce here the details of the calculation.

Eq. (23) is also plotted in Fig. 1, again assuming ω to be independent of ν. As before, the value $2\pi\lambda^2$ has been chosen for ω; this means that the base of the triangle is equal to three times the shift of the maximum of $I'(\nu)$. Strictly speaking, curves 2 and 3, Fig. 1, are not comparable quantitatively because curve 2 has an "impact half width" twice that of curve 3. By taking ω in Eq. (23) to be larger the curves can be made almost to coincide. It is of interest to notice how little the statistical distribution at larger frequencies is changed by the process of diffusion. We wish to emphasize again that Eq. (23), as well as (21), breaks down when $\omega>\pi\lambda^2$, for in that case the accurate impact distribution becomes important. It would then be necessary to evaluate (18).

The position of the maximum of (23) requires comment. We state merely the results without discussing the work involved: For $\omega\ll\pi\lambda^2$ the maximum ν_0 increases with the square of the relative density, as is clear without calculation. If $\omega\gg\pi\lambda^2$ the increase of ν_0 is not strictly linear with n_1, as was found in example 1), but proportional to a power of n_1 intermediate between the first and second. In this case ($\omega\gg\pi\lambda^2$), ν_0 is again far greater than $\frac{3}{2}\pi\lambda^2$, the position of the maximum of $I'(\nu)$. As before, the transition region in which the lower power changes into the second is defined by $\omega\approx\pi\lambda^2$.

The results of this section are definitely oversimplified. But before developing the theory further it seems well to determine whether the simple functions here derived (Eqs. (21) and (23)) agree with observations in the pressure range for which they are theoretically valid. This pressure range depends, of course, upon the gases used (cf. next section) since both ω and λ are functions of α, the parameter measuring the strength of the interactions. For the purpose of such comparison it would be necessary to measure the entire line contour rather than shift and half-width alone, as is customary. We regard as significant the fact that the maximum of the true distribution depends at small pressures largely upon the impact width, and that the position of this maximum moves toward longer wave-lengths first nearly linearly with n_1, at higher pressures with n_1^2.

§4. Comparison of Results with Experiments

The pressure shift of the line maximum is well known to be nearly proportional to the relative density of the perturbing gas. Füchtbauer and collaborators[10] have traced this linear law up to pressures of 50 atmos. Their observations are made on the 2537A-line of Hg. An essentially similar behavior is shown by the D lines of Na[11] up to relative density ≈ 10.

Recently, however, Watson and the author[12] have extended their measurements on the shift of the potassium resonance lines to relative densities above 20 and found definite departures from linearity in this region in qualitative confirmation of the theory, the perturbing gas being N_2.

The difference in the behavior of Hg and K is easily explained. The following is a list of the values of ω and $\pi\lambda^2(=4/9\pi^3 n_1^2\alpha)$ for 1 atmos. of pressure, together with the α's used in the computation of λ^2. These α's are computed for similar cases in reference 2, their numerical values are not very accurate, but the ratio of the two should not be greatly in error. The values of ω, the half-width at 1 atmos., are taken from experiment.

---

[10] C. Füchtbauer, G. Joos and O. Dinkelacker, Ann. d. Physik **71**, 204 (1923).

[11] H. Margenau and W. W. Watson, Phys. Rev. **44**, 92 (1933).

[12] W. W. Watson and H. Margenau, Phys. Rev. **44**, 748 (1933).

	$Hg-N_2$	$K-N_2$
α	1.5×10^{-32} cm^6 sec.$^{-1}$	7×10^{-32} cm^6 sec.$^{-1}$
ω	8.3×10^{9} sec.$^{-1}$	13×10^{9} sec.$^{-1}$
$\pi\lambda^2$	1.5×10^{8} sec.$^{-1}$	7×10^{8} sec.$^{-1}$

The statement previously made, that at pressures of a few atmospheres $\omega \gg \pi\lambda^2$, and hence the impact width dominates the position of the maximum as well as the width of the line, is thus seen to be true. Since ω varies as n_1, and λ^2 as n_1^2, ω becomes equal to $\pi\lambda^2$ at about relative density 55 for the case $Hg-N_2$, at relative density 19 for $K-N_2$. It is therefore clear why strong curvature in the shift curve should not have been detected by Füchtbauer and collaborators, but should have revealed itself even at lower pressures in the other experiments referred to.

In the pressure effects of foreign gases upon the D lines or the resonance lines of K, the statistical intensity distribution impresses its characteristics more and more markedly upon the lines from 20 atmos. onward. At pressures of this magnitude $I'(\nu)$ is already in error for large ν, but corrections can probably be applied by single impact considerations.

As regards half-widths the theory, since it incorporates all the features of impact broadening, must be in agreement with experiment wherever the impact theories agree, that is at low and medium pressures. This has been amply tested. At higher pressures the width of the line should increase according to the statistical distribution, i.e., like n_1^2, the turning point being as before $\omega \approx \pi\lambda^2$. This fact is also verified in the experiments above considered.

The shift of the maximum is usually supposed to be independent of the temperature. This is true only for high pressures, when the statistical distribution determines the shift. For the latter depends on temperature only through the Boltzmann factor which we have here neglected, and this dependence is slight. At low pressures the maximum should exhibit much the same behavior with respect to temperature variations as does the impact width. This point has not been experimentally tested.

It has been pointed out that ω should be about twice the shift of the maximum in cases to which the theory applies. The actual half-width $\nu_{\frac{1}{2}}$ is a little larger than ω, being compounded from impact width and statistical width. We expect therefore that the ratio of $\nu_{\frac{1}{2}}$ to ν_0 (shift of maximum) exceeds 2 somewhat. Table I contains experimental values of $\nu_{\frac{1}{2}}$ and ν_0 at 1 atmos. of pressure. The first column indicates the spectral line investigated together with the perturbing gas. The four cases below the horizontal line should not follow the present rule, as we shall see.

TABLE I.

	$\nu_{\frac{1}{2}}$ PER UNIT RELATIVE DENSITY ($\times10^9$ sec.$^{-1}$)	ν_0 PER UNIT RELATIVE DENSITY ($\times10^9$ sec.$^{-1}$)	$\frac{\nu_{\frac{1}{2}}}{\nu_0}$
Hg 2537 – A	9.66	3.73	2.6
Hg 2537 – N_2	8.26	3.73	2.2
Hg 2537 – O_2	7.86	3.69	2.13
Na 5890 – A	17	6	2.84
Na 5890 – N_2	11.7	5.2	2.25
K 7665 – N_2	13.2	6.2	2.13
K 7699 – N_2	13.2	6.55	2.0
K 4044 – N_2	33	16.5	2.0
K 4047 – N_2	33	19	1.75
Hg 2537 – CO_2	13.1	3.2	4.1
Hg 2537 – H_2O	10.6	2.34	4.5
Hg 2537 – H_2	12.36	1.97	6.3
Na 2537 – H_2	19.5	4.5	4.3

Both CO_2 and H_2O have complicated molecules with permanent electric moments. Their interaction with the emitting atom calls into play additional forces which have not been considered in §1. These forces can extend the distribution $I'(\nu)$ to negative ν, thereby increasing the width and decreasing the shift. A similar situation exists with regard to H_2, although for a different reason. H_2 produces a large impact width through the factor $v^{\frac{1}{2}}$ in ω because of its lightness, which explains its efficiency in broadening the line. But the statistical distribution (7) is inadequate for this case for reasons which have been discussed in a previous communication.[13] It is there shown in connection with simple examples (Fig. 2) that, if one adds to $\Delta\nu$ of Eq. (1) a range in which $\Delta\nu$ is positive, the statistical distribution becomes nearly symmetrical and the shift of the maximum very small. Superposition of the impact width then leads to an explanation of the anomalies shown by H_2 in Table I.

Although the present treatment is restricted to resonance lines since for high series lines

[13] H. Margenau, Phys. Rev. **44**, 931 (1933).

Eq. (1) is not valid, the lines K 4044 and 4047 have been included in Table I. For higher series lines, $\Delta\nu$ may have a large positive range, and therefore $I'(\nu)$ may contain appreciable "blue" intensities. The present treatment is entirely inadequate for dealing with the highest series members of the alkali spectra, where the atom in its excited state embraces thousands of perturbers.[14]

While this work was in progress there has appeared a paper by Minkowski[15] in which the intensity distribution of the D lines perturbed by small pressures of A is investigated and compared with the results of Lenz[5] and Kuhn.[6] The agreement is found satisfactory. The considerations here presented do not conflict with these results in their respective ranges of validity (cf. in particular the remarks on the limiting form of Eq. (18)), and hence are not in disagreement with Minkowski's data. It is to be observed that for his experiments, (7) represents the accurate statistical distribution. Moreover, $\omega \gg \pi\lambda^2$. If then the center of the line is completely absorbed and measurements are confined to its wings, $|\nu| \gg \omega \gg \pi\lambda^2$. Under this condition $I \sim \nu^{-2}$ on the blue side, $I \sim \nu^{-1}$ on the red side of the line, as was found.

[14] A theory pertaining to these effects has been given by Fermi, Nuovo Cimento **11**, 157 (1934).
[15] R. Minkowski, Zeits. f. Physik **93**, 731 (1935).

NOVEMBER 1, 1935 PHYSICAL REVIEW VOLUME 48

The Effect of Crystalline Fields on the Magnetic Susceptibilities of Sm^{+++} and Eu^{+++}, and the Heat Capacity of Sm^{+++}

AMELIA FRANK, *Department of Physics, University of Wisconsin*

(Received August 17, 1935)

The temperature variation of the paramagnetic susceptibility of Sm^{+++} is calculated on the assumption that the ion is subject to a crystalline field which can be represented by the potential

$$V = \sum_i [D(x_i^4 + y_i^4 + z_i^4) + Ax_i^2 + By_i^2 - (A+B)z_i^2],$$

the cubic portion of this potential predominant. The susceptibility is decreased by about 25 percent with respect to that of the free ion at 74°K when the cubic potential is so chosen as to give a separation of the $J = 5/2$ levels of about 200 cm^{-1} which is of the order indicated by Spedding's work on the absorption spectrum of samarium compounds. The theoretical values of the susceptibility are then in satisfactory agreement with the experimental data of Freed over a temperature range from 74°K to room temperature. The rhombic portion of the field separates the lowest excited level into two but the contribution to the susceptibility is negligible if the rhombic separation is small compared with the cubic separation. In striking contrast with Sm^{+++}, Eu behaves like the free ion even in the presence of a crystalline field. The contribution to the heat capacity of Sm^{+++} at various temperatures due to the excited levels is computed. When the levels which give good agreement with susceptibility data are used, the general shape of the curve is the same as that obtained experimentally by Ahlberg and Freed but the theoretical values are consistently lower than the experimental values.

THE EFFECT OF CRYSTALLINE FIELDS ON Sm^{+++}

Introduction

Van Vleck[1] has pointed out in his treatment of the paramagnetic susceptibilities in the rare earth ions that Sm^{2} and Eu are anomalous in that some of the consecutive multiplet intervals are only of the order of kT even though the overall multiplet widths are large. This makes it necessary to consider the populations of levels other than the ground state and also second order Zeeman terms. The theoretical values thus calculated were shown in a previous paper[3] to give good agreement with experimental data on liquids and solids over a wide temperature range even though the theory is for the free ion. This theory can be applied only when the distortion by interatomic forces is negligible, that is, the energy to "turn over" an ion against interatomic

[1] J. H. Van Vleck, *Theory of Electric and Magnetic Susceptibilities*, Chapter IX.
[2] Here as well as throughout the rest of the paper, the three plus signs are omitted. Whenever the chemical symbol Sm or Eu appears, it stands for the triply charged samarium or europium ion.
[3] A. Frank, Phys. Rev. **39**, 119 (1932).

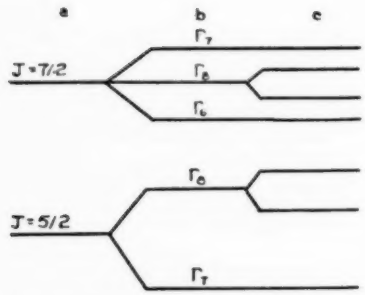

FIG. 1. The energy levels, $J=5/2$, $7/2$, of the ^6H configuration: (a) for the free ion and (b) in the presence of a field of cubic symmetry. The addition of a rhombic field splits the levels further as in *c*.

forces must be small compared with kT. It is not surprising, therefore, that the calculated values deviate considerably from the experimental data on liquid and solid compounds of samarium at low temperatures. The deviation becomes apparent at 150°K and increases as the temperature decreases.

The calculations are extended in this paper to take into account the interatomic forces for Sm and thus extend the data to lower temperatures than in the preceding article. Since the type of ionic field is unknown, the general procedure used by Penney and Schlapp[4] for other rare earths is followed, that is, we assume crystalline fields of simple symmetries and determine which types give good agreement with experimental data. The effect of such fields is to remove the degeneracy in the energy levels which exists when the intra-atomic spin-orbit interaction alone is considered. A type of field used successfully for the hydrated sulphates of other rare earths is one represented by a potential

$$V=D\sum_i(x_i^4+y_i^4+z_i^4).$$

in which the summation is taken over all of the electrons in the incomplete shell of the ion and the values of D are assumed positive. The significance of the sign of D has been discussed by Gorter,[5] the positive sign in the case of the rare earth salts suggesting an octahedral arrangement of the 6 oxygen atoms surrounding the metal ion.

Bethe[6] has shown that a field of cubic symmetry breaks up the $J=5/2$ state into two levels, corresponding in his notation to the irreducible representations Γ_7 and Γ_8 of the cubic group which have twofold and fourfold degeneracy, respectively. An interatomic field of rhombic symmetry splits Γ_8 further into two doubly degenerate levels. There remains the Kramers degeneracy, always present in systems with an odd number of electrons, which is removed only by a magnetic field. For the $J=5/2$ state of Sm, whose multiplet type is ^6H, the level Γ_8 is of higher energy than Γ_7. Similarly, $J=7/2$ breaks up into three levels corresponding to Γ_6, Γ_7 and Γ_8, the fourfold degenerate level Γ_8 lying between the other two which are doubly degenerate. The $J=5/2$, $7/2$ levels of the ^6H configuration in the presence of crystalline fields are shown diagrammatically in Fig. 1.

An added interest in this problem arises from the experiments of Spedding,[7] who has studied the absorption spectrum of the samarium ion in solids. His work indicates an appreciable splitting of the normal state of Sm such as one would obtain with a crystalline field. However Spedding gives the separation of the normal state into four levels with a possible fifth, whereas, if the method of crystalline potentials is applicable, it is impossible to obtain more than three. Some of Spedding's observed levels fit the susceptibility data very satisfactorily. Van Vleck has suggested that the additional levels of Spedding may possibly be vibrational effects.[8]

The Hamiltonian matrix with a cubic crystalline potential

The complete Hamiltonian function is given by

$$\mathcal{H}=A(\mathbf{L}\cdot\mathbf{S})+D\sum_i(x_i^4+y_i^4+z_i^4)+(L_z+2S_z)H\beta$$

where z is taken as the direction of the applied

[4] W. G. Penney and R. Schlapp, Phys. Rev. **41**, 194 (1932).
[5] C. J. Gorter, Phys. Rev. **42**, 437 (1932).
[6] H. Bethe, Ann. d. Physik **3**, 133 (1929).
[7] F. H. Spedding, Phys. Rev. **46**, 975 (1934).
[8] Spedding (J. Am. Chem. Soc. **54**, 2593 (1932)) has imputed some of his extra levels to "electronic isomers," thereby attributing some of the states to electronic configurations other than $4f$. However, such an idea appears at variance with the whole Hund scheme of the magnetic susceptibilities of the rare earths, notably its success in Pr and Nd when amplified by crystalline potentials in the Penney–Schlapp fashion. Also it is doubtful whether the existence of electronic isomers would be compatible with the chemical near-identity of the various rare earths. Even if Spedding's electronic isomer model were accepted, his attempted calculation of the magnetic susceptibility of Sm by this model would be in error. Among the mistakes we may mention the fact that, if the orbital magnetic moment were quenched, the statistical weight of the upper state would be 2 and not 18.

	1	6	7
1	$W_{5/2}-348Q-G/7$	$1560(6)^{\frac{1}{2}}Q/11$ $+5(6)^{\frac{1}{2}}G/14$	$(210)^{\frac{1}{2}}G/14$
6	$1560(6)^{\frac{1}{2}}Q/11$ $+5(6)^{\frac{1}{2}}G/14$	$W_{7/2}-17{,}048Q/33$ $+286G/189$ $+1183G^2/810F$	$-52(35)^{\frac{1}{2}}G/189$
7	$(210)^{\frac{1}{2}}G/14$	$-52(35)^{\frac{1}{2}}G/189$	$W_{7/2}-19{,}544Q/33$ $+26G/27$ $+91G^2/54F$

FIG. 2. Cubic factor of the secular determinant $\mathfrak{K}'$. Numbers designating rows and columns correspond to subscripts on the wave functions ψ_n'.

	2	5	3	4
2	$W_{5/2}-348Q$ $-11G/21$	$1560(6)^{\frac{1}{2}}Q/11$ $-5(6)^{\frac{1}{2}}G/14$	$4(5)^{\frac{1}{2}}G/21$	$-5(2)^{\frac{1}{2}}G/14$
5	$1560(6)^{\frac{1}{2}}Q/11$ $-5(6)^{\frac{1}{2}}G/14$	$W_{7/2}-17{,}048Q/33$ $+26G/63$ $+1547G^2/810F$	$-(30)^{\frac{1}{2}}G/7$	$-52(3)^{\frac{1}{2}}G/63$
3	$4(5)^{\frac{1}{2}}G/21$	$-(30)^{\frac{1}{2}}G/7$	$W_{5/2}-816Q$ $+5G/21$	$-1560(10)^{\frac{1}{2}}Q/11$ $+2(10)^{\frac{1}{2}}G/7$
4	$-5(2)^{\frac{1}{2}}G/14$	$-52(3)^{\frac{1}{2}}G/63$	$-1560(10)^{\frac{1}{2}}Q/11$ $+2(10)^{\frac{1}{2}}G/7$	$W_{7/2}-12{,}888Q/33$ $-26G/21$ $+91G^2/54F$

FIG. 3. Quartic factor of the secular determinant $\mathfrak{K}'$.

magnetic field and β is the Bohr magneton $eh/4\pi mc$. $A(\mathbf{L}\cdot\mathbf{S})$ is the spin-orbit interaction which is diagonal in J (and independent of M) since we assume that the crystalline field does not destroy the Russell-Saunders coupling. The eigenvalues of $A(\mathbf{L}\cdot\mathbf{S})$ will be referred to as W_J.

$(L_z+2S_z)H\beta$ is the contribution to the energy due to the presence of the magnetic field. This is regarded as a small perturbation in calculating the susceptibility, inasmuch as the magnetic separation is small compared with kT. As has been emphasized previously,[3] the calculations for Sm and Eu differ from those of the rest of the rare earth group in that the separation between the lowest multiplet levels is comparable with kT. It is therefore necessary to take into account the off-diagonal elements of the energy due to the magnetic field, formulae for which are given elsewhere.[9] In the complete secular determinant only the levels $J=5/2$ and $J=7/2$ are considered since, at low temperatures higher levels are not appreciably occupied, whereas at high temperatures the interaction between ions in the crystal, accounted for by the cubic potential, is not important. However, the interaction between $J=7/2$ and $J=9/2$ is not neglected insofar as the magnetic moment is concerned. This contribution to the magnetic moment is taken care of by adding to the diagonal elements of $J=7/2$ the second-order perturbation term $[(L_z+2S_z)(J, M; J+1, M)]^2/(W_J-W_{J+1})$ with $J=7/2$.

General expressions for the elements of the cubic field potential are given by Schlapp and Penney[10] in either the J, M or M_L, M_S systems of representation and so need not be repeated here. These, however, do not include the elements off-diagonal in J which may be obtained by expanding the wave functions in the form

$$\psi_{J,M}=\sum_{M_L} S^{L,S}_{J,M,M_L}\,\psi^{L,S}_{M_L,M-M_L}.$$

The coefficients in the expansion are given by Wigner.[11] For the multiplet type ^6H, the elements

[9] J. H. Van Vleck, reference 1, p. 167.

[10] R. Schlapp and W. G. Penney, Phys. Rev. **42**, 666 (1932). See also reference 4.

[11] E. Wigner, *Gruppentheorie*, p. 206.

of $V=D\sum_i(x_i^4+y_i^4+z_i^4)$ not diagonal in J are, for $J=5/2$:

$$V(J, M; J+1, M) = V(J+1, M; J, M)$$
$$= -1560\ (5)^{\frac{1}{2}}\ Q/11 \qquad (M=\pm 5/2)$$
$$= -2080\ (3)^{\frac{1}{2}}\ Q/11 \qquad (M=\pm 3/2)$$
$$= \ \ 780\ (10)^{\frac{1}{2}}Q/11 \qquad (M=\pm 1/2)$$

$$V(J, M; J+1, M\mp 4) = V(J+1, M\mp 4; J, M)$$
$$= -520\ (15)^{\frac{1}{2}}Q/11 \qquad (M=\pm 5/2)$$
$$= \ 3120 \qquad Q/11 \qquad (M=\pm 3/2)$$
$$= -780\ (14)^{\frac{1}{2}}Q/11 \qquad (M=\pm 1/2)$$

with $Q=q'D/c$. D is the cubic field constant, q' is the ratio of the matrix elements calculated for a system of n electrons to those for a one electron system, and c is a constant computed for a one electron system. The constant q'/c is the same as the absolute value of the constant q used by Penney and Schlapp.[4] By use of spur relations as explained by Penney and Schlapp, q'/c is determined to be $+503I/165$ with $I=\int_0^\infty r^6R^2(r)dr$. $R(r)$ is the radial wave function for one of the equivalent electrons. The positive value thus obtained for q'/c requires Γ_7 to be of lower energy than Γ_8 for $J=5/2$ for the type of cubic field we have assumed in which D is positive (see Fig. 1).

If the elements off-diagonal in J are neglected, the secular determinant factors, no factor being of higher order than two. The complete determinant is therefore simplified by transforming to a system of representation which diagonalizes those terms of the cubic field potential already diagonal in J. The following transformation of the original wave functions ($\psi_{J,\ M}$) accomplishes this simplification:

$$\psi_{\pm 1}' = \psi_{5/2,\ \pm 1/2},$$
$$\psi_{\pm 2}' = (5/6)^{\frac{1}{2}}\psi_{5/2,\ \pm 3/2} + (1/6)^{\frac{1}{2}}\psi_{5/2,\ \mp 5/2},$$
$$\psi_{\pm 3}' = (5/6)^{\frac{1}{2}}\psi_{5/2\ \mp 5/2} - (1/6)^{\frac{1}{2}}\psi_{5/2,\ \pm 3/2},$$
$$\psi_{\pm 4}' = (3/4)^{\frac{1}{2}}\psi_{7/2,\ \mp 1/2} + (1/2)\psi_{7/2,\ \pm 3/2},$$
$$\psi_{\pm 5}' = (3/4)^{\frac{1}{2}}\psi_{7/2,\ \mp 5/2} - (1/2)\psi_{7/2,\ \pm 3/2},$$
$$\psi_{\pm 6}' = (5/12)^{\frac{1}{2}}\psi_{7/2,\ \pm 7/2} + (7/12)^{\frac{1}{2}}\psi_{7/2,\ \mp 1/2},$$
$$\psi_{\pm 7}' = (5/12)^{\frac{1}{2}}\psi_{7/2,\ \mp 1/2} - (7/12)^{\frac{1}{2}}\psi_{7/2,\ \pm 7/2}.$$

Figs. 2 and 3 give the secular determinant $\mathcal{H}'$ in this new system of representation, factored into two identical quartics and two identical cubics with F substituted for $(W_{7/2}-W_{9/2})$, and G for $H\beta$.

TABLE I. *Effective Bohr magneton numbers for Sm.*

$T°K$	μ_{eff} (THEORY) $\nu=0$ (cm)$^{-1}$ (FREE ION)	173.6 (cm)$^{-1}$	207 cm^{-1}	μ_{eff} (EXP.) FREED[12]
74	1.06	.94	.91	.91
85	1.09	.99	.97	.96
112	1.16	1.11	1.09	1.08
170	1.29	1.28	1.27	1.26
205	1.37	1.37	1.36	1.35
240	1.44	1.44	1.44	1.44
293	1.55	1.56	1.56	1.57

The terms off the diagonal which depend on the cubic field occur in such a way as to require the solution of nothing more complicated than a quadratic to completely diagonalize them. Such a transformation, however, presents numerical difficulties because of the scrambling of the $J=5/2$ and $J=7/2$ terms. It would be possible to carry out the calculation in general terms by expanding the radicals which occur in the transformation matrix in terms of $Q/(W_J-W_{J+1})$. It is less laborious to make this second transformation by the substitution of numerical values for W_J and Q, until by trial and error a value of Q is found which gives results in agreement with experimental data. The values substituted for W_J are the multiplet energies used in the previous work on Sm, with the screening constant σ taken as 33.

Energy values are obtained to second powers in the magnetic field H by applying perturbation theory to the matrix $\mathcal{H}''$ which results from the second transformation and which is therefore diagonal except for linear terms in H. Thus

$$W_n = \mathcal{H}''(n; n) + \sum_{n'} \frac{[\mathcal{H}''(n; n')]^2}{W^0(n; n) - W^0(n'; n')},$$

where $W^0(n; n)$ is that part of $\mathcal{H}''(n; n)$ independent of the magnetic field.

Comparison of computed and experimental susceptibilities

Several sets of energy levels W_n corresponding to several choices of the constant Q were used and the molar susceptibility (χ) readily calculated from

$$\chi = \frac{NkT}{H}\frac{d\log Z}{dH},$$

[12] S. Freed, J. Am. Chem. Soc. **52**, 2702 (1930).

where Z is the partition function

$$Z=\sum_n e^{-W_n/kT}.$$

Table I gives computed and experimental values at various temperatures of the effective Bohr magneton number defined as

$$\mu_{eff}=[3kT\chi/N\beta^2]^{\frac{1}{2}}.$$

The values of ν referred to in the table are values of the separation of the $J=5/2$ level due to the cubic field corresponding to different choices of the constant Q. It is evident from the table that satisfactory agreement is obtained when the splitting of the $J=5/2$ level due to the cubic field is in the neighborhood of 200 cm^{-1}.

Experimental values of μ_{eff} at room temperature reported by other observers are

1.58 (anh. sul.) Cabrera and Duperier[13]
1.55 (hyd. sul.) Selwood[14]
1.66 (hyd. sul.) Rodden.[15]

The high effective magneton number given by Rodden would be in satisfactory agreement with the theory if the screening constant were taken as 34 instead of 33. Experimental values for the oxides of samarium are not included since it is not expected that the same type of crystalline field applies to both oxides and sulphates.[16]

The effect of adding a small rhombic potential to the crystalline field

Spedding[7] has reported excited levels at 160 cm^{-1}, 188 cm^{-1}, 225 cm^{-1}, and possibly one at 245 cm^{-1} from the absorption spectrum of $Sm_2(SO_4)_3\cdot 8H_2O$. The values of ν chosen for Table I are approximately the mean of 160 cm^{-1} and 188 cm^{-1}, and the mean of 188 cm^{-1} and 225 cm^{-1}. An interatomic field of rhombic symmetry will remove the degeneracy in the upper $J=5/2$ level but will leave the center of gravity unchanged. The calculation which follows shows that the inclusion of a rhombic field which will separate this level into two of those reported by Spedding will not destroy the good agreement with experimental data insofar as the susceptibility is concerned.

The rhombic field can be represented by the potential

$$\sum_i[Ax_i^2+By_i^2-(A+B)z_i^2],$$

the matrix elements of which are given by Schlapp and Penney.[10] If this rhombic field is assumed to be a small perturbation, it is sufficient to consider the effect only on the lowest levels of Sm. In the Hamiltonian matrix which results from the first transformation of the wave functions, new elements $\mathcal{H}'(n;\ n')=\mathcal{H}'(n';\ n)$ are added as follows:

$$\begin{aligned}
&\mathcal{H}'(1;\ 1)=-\mathcal{H}'(2:\ 2)=4a(A+B),\\
&\mathcal{H}'(1;\ 2)=4a(A-B)/(3)^{\frac{1}{2}},\\
&\mathcal{H}'(1;\ 3)=-(5)^{\frac{1}{2}}a(A+B),\\
&\mathcal{H}'(2;\ 3)=(5)^{\frac{1}{2}}a(A-B)/(3)^{\frac{1}{2}}
\end{aligned}$$

with $a=a'/b'$, where a' is the ratio of the matrix elements calculated for a system of n electrons to those for a one electron system, and b' is the constant calculated for a one electron system.

The addition of the rhombic terms to the complete secular determinant complicates it considerably. For example, the addition of the elements $\mathcal{H}'(1;\ 2)$ and $\mathcal{H}'(1;\ 3)$ spoils the factorization into quartics and cubics as given by Figs. 2 and 3. However, if we assume the energy (R) due to the rhombic field small compared with kT and also small compared with the separation ($h\nu$) due to the cubic field, it is possible to expand the susceptibility in terms of R/kT and $R/h\nu$. Then, by using spur relations, the contribution due to the rhombic field can be determined without solving the secular determinant which includes these terms. A general expression for this expansion in terms of spurs is given by Serber.[17]

Since the matrix elements of the magnetic moment were originally given corresponding to the application of the magnetic field along the z axis, it is necessary to determine the magnetic moment along the x and y axes in order to compute the average susceptibility. This can be done most conveniently by a cyclic permutation of the rhombic parameters, A, B, and $-(A+B)$.

[13] Experimental values on anhydrous sulphates of Sm and Eu were communicated by Professor Cabrera to Professor Van Vleck. Earlier work of Cabrera and Duperier on hydrous sulphates of Sm and Eu may be found in Compte rendus **188**, 1640 (1929).

[14] P. W. Selwood, J. Am. Chem. Soc. **56**, 2392 (1934).

[15] C. J. Rodden, J. Am. Chem. Soc. **56**, 648 (1934).

[16] Experimental values of the susceptibility of Sm_2O_3 of various observers are tabulated by C. Wiersma and B. H. Schultz, Physica **13**, 171 (1933), P. W. Selwood, reference 14, and A. Frank, reference 2.

[17] R. Serber, Phys. Rev. **43**, 1011 (1933).

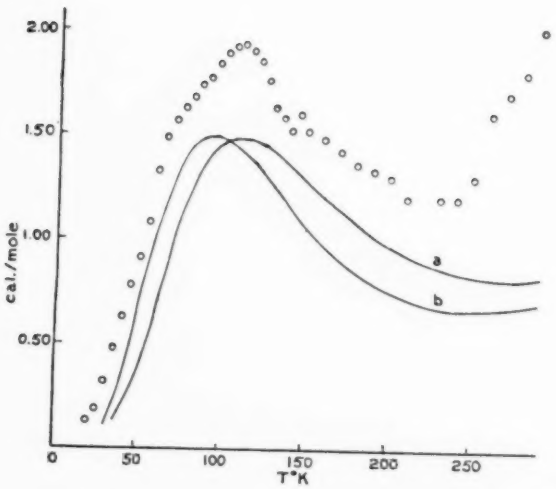

FIG. 4. Variation of electronic heat capacity of Sm^{+++} with temperature. Solid lines show theoretical values using levels at (a) 187 and 225 cm^{-1}, (b) 160 and 187 cm^{-1}. Circles designate experimental values of Ahlberg and Freed.

The terms in the expansion are symmetric in A, B, and $-(A+B)$ and therefore those which are of the first order in the rhombic field energy average to zero. The average contribution to the susceptibility is proportional to the square of the separation due to the rhombic field, to as good an approximation as is needed.

The computations show that the addition of the rhombic splitting has little effect on the susceptibility, as long as it is small compared with the cubic portion of the field. For example, with $\nu = 192$ cm^{-1}, a rhombic separation of 65 cm^{-1} (giving Spedding's levels 160 and 225 cm^{-1}) lowers μ_{eff} by only 0.8 percent at 74°K, the change in μ_{eff} decreasing with increasing temperatures. For smaller rhombic separations, the decrease in μ_{eff} rapidly becomes less so that, with $\nu = 174$ cm^{-1}, the effect of a rhombic separation of 25 cm^{-1} (giving Spedding's levels 160 and 187 cm^{-1}) is negligible. Thus the important factor is the mean of the excited levels and any two of the levels reported by Spedding give values for the susceptibility in satisfactory agreement with the experimental data available. Therefore we may conclude that the samarium ion in a solid such as $Sm_2(SO_4)_3 \cdot 8H_2O$ is probably in a crystalline field, predominantly of cubic symmetry such that the separation of the $J = 5/2$ level is in the neighborhood of 200 cm^{-1}.

TABLE II. *Effective Bohr magneton numbers for Eu.*

	μ_{eff} (THEORY)[2]			μ_{eff} (EXPERIMENT)		
T°K	$\sigma = 33$	$\sigma = 34$	SELWOOD[18]	HUGHES & PEARCE[19] (hyd. sul.)	CABRERA & DUPERIER[13] (hyd. sul.)	(anh. sul.)
83	2.18	2.33	2.06			
153	2.84	2.97	2.73			
223	3.18	3.29	3.14			
293	3.40	3.51	3.41	3.63	3.61	3.53
343	3.53	3.63	3.58			
400	3.65	3.75				3.75

Temperature variation of the heat capacity in Sm

The contribution of the multiplet levels to the heat capacity of Sm at various temperatures is given in a previous paper but these values are increased considerably by the assumption of a crystalline field which splits the lowest multiplet level. The solid lines of Fig. 4 show the theoretical curves for the temperature variation of the heat capacity. Curves for other combinations of levels which give good agreement with the susceptibility data lie close to those given on the graph. The lack of good agreement with the absolute values found experimentally by Ahlberg and Freed[20] is not surprising. These experimental values represent the difference between the heat capacities of $\frac{1}{2}[Sm_2(SO_4)_3 \cdot 8H_2O]$ and $\frac{1}{2}[Gd_2(SO_4)_3 \cdot 8H_2O]$. Since these are large quantities relative to their difference, possibly the error in the difference may be considerable. Moreover additional levels as reported by Spedding would contribute to the heat capacity.

EFFECT OF CRYSTALLINE FIELDS IN EU

Experimental data

Since the previous work on the theoretical susceptibility for the free europium ion,[2] several experimenters have published values of the susceptibilities of europium compounds. Table II lists the data on sulphates as one may expect these values to give better agreement with the theory for the free ion than values obtained from the oxides, since the latter are firmer chemical compounds. The fact that Selwood's values at temperatures below room temperature are lower

[18] P. W. Selwood, J. Am. Chem. Soc. **55**, 4869 (1933).
[19] Hughes and Pearce, J. Am. Chem. Soc. **55**, 3277 (1933). It is not stated in this paper whether diamagnetic corrections had been made.
[20] J. Ahlberg and S. Freed, J. Am. Chem. Soc. **57**, 431 (1935).

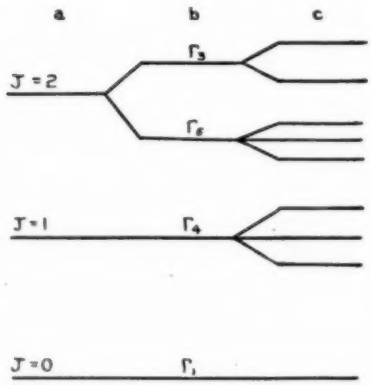

FIG. 5. The energy levels, $J=0$, 1, 2, of the ^7F configuration: (a) for the free ion and (b) in the presence of a field of cubic symmetry. The addition of a rhombic field splits the levels further as in *c*.

than the theoretical values suggests the possibility that the susceptibility is lowered by a crystalline field as in the case of Sm. However, calculations similar to those for Sm show that the presence of fields of cubic and rhombic symmetry has very little effect upon Eu.

Effect of crystalline fields on the energy values and the susceptibility

It is not surprising that the effect of a crystalline field of cubic symmetry is less for the europium ion than for samarium because the lowest state ($J=0$) is nondegenerate and the degeneracy in the $J=1$ level is not removed by the cubic field. The analysis of Bethe shows that the $J=2$ level separates into two levels corresponding to the irreducible representations Γ_3 and Γ_5. Furthermore, since $J=2$ and $J=1$ belong to different representations of the cubic group, there are no matrix elements of the cubic field between them. For Eu, whose multiplet type is ^7F, the doubly degenerate Γ_3 level is of higher energy than the triply degenerate Γ_5 level. A diagram of these levels is given in Fig. 5.

It is sufficient for the purpose of this calculation to consider the effect of a cubic field which partially removes the degeneracy in the $J=2$ level, and a rhombic field which completely removes the threefold degeneracy in the $J=1$ level. If the effect of the rhombic matrix elements between $J=1$ and $J=2$ and of cubic elements between $J=2$ and $J=3$ are neglected, the secular determinant is readily diagonalized in all but the magnetic terms, and their contribution to the energy may be obtained by perturbation theory.

With the rhombic field absent and the cubic separation equal to 200 cm^{-1}, the effective Bohr magneton number is smaller than that for the free ion by 1 percent at room temperature when the screening constant is taken as 34. The change in μ_{eff} is less when the screening constant is taken as 33. At low temperatures the change is negligible since only the normal state has an appreciable population and the normal state is not affected by the cubic field. Moreover a cubic separation as great as 200 cm^{-1} is improbable in Eu. In terms of constants defined previously in connection with the discussion of the cubic field in Sm, the energy of separation of the $J=2$ level due to the cubic field is $440Q/7=260ID/63$. If we assume the integral I to be nearly the same in both cases, the value of D necessary to separate the $J=2$ level of Eu by 200 cm^{-1} must be about 350 times the value to separate the $J=5/2$ level of Sm by the same amount. And since even the improbable separation of 200 cm^{-1} produces little change in the effective magneton number, Eu may be considered gas-like in the presence of a cubic field, a result which one should expect from the group theory analysis since the cubic field has no effect on the lowest two levels of Eu.

The average contribution due to the rhombic field may be determined by expanding the expression for the susceptibility if we assume the rhombic energies small compared with kT and small compared with the multiplet energies. The rhombic terms increase μ_{eff} by less than 1 percent at 83°K if the maximum separation introduced by the rhombic field is 100 cm^{-1}. The change due to the rhombic field is less at higher temperatures. Thus the effect of crystalline fields may be considered of little importance in the case of Eu.

In conclusion I wish to express my gratitude to Professor J. H. Van Vleck under whose guidance this work was done.

LETTERS TO THE EDITOR

Prompt publication of brief reports of important discoveries in physics may be secured by addressing them to this department. Closing dates for this department are, for the first issue of the month, the twentieth of the preceding month; for the second issue, the fifth of the month. The Board of Editors does not hold itself responsible for the opinions expressed by the correspondents.

Theory of Radioactive Fluctuations

Experiments on radioactive fluctuations have been confined to constant sources, and little has been done on the theory of fluctuations in the emission of sources which decay appreciably during the time of a single experiment.[1] Also, previous work dealt with fluctuations in disintegration, whereas the experimenter usually needs formulas for the fluctuations in the counts recorded by a detector which receives only a fraction of the particles or rays emitted by a source. In securing formulas suitable for analyzing experimental results, we first generalize Bateman's differential equation for the probability, $W_n(0, t)$, that n atoms of a source will disintegrate in the interval $(0, t)$. If $f_r dt$ is the chance of a disintegration in dt at t after r have occurred in $(0, t)$, then $dW_n/dt = f_{n-1}W_{n-1} - f_n W_n$. For a source with decay constant λ, containing N atoms initially, $W_n(0, t) = C_n^N(e^{\lambda t}-1)^n e^{-N\lambda t}$. From this we have obtained the fluctuations in counts recorded by a detector of efficiency g, subtending solid angle $4\pi A$ at the source. The chance P_n of n *counts* in the interval (T_1, T_1+T_2) is

$$C_n^N(e^{\lambda T_2}-1)^n e^{-N\lambda(T_1+T_2)}(gA)^n[1+e^{\lambda T_2}(e^{\lambda T_1}-1) + (1-gA)(e^{\lambda T_2}-1)]^{N-n},$$

provided each disintegrating atom emits just one particle or ray.[2]

For a decaying source the probability that the $(n+1)$th interval between disintegrations will exceed t is $e^{-(N-n)\lambda t}$. Therefore, if we measure a great number, r, of intervals, the expected value of the fraction of the intervals which exceed is $[e^{-N\lambda t}-e^{-(N-r)\lambda t}]/r(1-e^{\lambda t})$.

When one has obtained experimentally the fluctuations in counting (i.e., the functions P_n), the next step is to derive the probability W_s of s emissions in the interval (T_1, T_1+T_2). Now $P_n = \sum_{s=n}^{N} W_s C_n^s (gA)^n (1-gA)^{s-n}$, and the solution of these equations is

$$W_s = (1-gA)^{-s}\sum_{i=s}^{N} C_s^i [(1-gA)/gA]^i (-1)^{i+s} P_i. \quad (4)$$

We have obtained the probability P_0' of no counts in the interval $(0, t)$, in a detector of finite recovery time, τ, after a count has occurred at $t=0$. Our formula applies to counts produced by a constant source. Using Skinner's[3] formula for the frequency distribution of recovery times, $\omega(\tau)$, we obtain $P_0'(0, t) = e^{-f(t-\tau')}$ where t is greater than the maximum recovery time, f = number of rays which would be counted per sec. if τ were zero, and $e^{f\tau'} = \int_0^{\tau_{\max}} \omega(\tau) e^{f\tau} d\tau$.

We have derived formulas for the stock fluctuations of each substance in a source containing several members of a radioactive series, subject to any desired initial conditions. The probability of a stock n of a daughter substance (decay constant λ), in equilibrium with a constant parent which yields f disintegrations per sec., is $S_n = (f/\lambda)^n e^{-f/\lambda}/n!$. The emission fluctuations of the daughter are given by $W_n = (ft)^n e^{-ft}/n!$, the same formula as that for the emission of the parent. However, *the fluctuations of the parent and the daughter are coupled*, so that the Bateman type of formula does not apply to their combined emission. In fact, the probability of an interval greater than t between the emissions from *both* substances is exp $[-ft-(f/\lambda)(1-e^{-\lambda t})]$.

ARTHUR E. RUARK
LEE DEVOL

University of North Carolina,
September 3, 1935.

[1] See however Peierls, Proc. Roy. Soc. **A149**, 467 (1935).
[2] The modifications necessary when this is not the case are easily obtained. The fluctuations in counts produced by several sources containing different substances can also be obtained.
[3] Skinner, Phys. Rev. **48**, 438 (1935).

The Uncertainty Principle as an Eigenwert Problem

The quantum-mechanical uncertainty principle is usually stated as $\Delta p \Delta q \gtrsim h/4\pi$, where p and q are conjugate momentum and coordinate. In this note we push the problem further by finding all those wave functions which make $\Delta p \Delta q$ stationary. Using the calculus of variations method[1] in the usual way on the quantity

$$(\Delta p)^2(\Delta x)^2 = \frac{\int \psi^* q^2 \psi dq \cdot \int ((h/2\pi)d\psi^*/dq)((h/2\pi)d\psi/dq)dq}{(\int \psi\psi^* dq)^2},$$

we obtain the equation

$$[(\Delta q)^2(h/2\pi)^2 d^2/dq^2 - (\Delta p)^2 q^2 - 2(\Delta p)^2(\Delta q)^2]\psi = 0$$

for those functions which make $\Delta p \Delta q$ stationary. Using the change of variables $q = (h\Delta q/2\pi\Delta p)^{1/2} z$, we find $[d^2/dz^2 - z^2 + 4\pi\Delta p\Delta q/h]\psi = 0$, which is equivalent to the Schrödinger equation for the linear oscillator, even with the correct boundary conditions since ψ must approach zero for $x = \pm\infty$ in order that Δq may have a proper meaning.

From the known stationary values for the linear oscillator we find $(\Delta p \cdot \Delta q)_{\text{stationary}} = (n+1/2)h/2\pi$, the lowest value being $h/4\pi$, and the lowest stationary state being given by a Gaussian error curve as was shown by Heisenberg by a more complex method some time ago.[2]

CLARENCE ZENER

Wayman Crow Hall of Physics,
Washington University,
October 4, 1935.

[1] Courant and Hilbert, *Methoden der Mathematische Physik I* (1924), p. 142.
[2] Heisenberg, *The Physical Principles of the Quantum Theory* (1930), p. 18.

Shower Production in Small Thicknesses of Lead and Other Elements

It is generally assumed that the increased frequency of "shower coincidences," associated with the disposition of increasing thicknesses of lead above a set of Geiger-Müller counters, is a linear function of the thickness of the lead above such counters.[1]

As part of a general program of investigation of cosmic-ray shower production we have had occasion to make observations on the production of showers by relatively small thicknesses of material above the counters. These observations were undertaken primarily on account of the probable simplification of results due to the diminished importance of absorption for small thicknesses of material.

In the experimental arrangement of Fig. 1 it will be noted that at least three particles must be involved in a coincident discharge of the three counters, since no single particle from the lead can pass directly through more than one counter.

In Fig. 2 we have plotted the observed increase in counting rate ($\Delta C/T$) in counts per hour as a function of material thickness t in cm. A dotted curve, proportional to t^2, is also plotted for comparison purposes. The data indicate that the increase in such observed "triples" is definitely not a linear function of thickness, and is, for small thicknesses, considerably faster than the first power of t. One would expect that any correction of such observed counting rates for the absorption of shower particles in the producing material would become of relatively greater importance as t increases.

In view of the fact that other data in the literature, as well as observations made in this laboratory, indicate a linear increase of counting rate ($\Delta C/T$) with t where a minimum of two particles from the lead can cause a coincident discharge of the counters, we have also recorded "doubles" using only the two outside counters (1 and 3, of Fig. 1). In this case the data of Fig. 3 were obtained. This indicates an approximately linear relation between

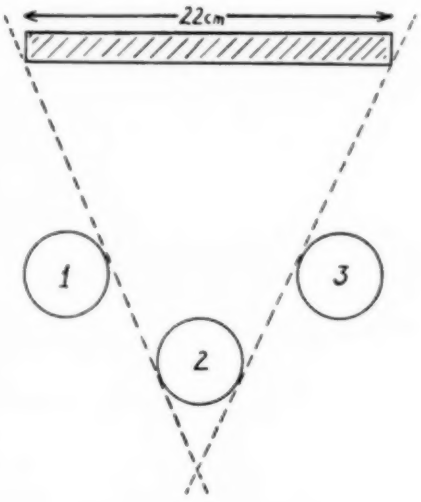

FIG. 1.

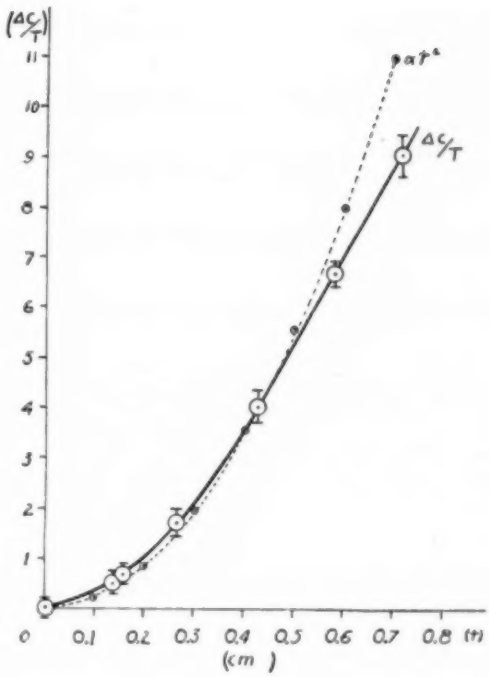

FIG. 2.

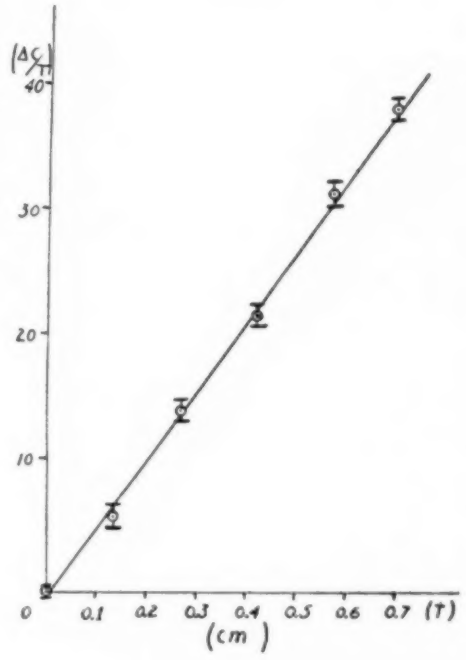

FIG. 3.

increase in coincidences and thickness of material for "two-particle" coincidences.

It must be emphasized that the above observations pertain to lead only. Our data on other materials (carbon, aluminum, copper and tin) show that the departure from linearity for "triples," as in Fig. 1, is a function of the

atomic number of the element concerned, and indicate that for the elements of lower atomic number the increase in counting rate is more nearly a linear function of t.

The significance of these observations and other data will be discussed after the completion of a series of rather lengthy experiments on the absorption of shower particles in the shower producing material.

J. E. MORGAN
W. M. NIELSEN

Department of Physics,
Duke University,
Durham, N. C.,
September 28, 1935.

[1] C. W. Gilbert, *et al.*, Proc. Roy. Soc. **A144**, 559 (1934).

Absorption and Detection of Slow Neutrons

Attempts to explain the capture of neutrons have generally included the assumption that the capture probability varies inversely as the velocity of the neutron. Accordingly the various reactions used as detectors should be velocity sensitive.

As the disintegrations[1] of boron and lithium according to the reactions[2]

$$_5B^{10}+{}_0n^1={}_3Li^7+{}_2He^4$$

and

$$_3Li^6+{}_0n^1={}_2He^4+{}_1H^3$$

are among the most useful detectors of neutrons, we have made a comparison of these in terms of the absorption observed in B, Li, and Cd.

The "slow" neutrons in these experiments are those from a paraffin sphere of 6 cm radius enclosing a Rn-Be source, and more specifically, are those that are stopped by cadmium, 0.9 g per square centimeter.

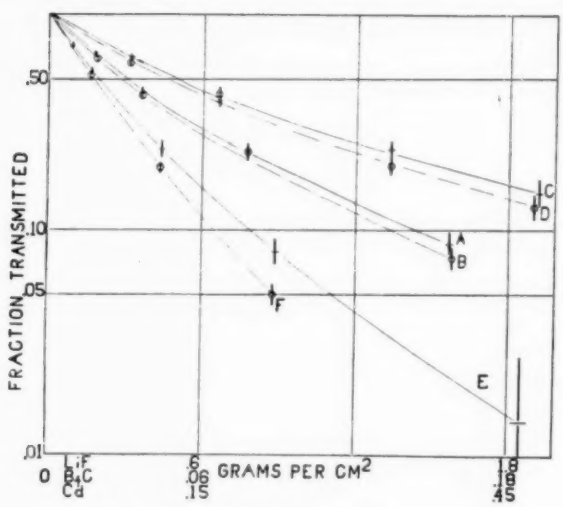

FIG. 1. The absorption of slow neutrons.

Curve	*Absorber*	*Detector*
A	boron	boron
B	boron	lithium
C	lithium	boron
D	lithium	lithium
E	cadmium	boron
F	cadmium	lithium

Identical ionization chambers were constructed except that the collector and all walls of one were coated with powdered boron with a little Aquadag (carbon) as binder, and the other with lithium foil. The details of such a chamber and the geometric arrangement of the source, sample and chamber were as previously described[3] except that in this case the distance from the source to chamber was 18 cm.

The data obtained in these experiments are disclosed in the accompanying plot, Fig. 1, of the logarithm of the fraction of slow neutrons transmitted against the mass per square centimeter of the absorbing sample. The vertical lines indicate the statistical error on the basis of the square root of the number of counts.

The cadmium was in the form of pure metal sheet, the lithium in LiF, and the boron in B_4C mixed with talc. The mass per unit area is the effective mass, account having been taken of the obliquity of part of the beam and the variation in intensity from different zones of the paraffin sphere. These correction factors have little effect on the result; e.g., in the case of B_4C, 0 at large transmissions to 3 percent at 0.08 transmission.

In order to get a reasonably large number of counts, these chambers were built with three successive, separate layers of B or Li. This arrangement permits the use of a total thickness sufficient to absorb most of the slow neutrons while at the same time permitting the detection of many disintegration particles produced by neutrons captured in the first layers. Such chambers should be relatively insensitive to neutron velocity. That the sensitiveness does not vary much with velocity seems to be borne out by the fact that the curves for the same absorber observed with Li and B as detectors are not very different.

Although the cadmium absorption curve by boron detection diverges more from the exponential than the earlier[4] curve by lithium detection, this divergence is of the same order as the experimental error. The departure of the B and Li absorption curves from the exponential form is outside the estimated experimental error. With the type of

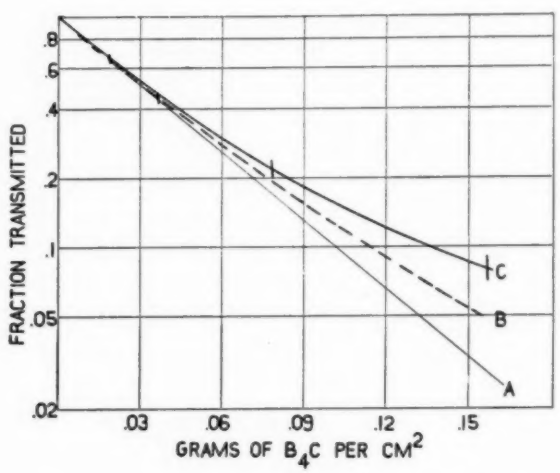

FIG. 2. *A*, the exponential form; *B*, the theoretical $1/V$ curve; *C*, observed for B with B detector.

chambers used, it appears that these departures from the exponential are chargeable to the nonhomogeneity of the neutron beam and the dependence of the absorption in the sample upon the velocity distribution of the neutrons, rather than to response of the detector.

Recent results[5] have shown that the velocity distribution of slow neutrons has a maximum closely coinciding with the maximum in a Maxwellian distribution. In view of the theoretical prediction that the absorption should vary inversely as the velocity, it is of interest to show the absorption curve that would result from a Maxwellian distribution in time, and an absorption proportional to $1/V$.

The departure of the $1/V$ curve from the exponential form is seen in Fig. 2 to be even less than that of the experimental one.

We are indebted to Mr. H. C. Torrey who supplied us with the values of the integral

$$f(q)=\int_0^\infty e^{-q^2y-y^3}dy$$

which he obtained in connection with another problem.

D. P. Mitchell
J. R. Dunning
E. Segrè
G. B. Pegram

Pupin Physics Laboratories,
Columbia University,
October 19, 1935.

[1] Amaldi, d'Agostino, Fermi, Pontecorvo, Rasetti and Segrè, Proc. Roy. Soc. **A149**, 522 (1935).
[2] Taylor and Goldhaber, Nature **135**, 341 (1935).
[3] Dunning, Pegram, Fink and Mitchell, Phys. Rev. **48**, 265 (1935).
[4] Dunning and Pegram, Phys. Rev. **47**, 796 (1935).
[5] Dunning, Pegram, Fink, Mitchell and Segrè, Phys. Rev. **48**, 704 (1935).

The Electrical Conductance of Colloidal Solutions at High Frequencies

Measurements of the electrical conductance and dielectric constant of suspensions and colloidal solutions have brought to light a number of interesting phenomena, originating, as it appears, at the interphases of the solution. In a recent letter to this journal[1] we have described the marked increase in dielectric constant which takes place at low frequencies. This note is concerned with a rise in electric conductance which is observed at high frequencies. The measurements were made up to 16,000 kc per sec. by comparison with potassium chloride solutions. On the basis of the theory of Debye and Falkenhagen[2] the frequency dependence of conductance of the potassium chloride solutions is sufficiently small to be disregarded in the present measurements. Associated with the rise in conductance, a small decrease in the dielectric constant of the colloidal solutions is observed.

Typical measurements on suspensions are shown in Fig. 1(A). They include powdered glass and kaolin suspended in potassium chloride and mineral oil in sodium oleate. The concentration of the potassium chloride has been varied to give specific conductances from 10^{-3} to 10^{-5} mho-cm^{-1} with no apparent change in the conductance-frequency curves. The specific conductance of the mineral oil emulsion was 7×10^{-4} mho-cm^{-1}.

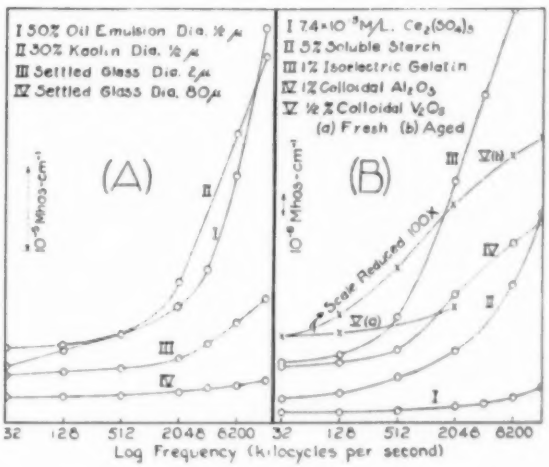
I 50% Oil Emulsion Dia. ½ μ
II 30% Kaolin Dia. ½ μ
III Settled Glass Dia. 2 μ
IV Settled Glass Dia. 80 μ
(A)
I 7.4×10⁻³ M/L. Ce₂(SO₄)₃
II 5% Soluble Starch
III 1% Isoelectric Gelatin
IV 1% Colloidal Al₂O₃
V ½% Colloidal V₂O₅
(a) Fresh (b) Aged
(B)
Scale Reduced 100X
32 128 512 2048 8200
Log Frequency (kilocycles per second)

FIG. 1. Variation of conductance with log frequency.

In Fig. 1(B) are shown results obtained for a number of colloidal solutions, including aluminum oxide, vanadium pentoxide, starch and gelatin. The gelatin was measured at its isoelectric point. The aluminum oxide and vanadium pentoxide solutions were prepared by chemical precipitation, followed by washing and peptization with distilled water.[3] The vanadium pentoxide was measured immediately after being prepared and again three months later. With aging, there is a marked increase in the high frequency conductance. The low frequency conductance of this solution was 1.2×10^{-3} mho-cm^{-1}, while the low frequency conductance of the other colloidal solutions of Fig. 1(B) were around 5×10^{-5} mho-cm^{-1}.

This increase in conductance of suspensions and colloidal solutions is probably due, at least in part, to an effect of the same type as the Debye-Falkenhagen[2] effect in strong electrolytes,[4] i.e., it is produced because the static forces between the charges on the colloidal particles and those in the adjacent portion of the continuous phase produce, in an external field of low frequency, an interference with the displacement of the ions of the continuous phase. This interference becomes negligible at high frequencies.

For soils, various investigators[5] concerned with the problem of radio communication have found indications of an increased conductance at high frequencies. This increase probably is of the same type as that studied here.

Howard J. Curtis
Hugo Fricke

Walter B. James Laboratory for Biophysics,
The Biological Laboratory,
Cold Spring Harbor, L. I., N. Y.,
October 3, 1935.

[1] H. Fricke and H. J. Curtis, Phys. Rev. **47**, 974 (1935).
[2] P. Debye and H. Falkenhagen, Physik. Zeits. **29**, 121 (1928). Compare also, H. Falkenhagen, *Elektrolyte* (Leipzig, 1932).
[3] H. Freundlich, *Kapillarchemie* (Leipzig, 1923), p. 715 ff.
[4] The measurements for cerium sulfate have been included in Fig. 1 (B) for the purpose of comparison.
[5] M. J. O. Strutt, Elek. Nach.-Tech. **7**, 387 (1930); C. B. Feldman, Proc. Inst. Rad. Eng. **21**, 764 (1933); R. L. Smith-Rose, J. Inst. Elect. Eng. (London) **75**, 221 (1934).

Note on γ-Transformation of Electromagnetic Fields

In his recent "Contributions to Born's Theory of the Electromagnetic Fields" Schrödinger[1] has given the name γ-transformation to a process which in relation to electromagnetic fields, must have been known previously to a number of mathematicians. For example, Whittaker in his paper on electromagnetic tubes of force[2] discusses the linear combination of the two electromagnetic 6-vectors to form one in which the component 3-vectors are mutually perpendicular, and it is a very short step from the consideration of this particular transformation to what really corresponds to Gibbs' bivector analysis.[3] Naturally, the above statements do not refer to Schrödinger's application of this method of representation. Independently of Born's work, this elegant device is quite proper to the theory of the electromagnetic symbolic differential forms,[4] which shows clearly that, in the representation, γ-transformation creates free magnetism.

Let α and β be the forms

$$\alpha = E_x dxdt + E_y dydt + E_z dzdt + H_x dydz + H_y dzdx + H_z dxdy,$$
$$\beta = E_x dydz + E_y dzdx + E_z dxdy - H_x dxdt - H_y dydt - H_z dzdt.$$

Following the method of Whittaker, set up the form

$$\lambda = a\alpha + b\beta,$$

where a and b are coefficients still to be determined. In order that

$$\sum_{x,\,y,\,z} (aH_x + bE_x)(aE_x - bH_x) = 0,$$

we must have

$$(a^2 - b^2)(\mathbf{E}\cdot\mathbf{H}) + ab(\mathbf{E}^2 - \mathbf{H}^2) = 0.$$

This means that, given a normalizing condition on a and b, there are two forms for which the condition of perpendicularity of the transformed field vectors holds, with important consequences with respect to the class of the forms. If we require that $a^2 + b^2 = 1$, the two forms are

$$\lambda = \cos\varphi\cdot\alpha - \sin\varphi\cdot\beta, \quad \mu = \sin\varphi\alpha + \cos\varphi\cdot\beta, \quad (1)$$

where $$\tan 2\varphi = G/F, \quad G = (\mathbf{E}\cdot H), \quad F = \tfrac{1}{2}(\mathbf{E}^2 - \mathbf{H}^2). \quad (2)$$

With regard to the derived forms, we have $\alpha' = 0$ always, and if β' is not zero, then, since

$$\lambda' = -\mu d\varphi - \sin\varphi\cdot\beta', \quad \mu' = \lambda d\varphi + \cos\varphi\cdot\beta',$$

neither λ' nor μ' vanishes. It follows that if we write

$$\lambda = E_x' dxdt + E_y' dydt + E_z' dzdt + H_x' dydz + H_y' dzdx + H_z' dxdy,$$
$$\mu = E_x' dydz + E_y' dzdx + E_z' dxdy - H_x' dxdt - H_y' dydt - H_z' dzdt,$$

and regard $\mathbf{E}'\mathbf{H}'$ as an electromagnetic field, we require at once the existence of free magnetism (which mathematicians seem to unearth every few years but which experiment continues to deny). The stress-energy-momentum tensor is of course unaltered by this transformation and would be so whatever the value of φ; $(F^2 + G^2)$ is unaltered when φ is given the value (2). On referring to Gibbs the reader will find that the transformation specified by (1) turns up as the multiplication of a bivector by $e^{i\varphi}$. It is unnecessary here to mention the fairly obvious development which follows from Gibbs' treatment.

When one considers the representation of an electromagnetic field by means of the motion of lines[5] one can use the inverse of (1) to obtain the line Hamiltonian appropriate to nonorthogonal fields; while with regard to the properties of the symbolic differential forms, $d\varphi$ is always an integrating factor of β', λ' and μ'.

In order that the motion of an electrified particle of charge e moving in the original field may be unaffected by the transformation it is necessary in the transformed field to endow the particle with electric charge $e\cos\varphi$ and magnetic pole-strength $e\sin\varphi$.

If one imagines the γ-transformations to correspond to physical possibilities then it becomes a question of some importance to ask the theorist what method he allows the experimenter to distinguish electricity from magnetism. With Schrödinger's assertion of the symmetry of theory with respect to electricity and magnetism, experimenters are invited to assign the names "electricity" and "magnetism" according to their own conventions which will have as little part in the theory as the conventions for naming "right" and "left" have in geometry.

W. H. Watson

Macdonald Physics Laboratory,
McGill University,
Montreal, Canada,
September 20, 1935.

[1] E. Schrödinger, Proc. Roy. Soc. **A150**, 465 (1935).
[2] E. T. Whittaker, Proc. Roy. Soc. Edin., Nov. 7, 1921.
[3] Willard Gibbs, *Collected Works*, Vol. II, pp. 87–88.
[4] W. H. Watson, Trans. Roy. Soc. Canada **3**, 1 (1934).
[5] Reference 4, § 4.

Enhancement of X-Ray Satellites by the Auger Effect

The satellites $L\beta_1'$ and $L\beta_1''$ of the x-ray diagram line $L\beta_1$ have been reported[1] for the atomic number range $29 < Z < 52$. It has been assumed[2] that within this range there are no sudden changes with atomic number in the relative energy (i.e., with respect to the parent line). D. Coster[3] has remarked, of these satellites, that "from Sb, (where they were observed for the first time) down to Rb they do not essentially change." Coster and Kronig[2] have pointed out that, for these satellites, the Auger effect cannot occur if $Z > 40$. We have observed photographically,

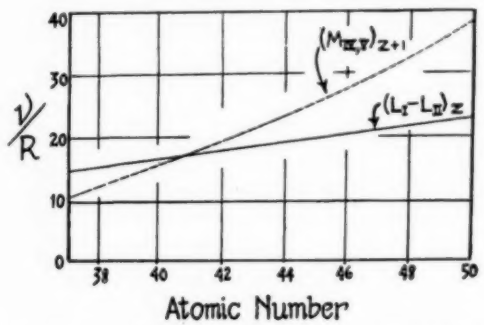

FIG. 1. The energy provided by the radiationless transition $L_I \rightarrow L_{II}$, and the energy required to eject an $M_{IV, V}$ electron, plotted against atomic number.

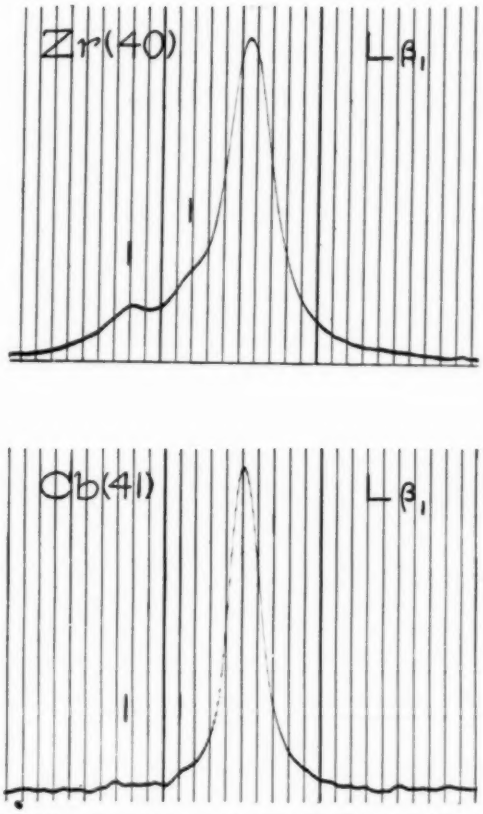

FIG. 2. Microphotometric records of the $L\beta_1$ lines of Zr(40) and Cb (41). Vertical dashes indicate positions at which satellites are known to occur.

and report herein briefly an intensity anomaly for these satellites, due to the Auger effect. A more complete report will be made later.

The line $L\beta_1$ arises from the transition $L_{II}M_{IV}$. According to the Coster-Kronig theory,[3] a cathode-ray electron ionizes the L_I shell of the atom; the radiationless transition $L_I \rightarrow L_{II}$ follows, with the simultaneous ejection of an $M_{IV, V}$ electron and the atom is left doubly ionized, (L_{II} and $M_{IV, V}$); a subsequent single electron transition, $L_{II}M_{IV, V} \rightarrow (M_{IV, V})$,[2] results in the appearance of satellites. If the energy difference $(L_I - L_{II})_z$ is greater than the ionization energy of the $M_{IV, V}$ shell (for $z+1$ since the L_I shell is also ionized), we may expect enhancement of the $L\beta_1$ satellites. This process is actually possible only when $Z<41$, as is shown in Fig. 1. Fig. 2 shows the $L\beta_1$ lines with their accompanying satellites for Zr (40) and Cb (41). (Both lines were excited by 20-kv cathode rays.) Satellites are observed visually at the positions indicated by the vertical dashes. These satellites are prominent for Zr (40), (integrated relative energy = 0.18), and have nearly vanished at Cb (41), (integrated relative energy <0.01), showing that the Auger effect strongly enhances the satellites of Zr $L\beta_1$. Above $Z=40$, when the Auger effect is eliminated, these same satellites are extremely faint, but persist because of double ionization by single impacts of cathode-ray electrons.

FREDERICK R. HIRSH, JR.

Cornell University,
Ithaca, N. Y.,
October 4, 1935.

[1] M. J. Druyvesteyn, Dissertation, Groningen (1928).
[2] D. Coster and R. DeL. Kronig, Physica **2**, 13 (1935).
[3] D. Coster, Phil. Mag. **43**, 1089 (1922).

Errata: Potential Drop and Ionization at Mercury Arc Cathode

E. S. LAMAR AND K. T. COMPTON, *George Eastman Research Laboratory of Physics, Massachusetts Institute of Technology*
(Phys. Rev. **37**, 1069 (1931))

DR. LEWI TONKS has very kindly called our attention to some numerical errors in our paper. In Table I, page 1075, the values for $N(10^{-11})$ should be, reading from left to right, 22.0; 3.45; 267.5; and 67.8. The value of I(amp. cm^{-2}) for 4.2 amp. arc d(cm) = 1.75 should read 0.74. The curves presented in the paper are correct.

THE AMERICAN INSTITUTE OF PHYSICS

INCORPORATED

GOVERNING BOARD

For The American Physical Society:

KARL T. COMPTON, *Chairman*
Massachusetts Institute of Technology

GEORGE B. PEGRAM, *Secretary*
Columbia University

JOHN T. TATE
University of Minnesota

For The Optical Society of America:

E. C. CRITTENDEN
Bureau of Standards

PAUL D. FOOTE
The Gulf Companies

F. K. RICHTMYER
Cornell University

For The Acoustical Society of America:

HARVEY FLETCHER
Bell Telephone Laboratories

VERN O. KNUDSEN
University of California at Los Angeles

WALLACE WATERFALL
The Celotex Company

For The Society of Rheology:

E. C. BINGHAM
Lafayette College

A. STUART HUNTER
du Pont Rayon Company

S. E. SHEPPARD
Eastman Kodak Company

For The American Association of Physics Teachers:

HOMER L. DODGE
University of Oklahoma

PAUL E. KLOPSTEG
Central Scientific Company

FREDERIC PALMER
Haverford College

ADMINISTRATIVE STAFF

HENRY A. BARTON, *Director* JOHN T. TATE, *Adviser on Publications*

MADELINE M. MITCHELL, *Editorial Secretary*

Office: 11 East 38th Street, New York, New York

JOURNALS

THE PHYSICAL REVIEW

REVIEWS OF MODERN PHYSICS

PHYSICS
JOHN T. TATE, *Editor*
J. W. BUCHTA, *Assistant Editor*
E. C. BINGHAM, *Rheology Editor*

THE JOURNAL OF THE OPTICAL SOCIETY OF AMERICA

THE REVIEW OF SCIENTIFIC INSTRUMENTS
WITH PHYSICS NEWS AND VIEWS
F. K. RICHTMYER, *Editor*

JOURNAL OF THE ACOUSTICAL SOCIETY OF AMERICA
F. R. WATSON, *Editor*

THE JOURNAL OF CHEMICAL PHYSICS
HAROLD C. UREY, *Editor*

THE AMERICAN PHYSICS TEACHER
DUANE ROLLER, *Editor*

The American Institute of Physics is a membership corporation of which five societies are the founding members. These five societies are the principal national societies devoted to pure and applied physics in America. Their names, and those of their representatives who form the Governing Board of the Institute, are given above. The principal work of the Institute is the publication of journals sponsored by the societies or by itself. The names and the editors of the journals are also listed above.

The broad purpose of the Institute is to represent, in all matters of wide or common interest, the five thousand or more members and subscribers associated with the Founder Societies and the journals. It aims to advance the science and profession of physics, and to promote cooperation between pure research, the applied sciences and the industries. To achieve these aims, it is greatly in need of an endowment and is empowered by law to administer grants and funds of any kind.

CONTENTS

PHYS. REV. 48 (1935) NOVEMBER 1

Beryllium Deuteride Spectra . . . . . PHILIP G. KOONTZ 707

Far Ultraviolet Absorption Spectrum of Oxygen . . . . . W. C. PRICE AND GEORGE COLLINS 714

Deep Terms in the Isoelectronic Sequence V I to Cu VII . . . . . P. GERALD KRUGER AND HELEN T. GILROY 720

Relative Energy of the $L\alpha$ Satellites Excited by Cathode Rays in the Atomic Number Range 47 to 52 . . . . . F. R. HIRSH, JR. 722

Hyperfine Structure and Nuclear Magnetic Moment of Caesium I . . . . . L. P. GRANATH AND R. K. STRANATHAN 725

***E* Band System of Calcium Hydride** . . . . . WILLIAM W. WATSON AND ROBERT L. WEBER 732

Photoelectric Properties of Pure and Gas-Contaminated Magnesium . . . . . R. J. CASHMAN AND W. S. HUXFORD 734

Disintegration of Lithium by Deuterons . . . . . T. W. BONNER AND W. M. BRUBAKER 742

On the Nuclear Moments of Lithium, Potassium, and Sodium . . . . . MARTIN FOX AND I. I. RABI 746

Positive and Negative Thermionic Emission from Molybdenum . . . . . H. B. WAHLIN AND J. A. REYNOLDS 751

Theory of Pressure Effects of Foreign Gases on Spectral Lines . . . . . HENRY MARGENAU 755

Effect of Crystalline Fields on the Magnetic Susceptibilities of Sm^{+++} and Eu^{+++}, and the Heat Capacity of Sm^{+++} . . . . . AMELIA FRANK 765

Letters to the Editor:

Theory of Radioactive Fluctuations . . . ARTHUR E. RUARK AND LEE DEVOL 772

Uncertainty Principle as an Eigenwert Problem . . . . CLARENCE ZENER 772

Shower Production in Small Thicknesses of Lead and Other Elements . . . . . J. E. MORGAN AND W. M. NIELSEN 773

Absorption and Detection of Slow Neutrons . . . . . D. P. MITCHELL, J. R. DUNNING, E. SEGRÈ AND G. B. PEGRAM 774

Electrical Conductance of Colloidal Solutions at High Frequencies . . . . . HOWARD J. CURTIS AND HUGO FRICKE 775

Note on γ-Transformation of Electromagnetic Fields . . . W. H. WATSON 776

Enhancement of X-Ray Satellites by the Auger Effect . . . . . FREDERICK R. HIRSH, JR. 776

Errata: Potential Drop and Ionization at Mercury Arc Cathode . . . . . E. S. LAMAR AND K. T. COMPTON 777

LANCASTER PRESS, INC., LANCASTER, PA.